A Systematic Methodology to Study Driving Adaptation Effects under Flooding Conditions

Cristino Pérez Lázaro

TU Delft

DELFT UNIVERSITY OF TECHNOLOGY

MSc. Civil Engineering

Transport & Planning

A Systematic Methodology to Study Driving Adaptation Effects under Flooding Conditions

Cristino Pérez Lázaro - 4745566

Chairman: Prof. Dr. ir. S.P. Hoogendoorn
Daily Supervisor 1: Dr. ir. A.J. Pel
Daily Supervisor 2: Dr. V.L. Knoop

A Systematic Methodology to Study Driving Adaptation Effects under Flooding Conditions

by

Cristino Pérez Lázaro

to obtain the degree of Master of Science
at the Delft University of Technology,
to be defended publicly on the 22^{nd} of January 2020 at 11AM.

Student number:	4745566
Project duration:	April 4, 2019 – January 22, 2020
Thesis committee:	Prof. Dr. ir. S.P. Hoogendoorn
	Dr. ir. A.J. Pel
	Dr. V.L. Knoop

Cover photo: Jason Fochtman. Downloaded from
https://www.chron.com

TU Delft

Executive Summary

Flooding events not only cause physical damage to the road infrastructure and roadside systems, yet they potentially lead to significant traffic disruptions over the network which have a large impact on the sustainability of urban cities. According to several climate change scenarios, flooding events as a result of intense precipitation are expected to continue into the future becoming more frequent and severe. Therefore, it is essential that engineers design and manage transport networks as efficiently as possible under adverse weather conditions in order to build more resilient transport systems. To do so, professionals need to understand and analyse the impacts of flooding on transport networks.

Traffic simulation models play a key role in allowing transportation engineers to evaluate complex traffic situations that cannot be analysed directly with other means [1]. Computer traffic simulation models are valuable analytical tools that enable the evaluation of traffic performance in road networks under predefined conditions. This allows the opportunity to assess traffic control and design strategies without the need of implementing those alternative strategies in the field. Modelling the impacts of flooding events on the road network is nowadays possible by the use of integrated simulation techniques that combine a flood simulation model with a microscopic traffic model. With this modelling techniques, the geographic location, severity and other impacts of flooding on the road network can be predicted and studied.

Nevertheless, in order to perform a consistent traffic simulation under flooding conditions, a thorough analysis of driving behaviour under such conditions need first to be accomplished, which is a research field that has been scarcely investigated thus far. Therefore, the main contribution of this thesis is to provide a systematic methodology for studying driving adaptation effects under flooding conditions at two complementary levels, namely microscopic and macroscopic level. This consists on a multilevel approach that uses microscopic traffic data of vehicles driving through flooding to extend the study to a macroscopic level. An video analysis procedure called the *'3-Step Video Analysis Approach'* (3SVAA) is developed by the author to extract microscopic traffic parameters from video recording of vehicles driving under different flood depths. This methodology is implemented through an empirical study that analyses two videos of vehicles crossing waterlogged stretches part of the A94 and A93 major roads in Scotland (UK).

First, the 3SVAA is introduced as a suitable data collection technique to extract microscopic traffic variables (i.e. vehicle's speed, time headways and spacing) from video recording of vehicles driving through flooding. More specifically, these parameters are obtained from the vehicle's trajectories in the space(m)-time(s) diagram, which is the main outcome of this video analysis approach. In order to provide the uncertainty or error committed by the 3SVAA when it comes to measure microscopic traffic parameters, a data collection plan is conducted in the province of Granada (Spain), the author's home town. A speed measurement error of $\pm$ 2.86 km/h and a time headway error of $\pm$ 0.74 s were estimated at a confidence level of 95%.

By applying a multilevel analysis, the study can be extended to a macroscopic level by correlating macroscopic variables (i.e. average speed, flow and density) with their microscopic counterparts through the fundamental relationship of traffic flow. This allows to estimate part of the fundamental diagrams of vehicles travelling under different flood depths, and therefore to study flood impacts on free-flow speed and capacity. Besides, this thesis carries out a comparison on the impacts of flooding on macroscopic variables with those found in previous studies by other adverse weather conditions. Furthermore, this thesis estimates two functions that correlate average vehicle speed and average headway to floodwater depth. It is found that average speed decreases with flood depth following a reverse polynomial function, whereas average time headway increases exponentially with flood depth. The significance of these functions is that they provide traffic practitioners with the possibility of including driving adaptation effects under flooding conditions within microscopic traffic models in order to conduct a consistent traffic simulation of the road network in urban cities under such circumstances. This will contribute to better understand flood impacts on driving behaviour providing valuable information to transport planners, operators and policy makers for designing and implementing management strategies before and during the aftermath of a flooding event.

Acknowledgments

First of all, I would like to express my great appreciation to my committee members: Professor Serge Hoogendoorn, Dr. Adam Pel and Dr. Victor Knoop for their invaluable feedback and guidance throughout this research. My special thanks go to Adam Pel, who has always been available for a 'short meeting' to discuss many aspects of this study. I owe special thanks to Panchamy Krishnakumari for her mentorship along the most challenging part of this research, the video analysis.

I would like to express my most sincere gratitude to some people without whom I would have never accomplished my thesis, and therefore my master's in Civil Engineering at Delft University of Technology. First, to my friend Pablo Sánchez Gómez who has been a mentor during both my bachelor's at Polytechnique University of Madrid and my master's at TU Delft. To my flat-mate and friend Anthony van der Pluijm for the amount of hours spent revising the Matlab code and for teaching me the functioning of LaTeX. To my colleague and friend Panagiotis Tzouras for introducing me to the world of research and for having travelled with me along this challenging journey in Delft. Finally, to Dr. Rob van Nes who has been the mentor of every Transport & Planning student, always willing to help and support us during our studies.

To my flat-mates and friends Jaime Quesada, Jaime Negro and Steph Contant for their sound advice during the most difficult moments, and for having made these years more fun. Also, to my friends from Delft Michael Lee, Pablo Garrido and Roberto Isacco for all the good moments lived in this small city of The Netherlands. I would also like to thank my friend Javier Guerrero, who despite the distance has always believed in me and has been there when needed during these past years.

Last but not least, I would like to thank my parents Maribel Lázaro and Cristino Pérez who have supported and encouraged me to continue forward throughout all the stages of my life. No words can express my gratitude to them.

I dedicate this thesis to my father, for his perseverance.

"Like all young men I set out to be a genius, but mercifully laughter intervened"

Lawrence Durrell

Contents

List of Figures

List of Tables

Chapter 1

Introduction

1.1 Problem Description

Transport network are often considered the backbone of modern cities [2, 3], since they have become an increasingly important enabler and driver for the globalized economy, allowing the movement of goods and workers as well as being a social asset, particularly in the maintenance of spatially extended social networks [4]. Extreme weather events not only cause physical damage to the infrastructures of transportation systems, yet they potentially lead to significant disruptions in their operations, which in turn yields to cascading impacts within the system and on other interconnected critical lifelines [5]. According to [2], flooding, especially as a result of intense precipitation, is the predominant cause of weather-related disruption to the transport sector. A number of trends suggest that the problem of urban flooding is expected to continue into the future; first, due to the growing population in urban areas, and secondly due to several climate change scenarios that show heavy rainfall events will be more frequent and intense in the future [6–8]. Different authors, such as [2, 9] state that the problem of flooding is particularly acute on the road network in urban areas due to the high proportion of impermeable surfaces that prevent infiltration of water into the soil. Meanwhile, studies have shown that roads are among the first cause of deaths in cities during flooding, due to vehicles being driven through flooded roadways [10, 11]. For instance, in July 2012, a pluvial flash flood took place in Beijin, leading to widespread transportation disruptions and claimed 79 lives, among which a large number of fatalities were caused by road inundations [9]. Other examples are the widespread flooding in Thailand that inundated Bangkok during the 2011 monsoon season or the series of floods that occurred in 2010 and 2011 in the state of Queensland in Australia, which left 200.000 people affected and 9.000 km of roadway and 3.000 km of rail track disrupted [12]. More recent events, such as the torrential rain and flash flooding in South-Eastern Spain in 2019 as a result of the 'cold drop', left at least 5 deaths and thousand of people affected, as well as several railway lines and road closures [1]. Also in 2019, Edinburgh and Stirling in Scotland were hit with flash floods and thunder leading to at least 14 people rescued and causing travel chaos across the cities with several disruptions to the road and rail networks. [2, 3].

[1] https://elpais.com/elpais/2019/09/13/inenglish/1568359828_120540.html
[2] https://www.bbc.com/news/uk-scotland-edinburgh-east-fife-48749009
[3] https://www.bbc.com/news/uk-scotland-edinburgh-east-fife-48755009

1.2 Motivation and Scientific Gap

Transport networks need to be designed and managed to operate as efficiently as possible in all weather conditions as well as having the capability to adapt and cope with the future impacts of climate change [3]. This is essentially the definition of a resilient road network, defined as 'the one with the ability to withstand the impacts of adverse weather conditions, operate during such adverse conditions and recover promptly from its effects' [13]. According to [7], it is therefore essential flood risk professionals and planners understand the impacts of flooding to build flood resilient cities. In addition, [14] argues that predicting the performance of the road network under extreme weather conditions is a key activity of building transport system resilience. That is the reason why different authors have proposed modelling techniques to predict the geographic location, severity and other impacts of flooding events on the road network [9,15–17]. These are essentially simulation techniques that integrate a flood simulation model and a microscopic traffic simulation for modelling the impacts of flooding on the road network. One of the key aspects of the micro and macroscopic simulation in adverse weather conditions is the introduction of adaptation effects of drivers travelling under such conditions. Several authors have demonstrated that a large number of weather-related effects influence driving behaviour as drivers tend to adapt their speed and time headways in such circumstances. If those driving adaptation effects are incorporated within traffic models, a consistent simulation would allow to test resilience measures and traffic strategies before severe weather conditions take place, making in such a way the road network more robust.

Nonetheless, the majority of those microscopic and macroscopic analysis carried out in the past have focused on day-to-day weather events such as light/heavy rain, snow or fog conditions. Practically no research can be found on the impacts of flooding on both microscopic and macroscopic driving behaviour. Some authors such as [2,16,17] have attempted to study the adaptation effects of drivers in flooding conditions, yet they have used data collection techniques that are highly questionable in terms of suitability for the type of data to be acquired. Therefore, this thesis provides with a new methodology that combines a data collection technique together with a multilevel analysis approach to study driving adaptation effects under flooding conditions at two complementary levels, namely microscopic and macroscopic level.

1.3 Research Questions & Objectives

The main contribution of this thesis is mentioned at the end of the previous section. That is, providing a systematic methodology to study driving adaptation effects under flooding conditions through a multilevel analysis approach. To do so, first an alternative video analysis procedure called the *'3-Step Video Analysis Approach'* (3SVAA) implemented in MATLAB is developed by the author of this thesis to extract individual traffic data from video recording of vehicles travelling through flooding. In doing so, changes in microscopic traffic parameters are first analysed, and subsequently the study is extended to a macroscopic level by correlating macro variables with their microscopic counterparts. This enables to study the impacts of flood depth on free-flow speed and capacity parameters, and therefore to estimate part of the fundamental diagrams of vehicles travelling through such conditions. This thesis seeks to answer the following research questions:

Research question 1: *How can microscopic traffic data (i.e. vehicle speed, time headways and spacing) of individual vehicles travelling through flooding be obtained?*

Research question 2: *What changes in microscopic variables (i.e. vehicle speed and time headways) occur when vehicles travel under different flood depths?*

Research question 3: *How can macroscopic traffic variables (i.e. average speed, flow and density) of vehicles travelling through flooding be obtained from their microscopic counterparts?*

Research question 4: *What changes in macroscopic traffic parameters (i.e. free-flow speed and capacity) occur when vehicles travel under different flood depths?*

In order to answer the above questions, this research achieves the following objectives:

1. It proposes an alternative video analysis procedure called the *'3-Step Video Analysis Approach'* (3SVAA) that enables to extract microscopic traffic parameters (i.e. vehicle speed, time headways and spacing) from video recording of vehicles driving through different flood depths.

2. It analyses changes in microscopic traffic variables when flooding conditions become more severe, that is when flood depth increases.

3. By a multilevel analysis approach, this thesis extends the study to a macroscopic level. First, two functions are estimated that relate vehicle's average speed and time headway with flood depth. Additionally, changes in macroscopic variables (i.e. free-flow speed and capacity) are analysed at three different flood depths, allowing in such a way to estimate part of the corresponding fundamental diagrams.

1.4 Thesis Outline

The outline of this thesis is represented in Figure 1.1 and discussed in more detail within this section. Chapter 1 is an introductory chapter that provides a brief description of the problem, the motivation which drove the author to embark on this research, the contribution and the research questions and objectives. Chapter 2 provides a comprehensive literature review on the main topics related with this research and explains the scientific gaps found and covered by this project in more detail. Chapter 3 presents the methodology, a multilevel analysis approach to study driving adaptation effects under flooding conditions at two complementary levels, namely microscopic and macroscopic level. Chapter 4 introduces the 3SVAA developed by the author to extract microscopic parameters from video recording, and applies it to videos of vehicles crossing two waterlogged stretches in the A94 and A93 major roads in Scotland (UK). In Chapter 5, the methodology proposed is implemented using the microscopic data obtained from the video analysis conducted in the previous chapter. By applying a multilevel approach, a macroscopic analysis is accomplished and part of the fundamental diagrams of vehicles travelling through different flood depths are estimated. Finally, Chapter 6 provides the conclusions drawn from this study and the suggestions for future research.

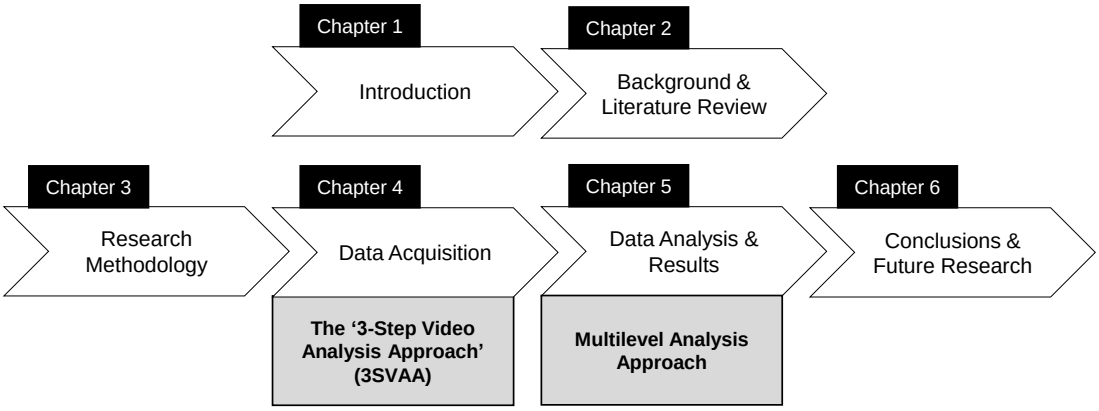

Figure 1.1: Thesis Outline.

Chapter 2

Background & Literature Review

Figure 2.1 displays the content of Chapter 2, providing a clear understanding on how the different sections are connected to each other. This chapter comprises a background and literature review of the most relevant topics related with this project and explains the scientific gaps found and covered in this research.

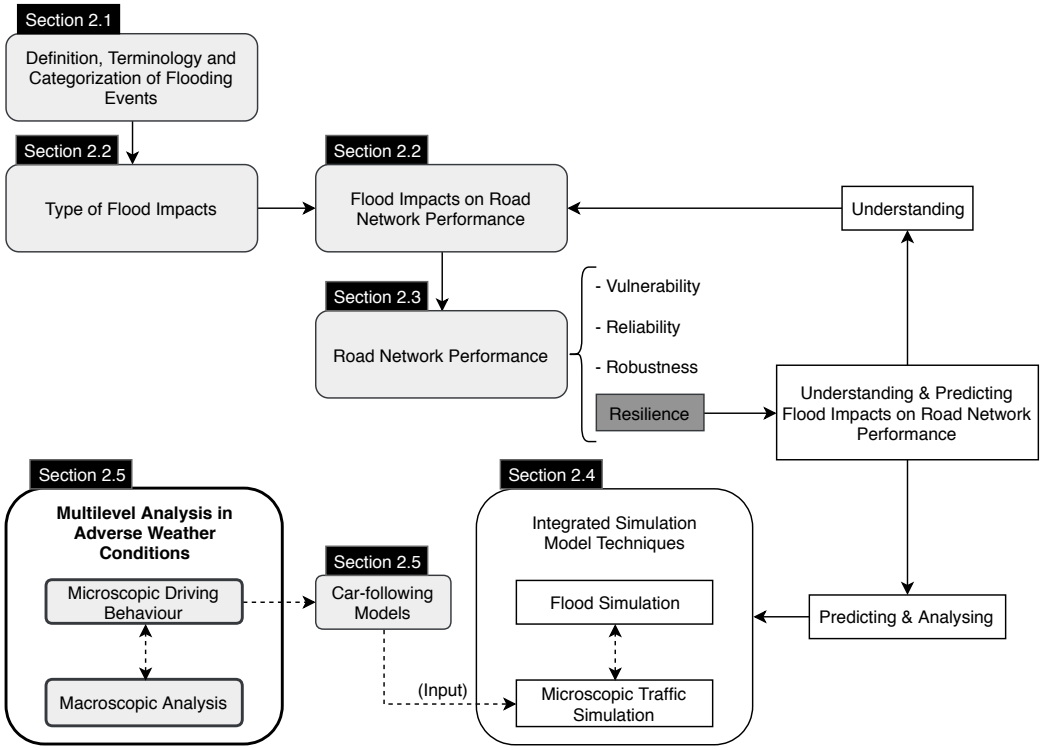

Figure 2.1: Graphical representation of the Background and Literature Review.

Section 2.1 gives a definition of flooding events, the terminology used by different authors and the type of flooding events that are distinguished in literature. In Section 2.2, this thesis gives its own classification of flood impacts on the road network performance based on other authors classification in different contexts. The level of performance of the road network is compromised when disturbances occur, and that is why several authors have provided different definitions of performance concepts in the past. Section 2.3 focuses on the concept of network resilience in the context of urban flooding to illustrate the importance of predicting the impacts of floodwaters on

road traffic. This section highlights the importance of pre-disaster and post-disaster activities when it comes to the preservation and restoration of the level of service in the network. As it is explained in Section 1.2, it is essential to understand and predict the impacts of a hazard in order to build transport system resilience, and that has become possible with the advent of simulation model techniques, since they enable the prediction of the geographic location, severity and other impacts of flooding events on the road network. A state-of-the-art review on those simulation model techniques is provided in Section 2.4, in which their main shortcomings are also highlighted. Those integrated simulation tools combine a hydraulic-hydrologic model and a traffic simulation model to analyse and assess the impacts of floods in road traffic. To simulate road traffic, driving adaptation effects under such adverse conditions need first to be studied, and that is why section 2.5 provides a thorough review on previous research on microscopic driving behaviour under adverse weather conditions. That section is indeed the core of the literature review as it provides the link with the following chapters. Moreover, in order to carry out traffic simulation analyses under such adverse conditions, microscopic models need to be developed/adapted to include driving adaptation effects under such conditions. Therefore, a review on previous studies that incorporate driver's adaptation effects under different weather conditions in microscopic models is conducted in that section. Finally, the scientific gaps covered by this research and the main conclusions drawn from this extensive review are summarised in Section 2.6.

2.1 Definition and Categorization of Flooding Events

Some authors use the term 'natural disaster' to refer to flooding events [19–22]. For instance, [21] define 'adverse conditions' in the context of transport as 'conditions following unplanned events with a relatively high impact and a low probability of occurring'. The latter authors distinguish between different adverse conditions such as evacuations due to man-made or natural disasters (e.g. earthquakes, flooding or terrorist attack), incidents in the road network (e.g. car accidents or road works) and adverse weather conditions (e.g. heavy rain, snow or fog). Other authors such as [22] however, use the term disturbances to refer to natural disasters (e.g. earthquakes, hurricanes or floods), extreme weather, incidents (e.g. road and lane closure), roadworks, social events, malicious attacks and signal failures that affect traffic in road networks. The authors of [5] argue that the term 'disaster' is used to describe an event in which a hazard, such as natural climatic/geological events (e.g. earthquake, hurricanes or floods) has caused extensive physical damage. According to the those authors, other hazards are operational or technological failures and intentional or malicious acts such as terrorist attacks. In [20], natural disasters are clustered within the term 'extreme weather phenomena' such as hurricanes, tornados or sandstorms. The use of different terms to refer to 'natural disasters' is essentially due to their different scale sizes, and hence due to the impacts those natural disasters can cause. This author explains that it is not easy to categorize between large or small-scale disasters. However, he argues that the scale of a disaster depends on the number of people affected and/or the extent of the geographic area involved, distinguishing between small, medium, large, enormous and gargantuan disasters.

This connects to [19], who argues that the impacts of flooding events strongly depends on both the characteristics of the flood itself and the area affected, which in turns have an influence on the lives of the inhabitants, resulting in different scale size inundations. It is worth noting that floods not necessarily lead to an evacuation of a region, which according to [23] 'evacuation is a risk management strategy that involves the movement of people to a safer location'. In fact, The Australian Bureau of Meteorology defines in [24] three flood classification levels, namely minor moderate and major, which describe in general terms the degree and nature of the flood impact. The main distinction between those levels is that moderate and major floods may require the evacuation of the affected area. Therefore, defining and classifying flooding events is

not straightforward either, due to the complex interrelated process that can cause and influence them [10]. That is the reason why several definitions and potential causes of flooding events have been adopted in literature by different authors. The Victoria State Emergency Response Plan gives a general definition of flooding 'as an overflowing or influx of water from its normal confines onto land not usually submerged' [25]. The authors suggest four potential mechanism that might cause flooding, namely heavy rainfalls, riverine flooding, storm surges, tsunamis and dam failure. In [19] six types of floods are distinguished, namely coastal floods or storm surges, flash floods, river floods, drainage problems, tsunamis and tidal wave. However, since the author focuses exclusively on natural disasters, dam breaks were excluded from the list. It is worth noting the inclusion of drainage problems as a flood type, which is caused by intense precipitation that are unable to be handle by regular drainage systems. According to the author, the difference with other flood types that can also be caused by heavy rainfalls such as flash floods or riverine flooding lies on the scale size of the inundation and the level of threat to lives of the inhabitants. Drainage problems usually pose a limited threat to life and mainly cause economic damage.

This thesis mainly focuses on urban flooding as a result of intense precipitation that overwhelm drainage capacity so that water accumulates on the roads. This phenomenon is particularly acute on the road network in urban areas due to the high proportion of impermeable surfaces that prevent the infiltration of water into the soil causing widespread damage and disruption to the road network [2, 9, 26].

2.2 Types of Flood Impacts

The authors of [7] provide in their research a state-of-the-art review on urban flood impact assessment, based on the classification given in [27] of various types of flood damages, which are classified according to two different criteria: tangible or intangible impacts and direct or indirect impacts. With regard to the first criterion, the authors define tangible impacts as those that can be measured in monetary terms (e.g. damage to properties or loss of profits if a business is disrupted). In contrast, intangible impacts are those that are hardly possible or impossible to be quantified in monetary terms (e.g. loss of life or impact on the mental well-being of those affected). With respect to the second criterion, the authors define direct impacts as 'any loss that is caused by the immediate physical contact of floodwaters with humans, property and the environment'. On the other hand, they define indirect impacts as those 'caused by the direct impacts and may occur - in space or time – beyond the immediate limits of the flood event'.

Other authors have taken this classification to define the impacts of adverse weather and flooding conditions in the context of road transport. For instance, [15] argues that indirect flood impacts in road transport are traffic disruptions, which are frequently intangible (e.g. loss of time, traveller's frustration or environmental degradation among others). On the other hand, [2] explain that flooding events influence the performance of transport systems through both direct (e.g. damage to transport infrastructures) and indirect impacts (e.g. traffic flow disruption). The authors of [8] also distinguish between direct and indirect effects of adverse weather events on the road network performance. They consider as direct impacts of weather events those which have an effect on both the capacity and demand of the road network, which in turns determine the road network performance in terms of congestion level, propagation of congestion and travel time delays. With demand effects, the authors refer to traveller's adaptation behaviour such as trip cancellation, changes in departure time, route choice or mode shifting due to the adverse weather conditions.

This thesis follows the classification of flood damages given in [27] and use the impacts of adverse weather impacts on the road network performance provided in [8] to give a more detail definition

of direct and indirect impacts of flooding on the road network performance. However, those impacts will not be further classified into tangible and intangible impacts since it is not the aim of this study to analyse whether those effects can be quantified or not in monetary terms. Therefore, this thesis considers as direct impacts of flooding the effects caused by the extent, propagation and depth of floodwaters on the roads (i.e. physical contact of floodwaters with the road infrastructure). The presence of floodwaters on the road not only damages the road infrastructure and roadside systems, yet it potentially reduces its capacity due to lane or road closure. Besides, vehicles can be washed away by the water flows putting road users at a high risk. Moreover, floodwaters also influence the traffic flow operations on the affected roads since drivers probably reduce their speed and increase time headways [2,16], which is also considered a direct impact. Furthermore, traffic disruptions over the road network such as road blockage due to spill back effects or traffic incidents may appear at different locations (beyond the limits of the flood) and caused by the direct impacts on the inundated roads. This thesis agrees with [8] that there will be also an effect on travel demand, which at the same time depends on the information provided by the different agencies to road users about the extent, propagation and depth of floodwaters over the network. Travellers may response to flooding conditions by cancelling their trips, changing their departure time, changing their routes or shifting mode. According to the latter authors, the effects on capacity and travel demand will determine the performance of the road network in terms of congestion level and total travel time.

2.3 Road Network Performance

Disturbances such as natural disasters (e.g. earthquakes, floods or hurricanes), extreme weather events (e.g. heavy rain, snow of fog), traffic incidents (e.g. lane or road closure), road works, social events, malicious attacks or signal failures [22] inevitably occur in urban cities causing staggering impact on safety as well as significant disruptions to the transportation systems. As it is explained in 2.2, these disturbances affect the supply side of the system, but also have an effect on the demand side, reducing therefore the level of the network performance. That is precisely the reason why a wide variety of performance concepts/metrics for analysing and evaluating the impacts of disturbances on transportation systems have been defined in literature by different authors. According to [28], when considering the performance of traffic flow on the road network, four main performance concepts are considered, namely vulnerability, reliability, robustness and resilience. As it is explained by the latter authors, those concepts are connected to each other, so that there is a certain amount of overlap between them. This section focuses on the concept of resilience in the context of urban flooding to illustrate the importance of predicting the impacts of floodwaters on road traffic.

In the context of road network, resilience is considered by different authors as one of the elements that makes the road network more robust [22, 29]. The first authors define resilience as 'the ability of a system to cope with disturbances and recover its original function after a loss of function'. On the other hand, they define robustness 'as the extent to which, under pre-specified circumstances, a network is able to maintain the function for which it was originally designed'. The reader may see that the word 'recover' actually makes the difference between these two performance concepts. The authors of [30] argue that the ability of a network to recover from disturbances not only depends on the network structure, but on activities that aim at preserving and restoring the level of service in the network. This connects with [5], who define resilience measures against hazards (e.g. hurricanes, earthquakes, floods or major traffic accidents) as interventions that aim at returning the transport system performance to nearly pre-disaster levels. According to the latter authors, the life cycle of a disaster is often described as having four phases, namely mitigation, preparedness, response and recovery. The first two phases involve pre-disaster actions and strategies aimed mainly at reducing the level of consequences of

a disaster, while the latter two contains post-disaster measures which objective is to restore the transport system performance. Figure 2.2 outlines the information provided in [5] with respect to the different phases in the life cycle of a disaster.

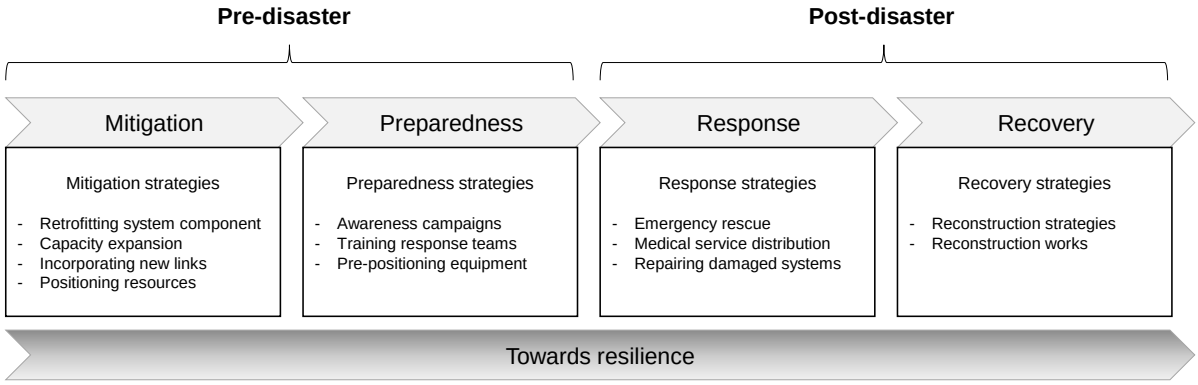

Figure 2.2: Resilience measures during the life cycle of a disaster event.

From the above figure the reader may realize that both pre-incident and post-incident activities play a key role in the resilience of road networks. According to [31], activities taken during the mitigation and preparedness phases of a disaster management cycle together with those adaptive actions during the response and recovery phases affect the resilience of a road network. In addition, these authors explain that one important aspect in adaptive actions that affect resilience is managing traffic flow in the aftermath of a disruptive event. As it is explained in Section 2.2, flooding events not only cause traffic disruptions at the vicinity of the flooding location, yet also beyond its limits since disruptions propagate over the road network. Therefore, it is essential to effectively plan weather-responsive traffic advisory and management strategies (e.g. route guidance, roadside variable message signs, variable speed limits or lane and road closure) to keep the performance of the road network at a high level during adverse conditions [32]. These authors already proposed a methodology for modelling the impacts of adverse weather conditions on traffic system performance and incorporating them in a simulation-based dynamic traffic assignment system with the aim of supporting the analysis and design of traffic management strategies during such conditions.

That is precisely the reason why different authors have proposed integrated simulation model techniques for modelling the impacts of adverse weather and flooding conditions on the road network. In the context of flooding events, the majority of those simulation techniques combine an hydraulic-hydrologic model to simulate urban flooding and a traffic simulation model to analyse flood impacts on the road network. These simulation modelling techniques contribute to better understand flood impacts on road traffic, providing in such a way valuable information to transport planners, operators and policy makers for developing and implementing traffic management strategies before and during the aftermath of the flooding event. Nevertheless, the traffic simulation requires the analysis of driving behaviour under such adverse conditions, which is a challenging matter due to the complexity of human behaviour and because microscopic data collection is expensive [33]. In Section 2.4, a thorough review on those integrated simulation techniques is carried out in the context of flooding, highlighting their weaknesses when it comes to the study of driving adaptation effects under such adverse conditions. Hence, in Section 2.5 the reader may find a detailed review on driving adaptation effects in adverse weather and flooding conditions.

2.4 Integrated Simulation Model Techniques

The authors of [8] proposed a methodology for modelling the effects of adverse weather conditions and adaptation measures on the road network performance. The authors applied the methodology by means of a case study in the city of Rotterdam (The Netherlands), in which different scenarios are simulated and compared using the total extra travel time or network delay as an indicator of road network performance. First, a reference scenario without adverse weather condition is simulated by using a macroscopic dynamic traffic assignment model 'Indy'. Secondly, in order to simulate the effects of weather related disturbances, the model requires quantitative inputs on how adverse weather conditions directly and indirectly affect both the supply and demand side of the road network. To do so, the authors use different empirical studies from literature (some of them are provided in Section 2.5 to incorporate effects on the supply side such as local capacity reductions. These disruptions can be caused by heavy rainfalls or snowfalls that lead to the blockage of on and off-ramps due to spill back effects, closed bridges or lane and road closure due to waterlogged. Because of the high uncertainty of these kind of disturbances, the authors performed a sensitivity analysis-based approach using five types of disturbances, which differ from each other in the percentage of local capacity reduction and duration. In the conclusions of their article, the authors highlight some shortcomings to be taken into account for future research. They argue that more empirical studies need to be carried out in order to gain a better understanding of the impacts of adverse conditions on the road network performance. As it is shown in Section 2.5 the majority of these empirical studies focuses on the impacts of rain and snow, yet there is a limited number of studies that consider other adverse conditions. Moreover, the authors incorporate the impacts of adverse weather conditions using a systematic approach in which five types of disturbances are included in the model, varying the percentage of local capacity reduction and the duration of the disruption. Other authors such as [32, 34] already proposed a traffic estimation system and prediction system for weather responsive traffic management by using a mesoscopic dynamic traffic model.

In 2015, the first dynamic integrated simulation tool for modelling the impacts of flooding conditions on road traffic was proposed by [15]. This simulation tool integrates a flood model (MIKE FLOOD) and the microscopic traffic simulation model of urban mobility (SUMO). The flood model provides the extent, propagation and depth of floodwaters over a geographic location, so that time-varying flood maps with a return period of a rainfall event can be obtained. Subsequently, the flood map is overlaid with a road network map of the same location in a GIS environment, which allows the identification of the affected roads within the network. The authors consider first the impacts of heavy rain on vehicle's speed and capacity reduction provided in literature (some of this studies are presented in Section 2.5). The moment the flood starts evolving over the transport network, road closure is carried out at a certain flooding depth (i.e. 0.3 metres), which is based on guidelines related to car stability in flood water [35]. The reader may have already noticed an important shortcoming in this methodology; the authors only assume, for those roads that are not close to traffic, the impacts of heavy rain on road capacity and on vehicle's speed. Nevertheless, they overlooked the impacts of floodwaters on road traffic, i.e. when the road surface becomes waterlogged, but is still open to traffic.

A similar study was conducted by [16], who proposed an integrated simulation method that combines an urban storm water model and a microscopic traffic simulation model in order to study the impacts of rainstorms on road traffic. The first model, based on the Storm Water Management Model (SWMM) is used to simulate the spatio-temporal distribution of floodwaters, deriving in such a way the flood depth on each road within the network. This model uses weather data and geographic information system (GIS) data. Subsequently, the authors use the same microscopic traffic simulation software of urban mobility (SUMO) for simulating the traffic situation. The improvement made by these authors with respect to the previous ones lies in the

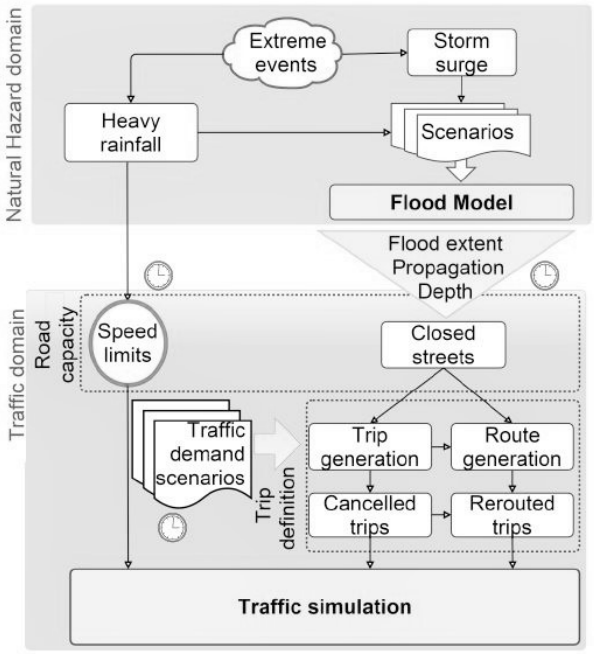

Figure 2.3: Structure of the Integrated Simulation Tool. [15].

study of driver's behaviour on waterlogged roads. In this article, a psychological questionnaire is carried out with the aim of studying drivers speed adaptation at different water depths and rainfall intensities. Respondents were asked to choose the speed at which they would travel in different rainfall and flooding scenarios, which were illustrated by using photographs. Figure 2.4 shows the structure of the integrated simulation tool proposed by the authors.

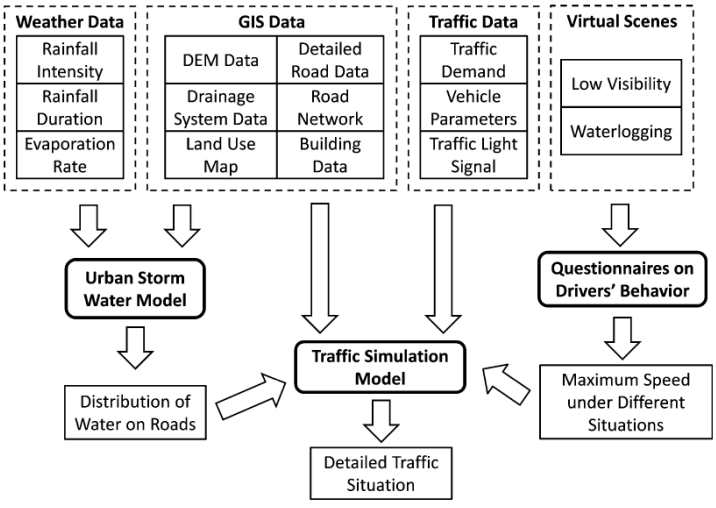

Figure 2.4: Structure of the Integrated Simulation Tool. [16].

The research of [9] also proposes a similar methodology as the previous one in order to assess the impacts and risk of pluvial flash flooding on intra-urban road networks. This integrated methodology consists of an inundation model (FloodMap) and a GIS-based road failure analysis and risk assessment model. The FloodMap simulates the extent and depth of floodwater over the study area, providing maximum inundation maps for different flood return periods. Sub-

sequently, the transportation impact assessment is carried out in each link within the network defining a critical threshold value of 0.3 metres for road closure. The authors assume a road is fully operational as long as the flood depth remains below 0.3 metres, and closed to traffic if the flood depth reaches this critical value. The reader may notice that the authors overlook the impacts of waterlogged roads (with a water depth below 0.3 metres) on road traffic, which is exactly the same assumption as in [15].

If one looks at more recent studies will realize there has not been improvement with regard to the study of driving adaptation effects under flooding conditions besides the one made in [16]. This can be seen from the research of [17] who propose another comprehensive method for studying the impacts of urban flooding on traffic congestion. This method combines again a flood simulation tool for predicting the spatio-temporal distribution of flooding, based on Storm Water Management Model (SWMM) and TELEMAC-2D, and an agent-based traffic simulation model (NetLogo) that generates the corresponding responses for the traffic in the road network. However, the authors study driver's behaviour under flooding conditions by using questionnaires, arguing measuring driver's behaviour through strictly physical ways is challenging, and that an accurate way to do it is by carrying out questionnaires as the one performed by [16].

2.5 Impacts of Weather Conditions on Traffic Operations

According to [28], a large number of weather-related effects have been proved to influence driving behaviour, and therefore traffic flow operations [36]. In the past, many authors have studied the impacts of adverse weather conditions such as rain, snow, fog or cold and high temperatures on traffic flow operations. Yet, the majority of the literature focuses on the impacts of day-to-day weather events such as light or heavy rain and snow on macroscopic traffic flow parameters (e.g. free-flow speed, capacity, speed at capacity or traffic demand). Nevertheless, there is a limited number of research on the impacts of those weather conditions on microscopic driving behaviour. Even less studies have been carried out on the impacts of flooding events on microscopic driving behaviour, first due to the complexity of human behaviour and second because microscopic data collection is expensive [33].

Therefore, this section aims at summarising the main findings on the impacts of adverse weather conditions on both macroscopic and microscopic traffic flow variables by reviewing previous research. Furthermore, it reviews the scarce research on the impacts of flooding events on road traffic. Nonetheless, it is not the aim of this section to provide an extensive review on the impacts of weather events on traffic flow operations, since this has been already carried out by different authors such as [2, 8, 33]. Hence, a short summary that highlights main findings on the impacts of weather conditions on macro and microscopic driving behaviour is provided first, and subsequently a detail review on previous research on the impacts of floodwaters on microscopic driving behaviour is conducted.

2.5.1 Macroscopic Traffic Analysis

As it is explained in the introduction of this section, the majority of the studies focuses on the impacts of day-to-day weather conditions, and more specifically on the impacts of precipitation on roadway capacity, free-flow speed, speed at capacity and traffic demand. An extensive qualitative and quantitative literature review on this subject can be found in [2, 8, 33] among others. The majority of this research consists on empirical studies that combine macroscopic traffic data, obtained normally by using loop detectors, and weather data gathered from stations located close to the study area.

According to [37], when it comes to the study of the impact of precipitation on traffic flow operations, probably rain and snow are the most researched weather conditions. Specially, articles

have focused on investigating capacity and free speed reduction in motorways/freeways across different countries due to heavy/light rain and snow compared to dry weather conditions. Altogether, these studies have found a greater impact of heavy rain than light rain on macroscopic traffic flow parameters [33,37–40]. Nevertheless, scare research can be found on the impacts of weather conditions on urban roads. The authors of [41] estimated changes in free-flow speed and capacity by using data collected in Austrian urban roads with speed limit of 50 km/h. The majority of these macroscopic studies collected traffic data by implementing loop detectors on the road. An overview of the results found by some authors that have studied the impacts of weather conditions in traffic flow operations is provided in Table 2.1. For a more extended review, the reader may read [2,8,33].

Weather condition	Article	Country	Road type	Capacity reduction	Free-flow speed reduction
Rain	Maze et al. (2006)	USA	Freeway	Heavy rain: 14%	Light rain: - 2km/h Heavy rain: - 4.2 to – 6.4 km/h
	Hranac et al. (2006)	USA	Freeway	Light rain: 10% to 11%	Light rain: 2% to 3.6% Rain: 6% to 9%
	Smith et al. (2004)	USA	Freeway	Light rain: 4% to 10% Heavy rain: 25% to 30%	5% to 6.5%
	Billot et al. (2009)	France	Motorway	Light rain: ~18.5% Medium rain: ~21%	Light rain: ~8% Medium rain: ~12.6%
	Asamer and Reinthaler (2010)	Austria	Urban road		Light rain: - 4.2km/h Heavy rain: until 12.6km/h
	van Stralen et al. (2014)	Netherlands	Motorway	Light rain: 4% to 9% Heavy rain: 4% to 11%	Heavy rain: 7.7%
Snow	Maze et al. (2006)	USA	Freeway	Heavy snow: 22%	Light snow: - 4.5 to – 9 km/h Heavy snow: - 10 to – 14.5 km/h
	Hranac et al. (2006)	USA	Freeway	Light snow: 12% to 20%	Light snow: 5% to 16% Snow: 5% to 19%
	Asamer and Reinthaler (2010)	Austria	Urban road		Light snow: - 8.4km/h Heavy snow: until 16.8km/h

Table 2.1: Some studies on the impact of rain and snow in Free-flow speed and capacity.

The reader may realize that the impacts of day-to-day weather events on macroscopic traffic flow variables have been widely studied in the past. However, to the best knowledge of the author of this thesis, there is very scarce research on the impacts of floodwaters on either macroscopic or microscopic traffic flow parameters. As it is explained in Section 2.2, the presence of water on road surface influence traffic flow operations since drivers probably adapt their speed and headways. Indeed, this is line with [33] who state that macroscopic impacts on traffic flow resulting from adverse weather conditions are the aggregate results of microscopic behaviour. Therefore, the following subsection provides a review on the impacts of weather events on microscopic driving behaviour, and it explains in detail the results of previous studies on the impacts of floodwaters on driving behaviour.

2.5.2 Microscopic Behaviour Analysis

According to [33], although microscopic driving behaviour models (e.g. car-following models) have been used for decades, knowledge of microscopic driving behaviour under adverse weather conditions remains limited, first due to the complexity of driver responses to those conditions and because microscopic data collection is expensive. The authors explain that adverse weather conditions modify the driving environment, which in turn change driver's behaviour such as individual speeds, vehicle headways or travel decisions that directly affect overall system performance. To date, scarce research has been conducted on the impacts of adverse weather

conditions on microscopic driving behaviour and even less research has studied the impacts of floodwaters on driving behaviour. An extensive literature review on this matter can be found in [33, 36].

In [42], an observational study is carried out in the A13 motorway in The Netherlands with the aim of quantitatively measure the effects of rain on driving behaviour, specifically on free-driving speed and vehicle headways. Data collected was conducted by means of inductive loop detectors, measuring for each lane mean speed and the percentage of vehicles with a time headway >1 s, >3 s and >5 s. ANOVAs test was carried out using weather, lane, volume category and carriageway factors and a main effect of weather on mean speed and vehicle headways was found. The results show that the mean speed in rain was 11 km/h lower than in dry conditions. In addition, the percentage of vehicles with headways >1s was smaller in rain conditions than in dry conditions, which also applied for headways >3s although the effect was smaller. Finally, for the >5s analysis, there was no main effect of weather.

The authors of [18] already proposed a multilevel approach for assessing the effects of rain on traffic; individual traffic data collected by double loop sensors in rainy conditions allowed the authors to assess the impact of rain at a microscopic level. Subsequently, the authors used the same data to extend the study to a mesoscopic and a macroscopic level. Three classes of rain were used, namely 'no rain' (0 mm/h), 'light rain' (2 mm/h) and 'medium rain' (from 2 mm/h to 3 mm/h). Results show a decrease of the frequencies of speeds higher than 90 km/h in the slow lane for light and heavy rain in comparison to dry conditions. In contrast, the results interestingly show an increase of the frequencies of speeds lower than 90 km/h in the slow lane for light and medium rain in comparison to dry conditions. With respect to vehicle headways, the results reveal a drop of 12.1% in the frequency of vehicles with a time headways lower than 2 s under light rain. However, the frequency of vehicles with time headways higher than 6, 8 and 10 s increases with the intensity of the rain.

Other studies have focused on the impact of reduce visibility due to fog conditions on microscopic driving behaviour [36, 43, 44]. In these three studies, however a driving simulator experiment was carried out to investigate the influence of fog on adaptation effects in longitudinal driving behaviour. For instance, [36] conclude from the results of the experiment that fog leads to significant adaptation effects in driving behaviour; a significant decrease in both speed and acceleration and a substantial increase in distance with the lead vehicle was found in the experimental conditions (i.e. foggy conditions).

The reader may realize again that the majority of the studies focuses on the impacts of day-to-day weather events on microscopic driving behaviour. Nonetheless, adverse weather events such as intense precipitation may lead to the inundation of roadways when the drainage system is unable to cope. As it is explained in Section 2.1, the presence of floodwaters on the road also influence traffic flow operations due to changes in driving behaviour such as speed or vehicles headways adaptation. However, to the best knowledge of the author of this thesis, there is very scarce research on the impacts of floodwaters on microscopic driving behaviour. Only a couple of authors have investigated driving adaptation effects under flooding conditions, and the majority of them as parallel study to the integrated simulation tool for assessing the impacts of flooding on road traffic. The reader may recall Section 2.4 in which those integrated tools are explained in detail.

In that section, the psychological questionnaire of [16] for deriving how drivers adjust their speeds at different water depths and rainfall intensities is introduced. Respondents were asked to choose at which speed they would travel at in the given rain and water depth scenario. The authors provided to the respondents some photographs taken from the driver position in common urban roads with speed limits of 60 km/h, in order to represent flooding scenarios more intuitively. Table 2.2 displays the average vehicle speed in km/h under 12 scenarios that

combine different conditions of water depth and rainfall intensities. In addition, the authors include a table that shows some relationships between driving speed and demographic variables under four different scenarios that combine different levels of flood depth and rainfall intensities. One of the conclusions taken from this study is that under normal conditions (i.e. no rain and no water on the road), there is practically no difference between male and female driving speed, yet female drivers reduce their speed more than male drivers when waterlogged occur. Subsequently, the authors performed bilinear interpolation to obtain a graph that displays the functional relationship between water depth, rainfall intensity and vehicle speed, which is depicted in Figure 2.5.

Rainfall intensity	Water depth (cm)			
	0	10	20	30
0 mm/h (no rain)	50.3	37.5	26.2	15.3
2.5 mm/h (light rain)	42.4	35.0	24.3	12.4
12.5 mm/h (heavy rain)	26.9	22.0	15.0	7.9

Table 2.2: Average vehicle speed (km/h) under different flood depths (cm). [16].

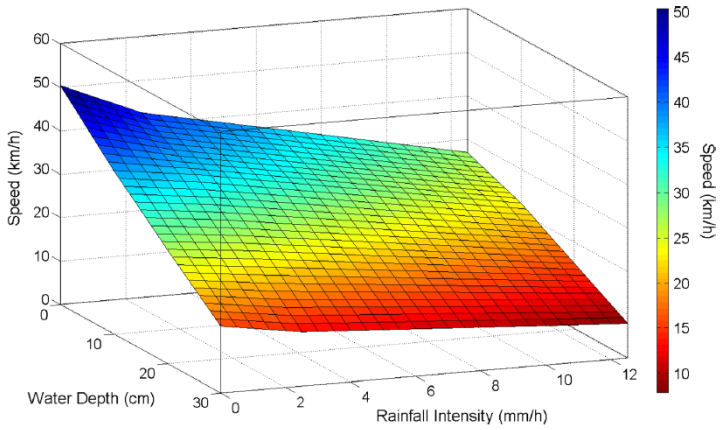

Figure 2.5: Functional relationship between water depth, rain intensity and vehicle speed. [16].

The authors of [17] explain that the results of the questionnaire obtained in [16] are quite accurate, so that they also combine socio-economic data with questionnaires in order to study driving behaviour under flooding conditions. They provide a table that shows average speed at different water depths based on several attributes.

Attribute	Water Depth (cm)			
	0	10	20	30
Male, Age < 35	50.9	38.4	27.6	16.9
Male, Age ≥ 35	49.8	37.1	26.0	14.9
Female, Age < 35	50.8	37.5	26.0	14.4
Female, Age ≥ 35	49.8	36.1	24.3	12.5

Table 2.3: Average vehicle speed (km/h) under different flooding conditions. [17].

In [2] vehicle's speed adaptation in flooding condition is also studied. The authors derived a depth-disruption function that relates flood depth to traffic speed (see Figure 2.6). This function was constructed by combining data from experimental studies, safety literature, expert's opinion and data collected from videos. Specifically, points number 3 and 5 were collected by observing two videos of vehicles driving through flooded roads in Perth and Bromsgrove (UK).

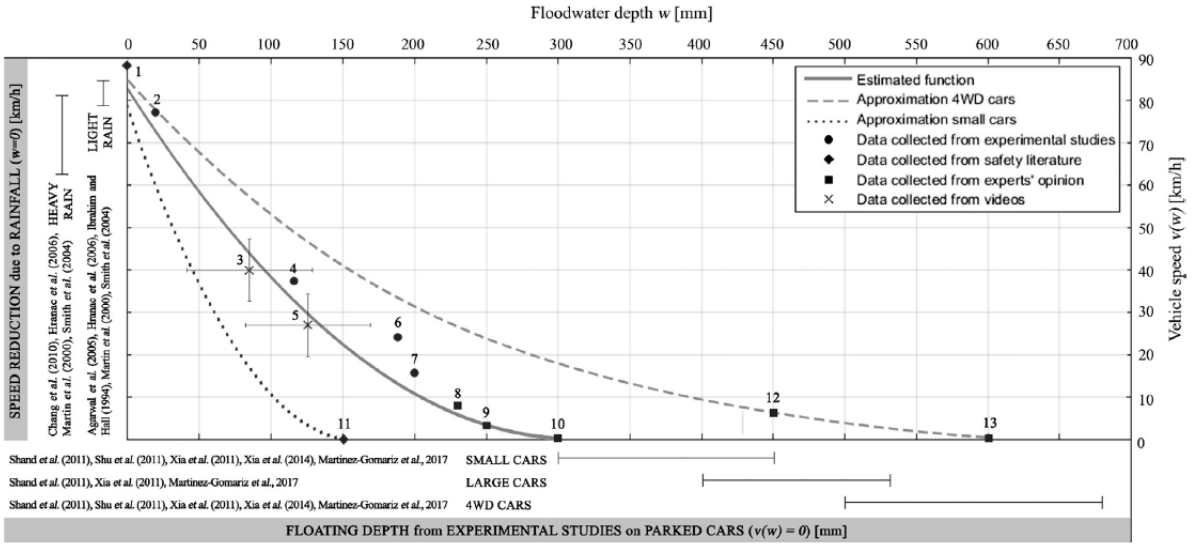

Figure 2.6: Correlation between flood depth and vehicle speed on a road. [2].

The reader may notice the difference in vehicle's speed at 0.3 m of water depth. While the results in the first two studies give a certain speed at a water depth of 0.3 m, [2] refer to different experimental and theoretical studies on car stability in floodwaters [35, 45, 46] to set the speed of vehicles driving at that flood depth equal to 0 km/h. According to those references, 0.3 m is the average flood depth at which passenger vehicles start floating. Furthermore, the guide of road design from [47] provides a road closure indicator based on trafficability of vehicles in floodwaters. These experts argue that in some cases, it is desirable to allow traffic on waterlogged roads, yet it is necessary to specify a certain limit at which the road should be closed. This limit is based on a combination of depth and velocity of flow over the road and is defined when the total head (depth and velocity of flow) at any point across the carriageway is equal to 0.3 m. This also connects with the guideline of [35], which provides a literature review on experimental and analytical studies of safety criteria for people and vehicles in flood in order to develop a draft, interim criteria for stationary vehicle stability considering three vehicle classes, namely small passenger cars, large passenger cars and 4WD vehicles.

2.5.3 Driving Adaptation Effects in Microscopic Traffic Models

The goal of this section is to provide the reader with some examples of previous studies that include driving adaptation effects under adverse weather and flooding conditions within microscopic traffic simulation models. Microscopic traffic models studied traffic phenomena by taking each individual vehicle as a starting point and analysing its interactions with other vehicles. The most popular microscopic model is the car-following model [17]. Car-following models generally relate acceleration of a driver-vehicle combination (a_i) at a certain time as a function of speed of the vehicle (v_i), speed of lead vehicle (v_{i-1}), net distance to the lead vehicle (s_i) and acceleration of the lead vehicle (a_{i-1}) [36]:

$$a_i(t) = f_{cf}(v_i, v_{i-1}, s_i, a_{i-1}) \tag{2.1}$$

According to the latter authors, each mathematical model of car-following behaviour has its own distinctive control objective. It is worth noting the aim of this section is not to provide a literature review on car-following models, since this has been carried out in [48]. Also, [49] provides a discussion on whether current of driving behaviour are adequate in incorporating this behaviour under adverse weather conditions. Different authors such as [16, 17, 36] have already noted the importance of studying driving adaptation effects under different weather and flooding conditions in order to adapt microscopic traffic models that will enable to simulate traffic microscopically.

The authors of [16] state that many traffic simulation models have been developed, but none of them takes rainfall and waterlogging into consideration. The authors of [16] improved the car-following model of the traffic simulation software of urban mobility (SUMO) in order to include the influence of rain and waterlogging on vehicle speeds. The default car-following model is based on the one established by Stefan Krauss [50, 51] cited in [16]:

$$v_{safe}(t) = v_1(t) + (g(t) - g_{des}(t))/(\tau_b + \tau) \tag{2.2}$$

$$v_{des}(t) = min[v_{max}, v(t) + a(v)\Delta t, v_{safe}(t)] \tag{2.3}$$

$$v(t + \Delta t) = max[0, v_{des}(t) - \eta] \tag{2.4}$$

$$x(t + \Delta t) = x(t) + v(t + \Delta t)\Delta t \tag{2.5}$$

Where t is time (s), v_{safe} is the maximum safe velocity (m/s), v_1 is the velocity of the leader car (m/s), g is the gap between the leader and the follower (m), g_{des} is the desired gap (m), τ is the reaction time (s), τ_b is the braking time (s), v_{des} is the desired velocity (m/s), v_{max} is the speed limit (m/s), v is the velocity of the follower (m/s), a is the maximum acceleration of the car (m/s^2), Δt is the time step (s), and x is the position of the follower (m). Random perturbation η is introduced to allow for deviations from optimal driving conditions. The authors adapt this model to include the effects of rain and waterlogging on traffic by introducing the function of rainfall intensity shown in Figure 2.5 within the v_{max} variable. Other authors such as [17], also attempt to incorporate in a very similar way driving adaptation effects under flooding conditions within traffic models.

In Section 2.4, the structure of the integrated simulation tool proposed by [15] was depicted in Figure 2.3. This tool integrates a flood model (MIKE FLOOD) and a microscopic traffic simulation model of urban mobility (SUMO) for modelling the impacts of flooding on road traffic. The reader may remember that one of the main drawbacks of this methodology is the fact that it considers the road either closed to traffic (when flood depth is equal or higher than 0.3 m) or fully operational at the speed limit of the road (when flood depth is lower than 0.3 m). In [52], the authors were motivated by [2] to improve their methodology by considering a speed reduction in those streets with shallow flood depth (i.e. less than 0.3 m).

2.6 Conclusions

In this chapter, an extensive literature review on the most relevant topics related with this research was conducted. Section 2.1 started giving a definition of flooding event, the types of flooding events and the terminology used in literature by different practitioners. It concluded explaining that this research mainly focuses on urban flooding as a result of intense precipitation that overwhelm drainage capacity in such a way that floodwaters accumulate on the road. Subsequently, Section 2.2 distinguished between direct and indirect impacts of flooding on the road network based on previous experts classification. It was concluded that the presence of floodwaters on the road not only damages the road infrastructure and roadside systems, yet it potentially reduces its capacity due to lane or road closure (direct impact). Additionally, floodwaters also influence traffic flow operations as drivers may adapt their speeds and headways (direct impact) when driving through flooding. Besides, traffic disruptions will also occur across the road network, that is beyond the limits of the inundated roads (indirect impact), which are essentially caused by direct impacts. Section 2.3 highlighted that predicting the performance of the road network under flooding conditions essential to build transport system resilience, and that is why different authors have proposed modelling techniques to predict the geographic location, severity and other impacts of flooding events on the road network.

Those are integrated simulation model techniques that combine a flood model and a microscopic traffic simulation model allowing to predict and analyse flood impacts on the road network. These modelling techniques contribute to better understand flood impacts on road traffic, providing valuable information to transport planners, operators and policy makers for developing and implementing traffic management strategies before and during the aftermath of flooding events. Nevertheless, traffic simulation requires the analysis of driving adaptation effects under such conditions, a research field that has been scarcely investigated so far. Only few authors have attempted to study the effects of floodwaters on individual vehicle's speed using data collection techniques highly questionable in terms of suitability for the type of data to be acquired. Therefore, if driving adaptation effects are not properly investigated and included within microscopic traffic models, will not be possible to conduct consistent microscopic traffic simulation studies on the road network under such conditions. This is why thesis proposes a systematic methodology to study driving adaptation effects under flooding conditions; first a data collection technique consisting on video analysis through the so-called *3-Step Video Analysis Approach* (3SVAA) is developed by the author of this thesis which allows to extract microscopic traffic data of individual vehicles travelling under different flood depths. Secondly, a multilevel analysis approach is conducted to study flood impacts at two complementary levels, namely microscopic and macroscopic level.

Regarding macroscopic analysis, Section 2.5 highlighted that although there is extensive research on the impacts of day day-to-day weather conditions on macroscopic traffic variables (i.e. free-flow speed and capacity), there is not any research available on the impacts of flooding conditions on those traffic parameters. The traffic fundamental diagram that relates the three macroscopic variables, namely average speed, flow and density are the basis of macroscopic traffic simulation, and therefore it is a valuable tool for traffic management [18]. Since there is not any study on the impacts of floodwaters on macroscopic traffic parameters, the estimation of the fundamental diagram of vehicles travelling through flooding has not been accomplished yet. The core of the methodology proposed in this thesis consists on a multilevel analysis approach that enables to extend the microscopic analysis to a macroscopic level, being possible to assess the impacts of flooding depth on traffic flow operations.

The reader may see now the need of conducting more empirical studies that collect and analyse micro and macroscopic traffic data in flooding conditions. This will enable to further study driving behaviour under such conditions and to assess the impacts on traffic flow operations. This will enable to estimate the complete fundamental diagrams of vehicles travelling under flooding conditions, which will be needed for macroscopic traffic simulation. These studies will also be used to validate future studies.

Chapter 3

Research Methodology

Chapter 2 concludes highlighting the importance of understanding and predicting the impacts of flooding events on road traffic in order to build resilient transport systems. That is precisely the reason why different authors have proposed integrated simulation model techniques for modelling the impacts of flooding events on the road network of urban cities. These simulation models contribute to better understand flood impacts on road traffic, providing valuable information to transport planners, operators and policy makers for developing and implementing traffic management strategies before and during the aftermath of the flooding event. Figure 3.1 outlines the steps towards the development of microscopic traffic simulation models. The methodology proposed in this thesis encompasses the first five boxes.

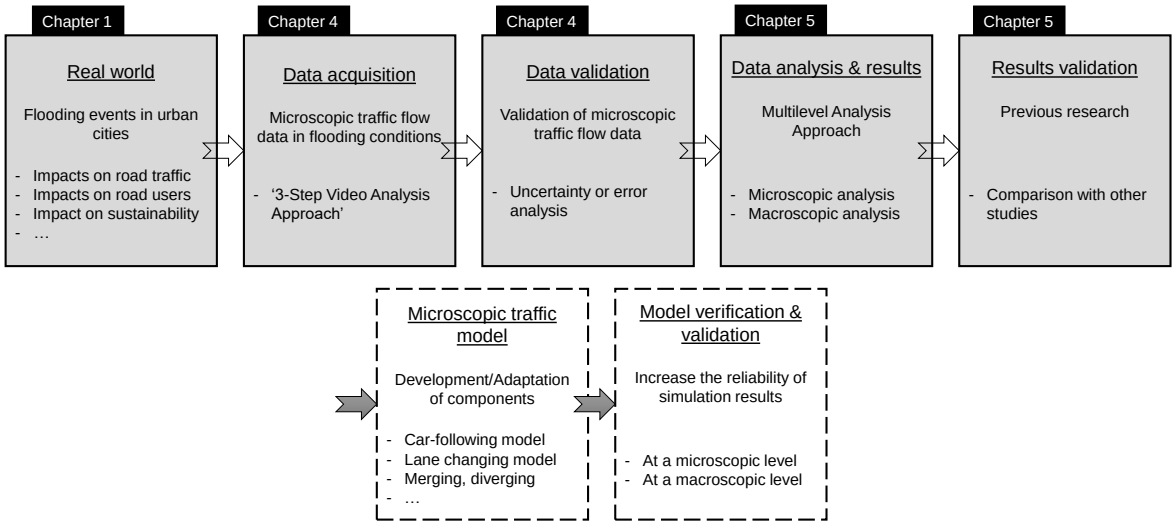

Figure 3.1: Towards microscopic traffic models in flooding conditions.

This thesis proposes a systematic methodology to study driving adaptation effects under flooding conditions. First, microscopic traffic data (i.e. vehicle speed, time headways and spacing) of individual vehicles driving through flooding conditions need to be collected. It is important to bear in mind that much effort has to go to the collection of accurate data, otherwise the results obtained from the model will be inaccurate [53]. Therefore, a discussion on the pros and cons of different data collection techniques for measuring microscopic traffic parameters in adverse and flooding conditions is provided in Section 3.1, which will enable to answer the first research

question of this thesis: *How can microscopic traffic data (i.e. vehicle speed, time headways and spacing) of individual vehicles travelling through flooding be obtained?*. The answer of this question drove the author to develop the so-called *'3-Step Video Analysis Approach'* (3SVAA) to extract microscopic parameters from video recordings of vehicles driving through flooding. This video analysis approach essentially is a measuring tool that is subjected to errors or uncertainties that need to be evaluated in order to estimate the level of confidence associated to the measures. Therefore, an uncertainty or error analysis is accomplished to validate microscopic traffic measurements obtained by means of the 3SVAA, which is explained in Section 3.2.

The core of the proposed methodology is explained in Section 3.3. By a multilevel analysis approach, the study can be extended to the macroscopic level by correlating macroscopic variables (i.e. average speed, flow and density) with their microscopic counterparts using the fundamental relationship of traffic flow. This will enable to study the impacts of flooding conditions on free-flow speed and capacity, and therefore to estimate part of the fundamental diagrams of vehicles travelling under such conditions. Finally, a result validation is conducted by comparing the outcomes of the macroscopic analysis to those found in previous research on both adverse and flooding conditions. The methodology proposed is implemented through an empirical study that analyses video recording of vehicles crossing two waterlogged stretches part of the A94 and A93 major roads in Perth (Scotland).

3.1 Data Acquisition

This section provides a discussion on the pros and cons of different techniques used to collect microscopic traffic data in adverse conditions. The assessment will enable to answer the first research question proposed in this thesis. Some examples of previous studies that collected microscopic data to study driving adaptation effects in adverse conditions are included in the discussion.

3.1.1 Type of Data

The analysis of driving behaviour such as car-following and lane changing requires highly dedicated data to generate adequate insight into the traffic features to be modelled [54]. According to these authors, trajectory data are typically used by researchers to investigate driving behaviour in general. In Table 3.1, the authors of [55] provide a traffic data categorization based on measurement perspective (i.e. microscopic and macroscopic) and measurement objective (i.e. local and global).

		Measurement objective	
		Local	Global
Measurement perspective	Microscopic	Trajectories	Routes Travel times
	Macroscopic	Counts Speed distribution Flow patterns over time	Densities over network OD matrix Travel times

Table 3.1: Traffic Data Categories. [55].

The authors explain that local measurements cover traffic dynamics at specific locations within the network such as junctions or road stretches, whilst global measurements refer to the traffic flow in the network. Besides, traffic measurements can be also classified into microscopic and macroscopic. The microscopic perspective deals with the movements of individual vehicles or

persons such as trajectories, whereas the macroscopic traffic perspective focuses on traffic flows, in which individual vehicles cannot be analysed independently.

As it is explained in Section 3.3, full information regarding microscopic parameters of individual vehicles can be extracted from vehicle's trajectories, which define the position of a vehicle over time. In order to study driving adaptation effects (i.e. changes in vehicle speed and headway), the trajectories of individual vehicles travelling under such conditions need to be collected and analysed. This type of data is classified within local microscopic traffic data, leading to the use of probe vehicles (i.e. vehicle-based trajectories) or external observations (i.e. non-vehicle-based), which mostly are video-based observations [54]. A discussion on the pros and cons of these techniques for studying changes in microscopic parameters of vehicles driving under flooding conditions is carried out in the following section.

3.1.2 Data Collection Techniques

The use of probe vehicles or floating cars, which are equipped with devices that store position, speed and travel times allows to measure microscopic traffic variables (i.e. vehicle speed, time headways and spacing) under adverse conditions. However, a plethora of uncertainties as a result of using this technique could potentially jeopardize the data collection activities. First, the probe vehicle will have to be submerged within the traffic in a flooding road, where any other vehicle around could hamper the data collection at any moment. This is an expensive technique that also requires the presence of a experienced driver and a person familiar with the equipment. Finally, it does not allow to classify data according to demographic variables such as gender or age, which could be useful for a studying diver's behaviour under such adverse conditions. Conversely, this technique allows to obtain data over longer road stretches compared to video-based trajectory technique.

Video recording can be also used to collect vehicle's trajectories along a selected road section. According to [54], the main advantages of this technique is that first allows to acquire data from large number of vehicles, and second the collected data can be considered unbiased since drivers are not influenced by the data collection method. The later authors explain the usability of cameras mounted on poles or on airborne vehicles such as helicopters, airplanes or drones. Mounting the cameras on road side poles or placing them within a protective case would give greater flexibility in terms of position, time and duration of the activities. Moreover, the cancellation of the activities due to any unforeseen reason will not be a big issue since the equipment can easily be uninstalled. This flexibility would enable to record videos across different countries in a much easier way, allowing the inclusion of regional differences in the driving behaviour analysis. However, this technique presents some drawbacks according to the latter authors. First, the range of vision captured by the camera is limited in space and time, so that the consistency of driver's following and lane changing behaviour cannot be evaluated. Second, the data post-processing will be difficult and time-consuming unless automated image processing method are used. A third drawback is the noise in the resulting trajectories due to potential errors in the frame-by-frame analysis that need to be conducted. Finally, this technique will probably not allow to classify data according to demographic variables since drivers are barely distinguished from the videos.

From the literature review conducted in this thesis, one can see there are barely studies that have collected neither microscopic nor macroscopic traffic data in flooding conditions. For instance, the authors of [16, 17] carried out a psychological questionnaires to study speed adaptation of individual drivers under flooding conditions. Essentially, respondents were asked at which speed they would drive under different scenarios of rainfall intensity and flood depth, by providing them with photographs that illustrated such scenarios. Although these pictures are useful to provide respondents with a clear view of the real scenario, one well-known drawback of Stated

Choice experiments is that the answers do not always match with what respondents actually do in reality, making the answers being hypothetical. It is important to know that respondents do not feel the actual consequences of being driving through flooding conditions when they are answering the questionnaire. In contrast, this technique allows to classify the answers based on demographic variables. Other authors such as [36] designed a driving simulator experiment to study driving adaptation effects under adverse conditions such as fog. Although driving simulators provide valuable information on driving behaviour, they have a clear drawback: the driving task in a simulator cannot be captured realistically [54]. Indeed, subjects are not driving on a real road, and therefore actions made during the experiment do not have any consequence in reality.

Other authors such as [18] have used local detector data to study changes in microscopic driving behaviour (i.e. changes in microscopic variables) under rain conditions by collecting individual traffic data. Local detector data provide traffic information collected at a single measurement point on a road using either inductive loop detectors or nonintrusive detectors (e.g. radar, ultrasonic or video cameras) [54]. An advantage of these techniques is that allow to obtain both disaggregate or single vehicle data and aggregate data over time intervals. The main difference between these two types of local detectors is that inductive loops are permanent detectors embedded in the pavement, whereas nonintrusive detectors are normally side-firing or mounted over the road. Although the latter ones are much easier to install and replace, the reader may see the lack of flexibility compared to the road-side video recording proposed by the author of this thesis. Furthermore, the use of local detector data does not allow to analyse unexpected actions that some drivers could undertake when adverse conditions become more severe, and which would provide useful information to study driver's behaviour under adverse conditions. Besides, detectors might fail to detect vehicles if flooding conditions become more severe, that is when flood depth increases.

The author of this thesis carried out a critical evaluation on the pros and cons of the different techniques that can be used to collect microscopic traffic data of vehicles driving through flooding, and agreed with [33] that videotaping drivers is a suitable technique to measure driving adaptation effects under adverse conditions. Therefore, the author of this thesis developed the 3SVAA to extract microscopic traffic parameters (i.e. vehicle speed, time headway and spacing) from video recording. Two clips that show vehicles driving under different flood depths through two waterlogged stretches part of the A94 and A93 major roads in Perth, Scotland (UK).

3.2 Data Validation

As it is explained in the introduction of this chapter, the 3SVAA developed by the author of this thesis is a measuring tool implemented in Matlab that extracts microscopic traffic parameters from individual vehicle's trajectories from video recording. As a measuring system, it is subjected to errors or uncertainties that need to be evaluated in order to estimate the level of confidence associated to the measures [56].

Key indicators of the quality of a measuring instrument are the reliability and validity of the measures [57]. The author of [58] explains that validity determines whether the means of measurement are accurate and whether they are actually measuring what they are intended to measure. They reader may see the term 'accuracy', which can be defined as 'the closeness agreement between measured value and a true or accepted value' [59, 60]. In other words, accuracy refers to the deviation of a measurement from its true or accepted value. Such deviation can have two components called systematic and random errors. According to [60], a systematic error is a 'reproducible inaccuracy introduced by faulty equipment, calibration, or technique'. These errors are difficult to detect and cannot be analysed statistically [56]. In case a systematic

error is identified, applying a correction factor to compensate it can reduce the bias. Random errors are however 'statistical fluctuations (in either direction) in the measured data due to the precision limitations of the measurement system'. In contrast, these errors can be evaluated through statistical analysis and can be reduced by averaging over a large number of observations.

A data collection plan was therefore designed and conducted by the author of this thesis with the aim of studying the uncertainty associated to the vehicle speed measurement given by 3SVAA. The data collection activities were carried out the 23rd of June (2019) in the province of Granada (Spain), the author's home town. The data collection plan, included in Appendix 6, consisted on video taping an experimental vehicle travelling at known speed through two dry road stretches very similar in layout to the A94 and A93 major road stretches in Perth (Scotland). Afterwards, the videos were analysed through the proposed video analysis procedure, so that the differences between the GPS speed and the speed reported by the 3SVAA are used to compute the speed measurement error. It is worth noting that, according to the *Regulation No 39 of the Economic Commission for Europe of the United Nations*[1], the speed displayed on the car's speedometer shall not be less than the true value of the vehicle speed. Although all measurements have sort of error associated with them, this thesis assumes that a GPS speedometer provides an accurate value of vehicle speed, since under normal conditions they compute errors down to about 0.1 and 0.2 m/s [61].

During the data collection activities was not possible to measure neither time headway nor spacing due to lack of equipment and devices, and hence a different technique consisting on frame-by-frame analysis was conducted to define the time headway error committed by the 3SVAA. A reference point is marked on the video image using a grid in order to measure the elapsed time between the front of the lead vehicle and the front of the following vehicle (i.e. time headway). These values are then compared to those obtained by applying the 3SVAA in order to define the time headway measurement error. Unfortunately, this technique is not precise when it comes to measure vehicle spacing, since the author does not dispose of the real size of elements displayed on the videos in order to build an scaled grid. Therefore, although this thesis does not define the spacing measurement error, it provides a feasible way to measure it in future studies.

In order to validate the measuring instrument, a theoretical validation is conducted as the three variables are related to each other through the fundamental relationship of traffic (see equation 3.1). A Pearson correlation can be computed between the spacing values obtained through the 3SVAA and those derived by applying the fundamental expression. In Section 3.2 on the following chapter, the results obtained from the data collection are first presented, and secondly the speed and headway measurement errors associated to the 3SVAA are estimated. Finally, the three microscopic variables, and therefore the 3SVAA are validated using the Pearson correlation coefficient.

3.3 Multilevel Analysis Approach

Figure 3.2 displays a flow chart of the multilevel analysis approach proposed by the author of this thesis to study driving adaptation effects under flooding conditions at two complementary levels, namely microscopic and macroscopic level. This is the core of the proposed methodology and the answer to the third research question: *How can macroscopic traffic variables (i.e. average speed, flow and density) of vehicles travelling through flooding be obtained from their microscopic counterparts?*. It is based on the conceptual methodology proposed in [18] and it is implemented in Chapter 5 using microscopic traffic data obtained in the 4 by applying the 3SVAA to the videos of Perth (Scotland).

[1] https://eur-lex.europa.eu/legal-content/EN/TXT/?uri=CELEX%3A42010X0513%2803%29

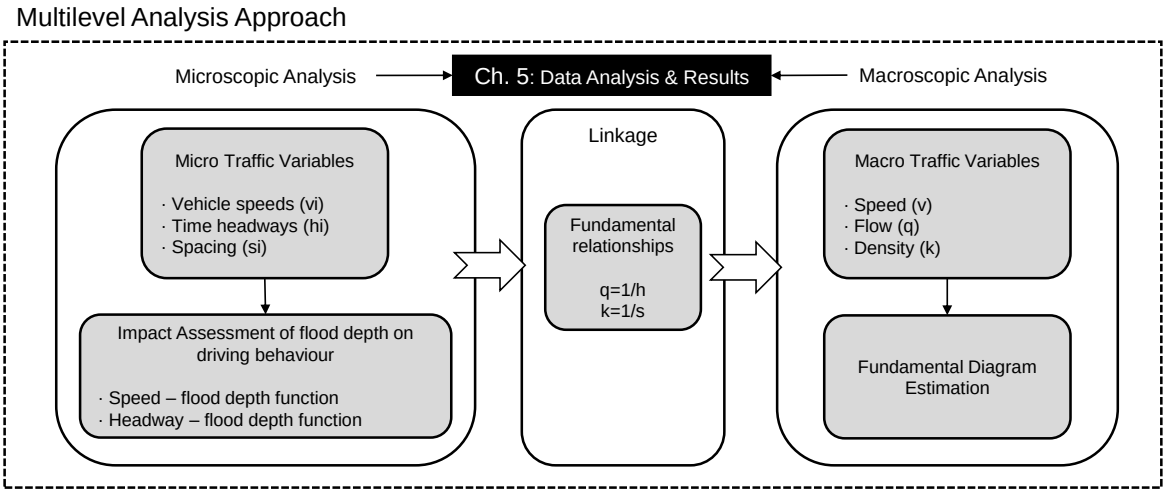

Figure 3.2: Multilevel Analysis Approach.

According to the figure, a microscopic analysis is first conducted to study changes in microscopic parameters when flooding conditions become more severe, that is when flood depth increases. To do so, a data collection technique consisting on video analysis through the 3SVAA is proposed with the aim of extracting microscopic traffic data (i.e. vehicle speed, time headways and spacing) from video recording of vehicles driving through flooding. This enables to answer the second research question: *What changes in microscopic variables (i.e. vehicle speed and time headways) occur when vehicles travel under different flood depths?*.

From microscopic traffic data, a macroscopic analysis can be accomplished by using the fundamental relationships of traffic flow, which correlate microscopic variables with their macroscopic counterparts. This enables to study the effects of flood depth on macroscopic variables (i.e. average speed, flow and density), which in turn allows to estimate part of the fundamental diagrams of vehicles travelling under different flooding depths. This provides the answer to the fourth research question: *What changes in macroscopic traffic parameters (i.e. free-flow speed and capacity) occur when vehicles travel under different flood depths?*.

Additionally, in order to assess the impacts of flooding depth on driving behaviour, two functions are estimated that correlate average vehicle speed and average headway with floodwater depth over a continuous flood depth interval from 0 to 300 mm. The reader may remember from literature that 300 mm is considered by different authors to be the threshold value at which passenger vehicles start floating. The significance of these functions is that they can be used to develop/adapt microscopic models needed for simulating the impacts of flooding on road traffic.

3.3.1 Microscopic Analysis

According to [62], there are two complementary levels at which traffic is generally described, namely microscopic and macroscopic level. In the microscopic level, every vehicle-driver combination, normally referred to as 'vehicles' are described individually, whereas at the macroscopic level traffic variables are aggregated over several vehicles, or usually over a road stretch.

The basic variables in microscopic traffic are individual speeds, time headways and spacing. Speed (v_i) is defined as the distance covered by a vehicle per unit of time. Distance between vehicles can be measured in time, normally referred to as headway (h_i) or in space, which is called spacing (s_i). In turns, distance between vehicles can be defined in two different ways: net headway/spacing or gross headway/spacing. The first one refers to the gap between two

consecutive vehicles, without considering the length of one of the vehicles. On the other hand, the gross headway/spacing refers to the distance between the rear bumper of the leading vehicle to the rear bumper of the following vehicle, which is the definition used in this thesis. These three variables are related to each other through a fundamental relationship.

$$s_i = h_i \cdot v_i \tag{3.1}$$

As it is explained by the previous author, full information regarding microscopic parameters of individual vehicles can be extracted from their trajectories, which define the position of a vehicle over time. Normally, the trajectories of a vehicles are plotted on the so-called space(m)-time(s) diagram. An example is included in Figure 3.3, which shows the trajectories of two vehicles: a truck and a passenger car.

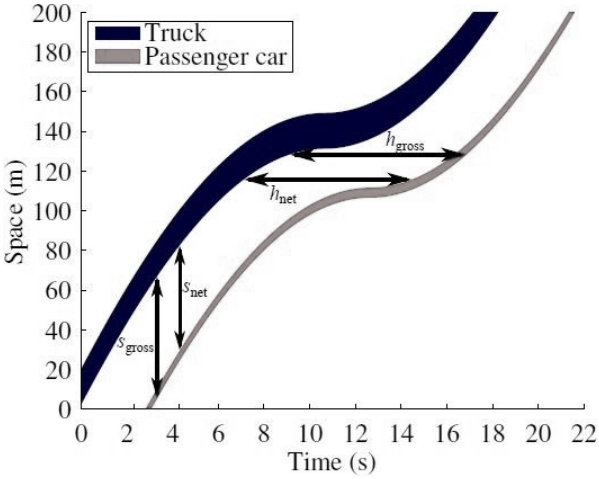

Figure 3.3: Vehicles trajectories in the space (m)-time(s) diagram. [62].

The slope of the curves at a certain point is equal the speed of the vehicles at that specific moment in space and time. Changes in the slope of the curves means the vehicles are accelerating/decelerating. Time headway between vehicles (s), measured at a reference point on the road stretch, can be obtained from the horizontal distance between the two points on the vehicles trajectories that pass through the reference point. Conversely, the spacing (m) between vehicles, measured at a certain moment in time, is obtained from the vertical distance between two points on the vehicles trajectories for the given time.

3.3.2 Macroscopic Analysis

In a macroscopic level, aggregated variables are described for a specific road stretch. The basic macroscopic parameters are the average speed of the vehicles on that stretch (u_i), the traffic flow (q_i) and the density (k_i). Traffic flow is defined as the number of vehicles that crosses a reference point on the road per unit of time, and is normally measured in vehicles per hour. Density is defined as the number of vehicles per unit of distance and is usually measured in vehicles per km. Every macroscopic variable has its microscopic counterpart. The following table shows how micro and macroscopic parameters are related to each other.

Microscopic variables	Symbol	Units	Macroscopic variables	Symbol	Units	Relationship
Headway	h	s	Flow	q	veh/h	$q = \frac{3600}{\langle h \rangle}$
Spacing	s	m	Density	k	veh/km	$k = \frac{1000}{\langle s \rangle}$
Speed	v	m/s	Avg. Speed	u	km/h	$u = 3.6\langle v \rangle$

Table 3.2: Relationship between micro and macroscopic variables. The brackets indicate the mean. [62].

Therefore, the macroscopic equivalent of relationship 3.1 is as follows:

$$q = k \cdot u \tag{3.2}$$

The relationship between macroscopic variables defines traffic states, which can be be represented graphically in the so-called fundamental diagram. The reader may notice that if two of the parameters are known for a given traffic state, the third one can be derived using the fundamental relationship. According to [18], the fundamental diagram is the basis of macroscopic traffic simulation and a valuable tool for traffic management. Figure 3.4 depicts the basic shape of the fundamental diagram that relates flow (q) with density (k), which is normally used in traffic analysis.

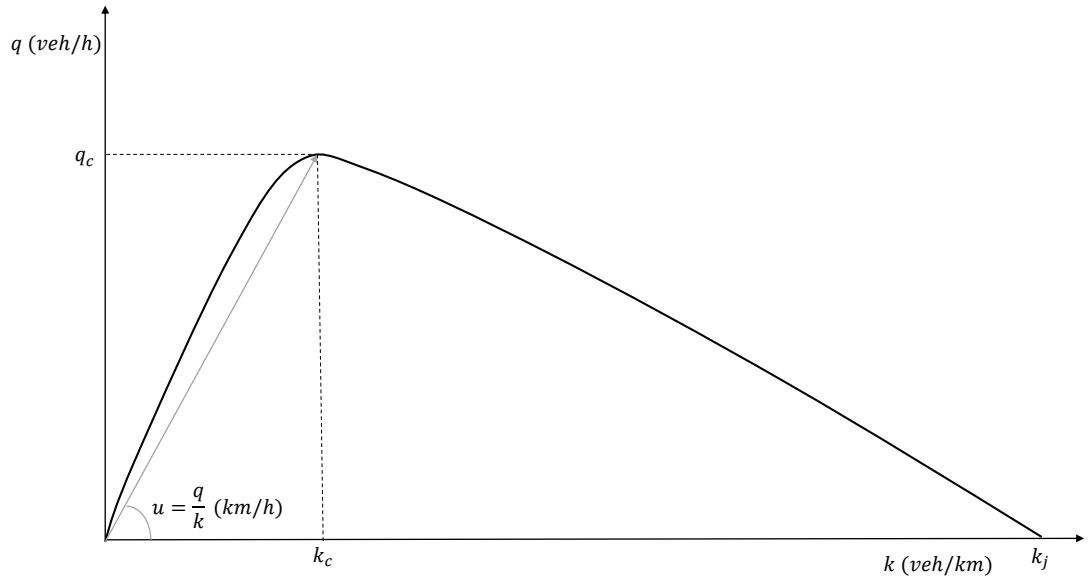

Figure 3.4: Basic shape of the fundamental diagram

The reader may realize that average speed can be obtained from the fundamental relationship 3.2 and it is equal the slope of the line from the origin to any point of the curve that represents a specific traffic state. It is important to know that the fundamental diagram can adopt many different shapes as it is estimated from empirical data. Different models has been fitted to data points representing different traffic states in order to estimate the shape of the fundamental diagram. In this thesis, the triangular shape will be used due to the short data set obtained

from the video analysis. The reader may notice the complete triangular fundamental diagram can be drawn defining only two traffic states: the capacity point and the end point of the congested branch.

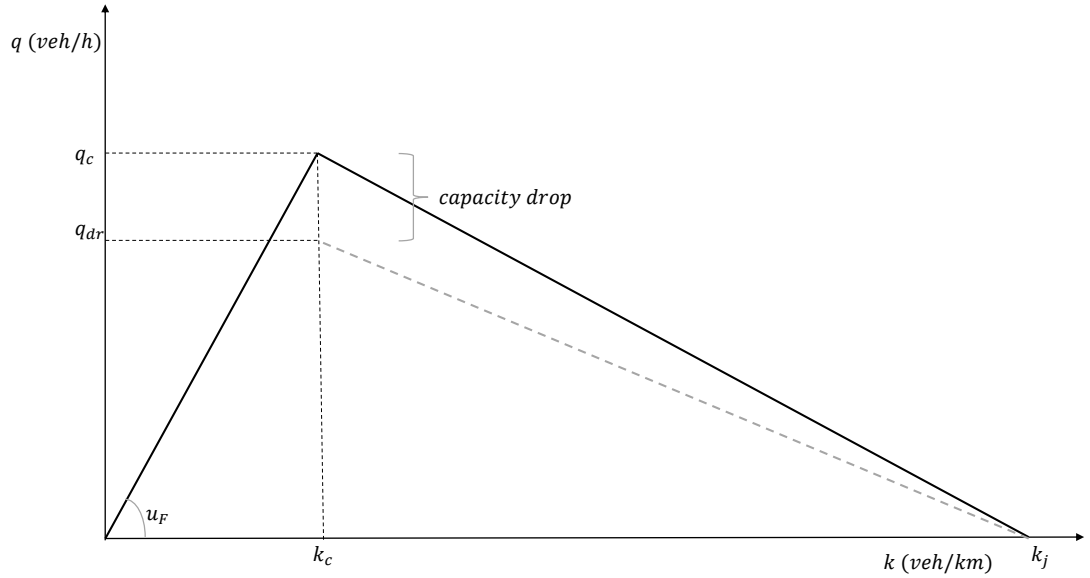

Figure 3.5: Triangular fundamental diagram and capacity drop phenomenon.

As it is explained in the literature review of this thesis, traffic practitioners have focused on studying the impacts of adverse weather conditions on traffic flow operations. Specially, research has been conducted on investigating the effects of weather conditions on highway capacity and free-flow speed. It is well known that these two are essential in the planning, design and operations of roads [63]. The capacity (q_c) of a road is defined as the highest flow a road can absorb before traffic congestion appears. Therefore, this point is found at the top of the fundamental diagram. The density and the average speed for this point are called critical density (k_c) and critical speed (u_c), which defines the boundary between the uncongested and the congested traffic states. According to [62], an estimation of the free-flow capacity can be given using the minimum average headway and maximum vehicle speed as these three variables are related to each other through the fundamental relationship. The reader may realize that when traffic flow reaches capacity, vehicles are driving in car-following mode or in other words, that is maintaining short headways with their leaders. In the uncongested branch of the diagram traffic flow increases with an increase of density, whereas in the congested part the traffic flow decreases with an increase of the density.

The average speed when the density is minimum is called free-flow speed. Nonetheless, if one assumes a triangular shape then the slope of the uncongested branch of the diagram corresponds to the free-flow speed (u_F). The remaining end point of the diagram is located at maximum density called jam density (k_j) and it corresponds to a traffic state in which the road is full of vehicles, that is vehicles coming to a complete stop and thus the traffic flow is equal to zero. Many practitioners have been interested in studying the join between the congested and the uncongested branch of the fundamental diagram, that occurs at critical density. Figure 3.4 shows how both ends meet at the same point, that is at the free-flow capacity point (k_c,q_c). Nevertheless, there is a phenomenon called 'capacity drop' that has been empirically observed by different experts and which explains why both branches would not merge in the same point. This phenomenon refers to the difference between the maximum flow on the road before the onset of congestion and the flow observed downstream of a location as long as congestion

exists. This traffic flow is normally referred to as queue discharge rate. This is also known as the discontinuity problem, which is discussed in [64, 65]. Figure 3.5 shows the discontinuity problem, and one can see how the congested branch (dashed grey line) do not end at the critical capacity (q_c), but at the queue discharge rate (q_{dr}).

3.4 Results Validation

One of the main outputs of the multilevel analysis approach is the estimation of the free-flow branches of the triangular fundamental diagrams of vehicle travelling through different flood depths. This allows to assess the changes in both free-flow and capacity variables when flooding conditions become more severe. One of the main conclusions of the literature review conducted in this thesis was that there is not any research available on the impacts of flooding on traffic flow operations, which prevents from comparing the results obtained in Chapter 5. However, many practitioners have carried out research on the impacts of adverse weather conditions (e.g. light/heavy rain and snow, fog, low visibility, wet pavement or snowed covered surface) on free-flow speed and capacity variables. The majority of these studies collects empirical data in motorways/freeways across different countries, and a few of them obtain data from urban roads with speed limit similar to the A94 and A93 major road stretches analysed in this thesis.

Therefore, a validation of the results obtained in Chapter 5 is accomplished in which the changes in free-flow speed and capacity caused by flooding are compared to those found in previous research under other adverse weather conditions. Although these studies differ on the type of weather phenomena, this comparison enables to see whether the speed and capacity drop found due to flooding are in line with those found in other studies. This will also contribute to extend the comparison of the effects of different weather phenomena on traffic flow operations.

Chapter 4

Data Acquisition

This chapter introduces the 3SVAA developed by the author of this thesis and implemented in Matlab to extract microscopic traffic data from video recording. Besides, it applies the proposed video analysis approach to videos that show vehicles driving through two waterlogged stretches part of the A94 and A93 major roads in Perth (Scotland). First, Section 4.1 gives information about the context of the videos (i.e. source, properties and exact location where they were recorded) and the characteristics of the road stretches. Section 4.2, explains the main functions of the 3SVAA and includes some examples of the information obtained when it was applied to the videos of Perth. In Section 4.3, an error analysis is conducted in order to report the uncertainty associated to 3SVAA when it comes to measure vehicle's speed and time headway. Finally, Section 4.5 explains how the depth of the waterlogging was inferred from the videos. The 3SVAA Matlab codes are included in Appendix 6, and it is recommended the reader follows the code while reading Section 4.2.

4.1 Context of the Videos

This thesis applies the 3SVAA to two video clips that are published on the video sharing platform *'YouTube'*. These clips display vehicles driving through two waterlogged stretches part of the A94 and A93 major roads in Perth, a city of central Scotland (UK). The first stretch is part of the A94 that connects Perth to Forfar [1], whilst the second one is located in the A93 public road between Perth and Blairgowrie [2].It is worth noting that the second clip was already used in [2] to estimate through video observation the speed of one vehicle crossing the waterlogged stretch using road markings as reference points. Figure 4.1 depicts the exact location of both road stretches in Perth (Scotland).

The first road stretch has a length of approximately 100 metres and is located right at the entrance of Scone, a small village in Perth and Kinross. The speed limit in this section is 30 *mph* as it traverses a build-up area. It seems that the waterlogging might be caused due to the reduce capacity of the drain located in the right lane, and that the flooding has spread over the road reaching the left lane. The frame rate of this video is 50 frames per second (fps).

[1] https://www.youtube.com/watch?v=sLWaSewuvtY&t=5s
[2] https://www.youtube.com/watch?v=tCqEARMI-_k&t=216s

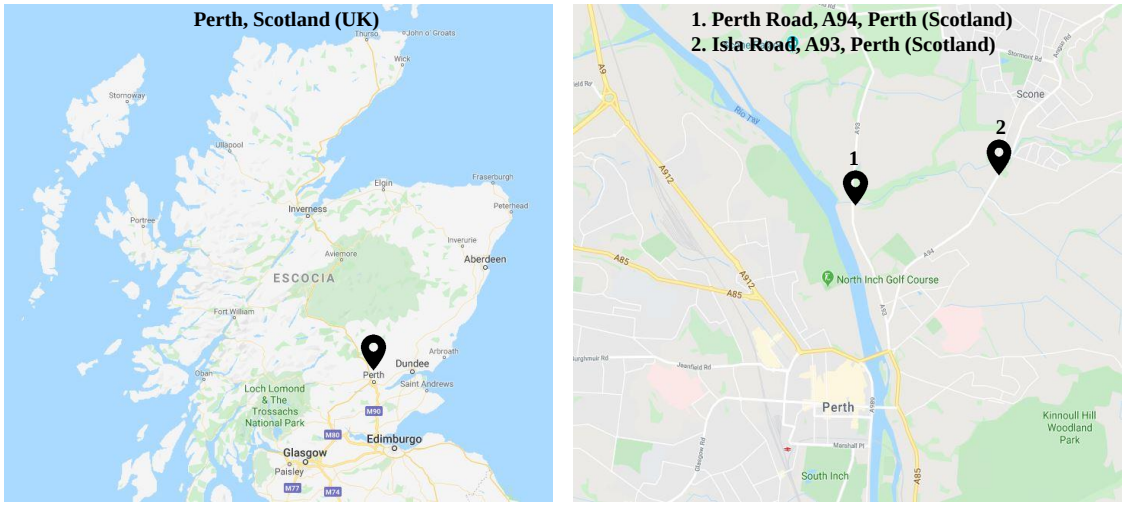

Figure 4.1: On the left, the city of Perth (Scotland). On the right, the location of the two road stretches. Google maps.

The road stretch displayed in video 2 is called Isla road and is located practically at the Quarrymill Bridge. It is approximately a 80 meters-long stretch and it is susceptible of becoming flooded during heavy rainfall events as it is located in a trough level. Two drains can be found at the lowest point of the trough, and they might be the cause of waterlogging when the overland flow exceeds their capacity. The speed limit in this stretch is also 30 *mph* as it traverses a build-up area. The frame rate of this video clip is 30 *fps*.

Figure 4.2: On the left, location of the A94 Perth road stretch. On the right, screenshot of video clip 1. Google maps

Along this report, the left lane according to Figure 4.2 of the A94 road stretch will be referred to as 'Stretch 1-L', while the right lane (i.e. vehicles coming towards the camera) will be called 'Stretch 1-R'. In the A93 road stretch, only vehicles driving on the left lane according to Figure 4.3 (i.e. vehicles driving towards the camera) are considered in the analysis, and therefore this lane will be referred to as 'Stretch 2-L'. Moreover, only small and large passenger cars including 4WD vehicles are considered in the analysis, while lorries are discarded. It is worth mentioning that either the day of the week and the time of the day in which the videos were recorded are unknown.

Figure 4.3: On the left, location of the A93 Isla road stretch. On the right, screenshot of video clip 2. Google maps

4.2 The '3-Step Video Analysis Approach'

Figure 4.4 outlines the methodology of the '3SVAA' implemented in Matlab to extract microscopic variables from video recording. As it is explained in the previous chapter, full information regarding microscopic traffic variables (i.e. vehicles speed, time headways and spacing) can be extracted from the trajectories of vehicles represented in the space-time diagram. This is precisely the idea followed by the author when developing the 3SVAA; first, it constructs the trajectories of vehicles driving through flooding in the space(m)-time(s) diagram, and then it extracts microscopic traffic variables from the vehicle's trajectories. To accomplish that, three Matlab codes were created which need to be implemented in three steps. These codes are included in Appendix 6 and it is recommended to read this chapter while looking at the codes for a better comprehension.

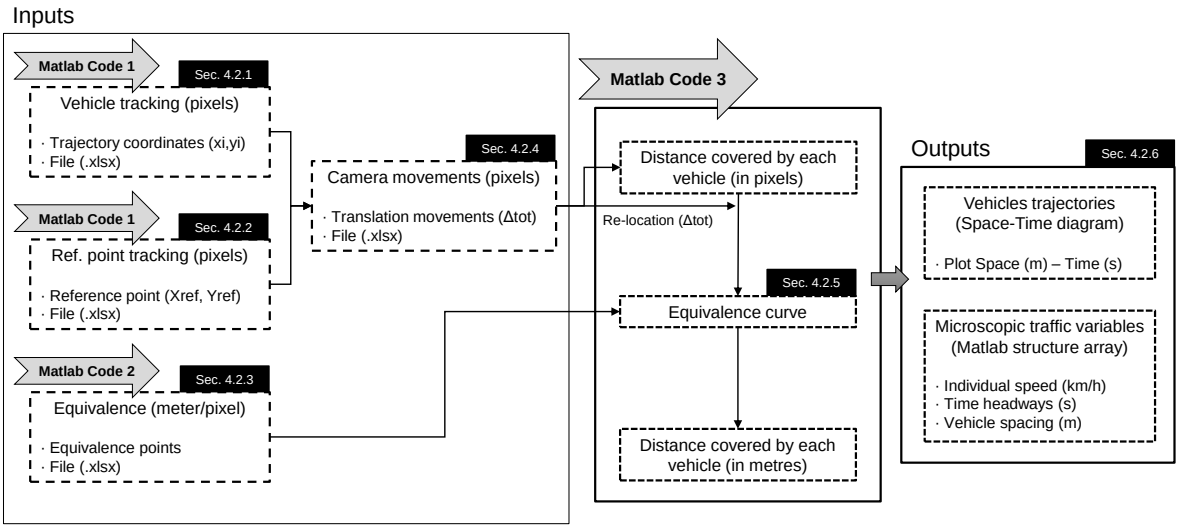

Figure 4.4: The '3-Step Video Analysis Approach'.

The first Matlab code is created to manually track the vehicles along the flooded stretches. It returns a convertible file with the trajectory coordinates of each vehicle in pixels. This first code is also re-used to track a static reference point on each video in order to correct for the camera movements. This will provide the 'corrected trajectories' file which is an input to the third Matlab code. Moreover, in order to convert the distances covered by the vehicles

from pixels to meters, a second Matlab code was created which allows to derive the so-called 'equivalence points' or ratios metre-pixel needed for the conversion. This file together with the 'corrected trajectories' file are the inputs to the third and main code. The third code essentially constructs the so-called 'equivalence curves' from the equivalence points that enable to convert the distances covered by the vehicles into metres. In doing so, the trajectories of vehicles can be plotted in the space(m)-time(s) diagram, so that microscopic variables (i.e. vehicle's speed, time headways and spacing) can be extracted and gathered in a Matlab structure array.

4.2.1 Vehicle Tracking

The first Matlab code enables the analyst to track manually the vehicles along the flooded stretch and returns a '.xlsx' file that contains the trajectory coordinates (xi,yi) of the vehicles in pixels. When running this code, video frames or images pop up on a new window allowing the analyst to manually track vehicles along the stretch by clicking on a specific reference point on the vehicles (i.e. wing mirrors, windscreens or license plates). As the analyst has to click on the same point on the vehicle along the stretch, the author strongly recommends to choose a small reference point in order to reduce the error as much as possible. The code is programmed to automatically gather the vehicle id, the lane on which vehicles are driving, frame number, video second and the trajectory coordinates in pixels in a Matlab table that is converted into an Excel file. As an example, the table obtained when tracking vehicles in stretch 1-R is shown in Table 4.1.

Vehicle Id	Direction	Frame	Sec	X_t (pixels)	Y_t (pixels)
1	R	151	4	1226	229,5
1	R	201	5	1192	232,5
1	R	251	6	1126	236,5
1	R	301	7	1024	251,5
1	R	351	8	916	266,5
1	R	401	9	781	299,5
1	R	451	10	639	334,5
1	R	501	11	437	384,5
1	R	551	12	4	470,5
2	R	601	13	1136	222,5
2	R	651	14	1001	248,5
...	...	...	...	...	...

Table 4.1: Trajectory coordinates in pixels of vehicles driving on Stretch 1-R.

From the table, one can see the first vehicle driving on the right lane in video 1 appears in frame 151 or video second 4. That is the first image that pops up when running the first Matlab code. Since it is a 50 fps clip, the following frame that pops up corresponds to the 201th frame. The first column, 'Vehicle id', associates each vehicle with a number, being number 1 the first vehicle tracked along the right lane. 'Direction' corresponds to the lane on which vehicles are driving. The fourth column called 'Sec' displays the second of the video in which the analyst has clicked on the screen. The last two columns show the x and y coordinates of the vehicles trajectories in pixels. From this table, one can see that the first vehicle takes in total 8 second to cross the flooded stretch. This vehicle drives away in second 12 when the second vehicle (id 2) appears on the screen.

4.2.2 Reference Point Tracking

If the reader observes the clips, will probably realize that the video maker is constantly moving the camera during the recording. It is therefore essential to define these movements in order to correct the coordinates of the vehicle's trajectories obtained from the first code. These movements are the result of rotating the camera during the recording, which can be defined as a translation movement of a pixel between two consecutive video frames. In order to define these translation movements, the first Matlab code can be re-used to track this time a static reference point (e.g. traffic sign in Figure 4.5). This provides with the coordinates of the reference points in every video frame, which allows to define the total translation movement (Δtot) of a pixel between two consecutive frames. Figure 4.5 displays one of the frames analysed in video 2-L. The reference point can be found at the back of the image on the traffic sign, whilst the centre of the wing mirrors are the points selected for tracking the vehicles.

Figure 4.5: Screenshot of a frame analysed in video 2.

4.2.3 Equivalence Points (m/px)

The 'equivalence points' are defined as the ratios metre/pixel derived along the road stretch to construct the so-called 'equivalence curves'. The significance of these curves is that they enable to convert the distance covered by the vehicles into metres. The equivalence points are first calculated by correlating the vehicle size in pixels with its real length in metres. To do so, the first Matlab code is slightly modified in order to be able to define the length of a reference vehicle by tracking the terminal points, (x4,y4) and (x5,y5) of the car throughout the stretch. Table 4.2 displays the ratios (m/px) obtained when tracking the length of the first vehicle that appears on 1-R.

From the table, one can see the reference vehicle is driving towards the camera, and thus the ratio metre/pixel becomes smaller on each frame, which makes sense since the closer the vehicle is to the camera lens, the larger its length in pixels, and therefore the smaller the ratio. As an example, two screenshots corresponding to frames 401 and 451 are shown in Figure 4.6, where the length of the reference vehicle is tracked on stretch 1-R. The reader may realize that for those vehicles driving on the other lane, the ratios would increase as vehicles separate from the camera.

Frame	x4	y4	x5	y5	Length. (px)	Length. (m)	Equivalence (m/px)
151	1253	260,5	1275	247,5	25,55	4818	0,18854
201	1222	267,5	1253	248,5	36,35	4818	0,13251
251	1153	283,5	1207	255,5	60,82	4818	0,07920
301	1044	307,5	1128	274,5	90,23	4818	0,05338
351	930	338,5	1050	293,5	128,16	4818	0,03759
401	787	385,5	948	325,5	171,82	4818	0,02804
451	617	445,5	843	366,5	239,41	4818	0,02012
501	376	528,5	710	410,5	354,23	4818	0,01360

Table 4.2: Equivalence points of the reference vehicle in stretch 1-R.

Figure 4.6: Sketch of how the length of the reference vehicle is tracked on frames 401 and 451 in stretch 1-R.

It is worth noting the importance of choosing a suitable reference vehicle to derive the equivalence points since the outcome of the 3SVAA strongly depends on the 'equivalence curves'. Three curves are estimated in total, which are essentially fitted curves to the equivalence points that contain the ratio metre-pixel at every single point along the road stretch. Based on the experience of the author when analysing the videos, there are some aspects to consider when choosing the reference vehicle; first, it is important to derive as many 'equivalence points' as possible, so that more accurate curves can be obtained. To this end, it is recommended either to choose a vehicle that crosses the stretch at low speed or to reduce the frame rate in the code. Moreover, one needs to make sure the vehicle's brand and model can be easily identified from the image, since the length of the vehicle in metres is obtained from its technical specifications.

4.2.4 Camera Movements

As it has been explained above, it is essential to compensate for the rotation movements of the camera during the recording. The rotation movement between two frames are calculated

as the root of the sum of squares of the horizontal and vertical translation of the reference point coordinates between those frames. For this analysis, the first frame in which the reference vehicle was tracked is used as the 'basis' frame, which means that all the vehicle's trajectory coordinates are corrected with respect to that frame. Continuing with the example of stretch 1-R, the 'basis' frame corresponds to the 151th (i.e. first frame in which the length of the reference vehicle is tracked). Table 4.3 shows how the total translation movements can are calculated in a '.xlsx' file with respect to the reference point coordinates (Xref, Yref) of frame 151. The reader may realize that Δtot is equal to zero in that frame, and it is negligible in the rest of the frames in which the reference vehicle was tracked along the stretch (i.e. from 201 to 501). For the rest, the Δtot is larger than zero and it defines the total translation movement of the reference point coordinates between each video frame and the 151th.

Vehicle Id	Direction	Frame	Sec	X_ref (pixels)	Y_ref (pixels)	ΔX (pixels)	ΔY (pixels)	Δtot (pixels)
1	R	151	4	Xref	Yref	0	0	0
1	R	201	5	X1	Y1	ΔX1=Xref – X1≈0	ΔY2=Yref – Y1≈0	$\sqrt{\Delta X1^2 + \Delta Y1^2}$≈0
1	R	251	6	X2	Y2	ΔX2=Xref – X2≈0	ΔY2=Yref – Y2≈0	$\sqrt{\Delta X2^2 + \Delta Y2^2}$≈0
1	R	301	7	X3	Y3	ΔX3=Xref – X3≈0	ΔY3=Yref – Y3≈0	$\sqrt{\Delta X3^2 + \Delta Y3^2}$≈0
1	R	351	8	X4	Y4	ΔX4=Xref – X4≈0	ΔY4=Yref – Y4≈0	$\sqrt{\Delta X4^2 + \Delta Y4^2}$≈0
1	R	401	9	X5	Y5	ΔX5=Xref – X5≈0	ΔY5=Yref – Y5≈0	$\sqrt{\Delta X5^2 + \Delta Y5^2}$≈0
1	R	451	10	X6	Y6	ΔX6=Xref – X6≈0	ΔY6=Yref – Y6≈0	$\sqrt{\Delta X6^2 + \Delta Y6^2}$≈0
1	R	501	11	X7	Y7	ΔX7=Xref – X7≈0	ΔY7=Yref – Y7≈0	$\sqrt{\Delta X7^2 + \Delta Y7^2}$≈0
1	R	551	12	X8	Y8	ΔX8=Xref – X8	ΔY8=Yref – Y8	$\sqrt{\Delta X8^2 + \Delta Y8^2}$
2	R	601	13	X9	Y9	ΔX9=Xref – X9	ΔY9=Yref – Y9	$\sqrt{\Delta X9^2 + \Delta Y9^2}$
2	R	651	14	X10	Y10	ΔX10=Xref – X10	ΔY10=Yref – Y10	$\sqrt{\Delta X10^2 + \Delta Y10^2}$
2	R	701	15	X11	Y11	ΔX11=Xref – X11	ΔY11=Yref – Y11	$\sqrt{\Delta X11^2 + \Delta Y11^2}$
...	...	...	...	...	...	...	...	...

Table 4.3: Total translation movements of the reference point in stretch 1-R.

4.2.5 Equivalence Curves

The third Matlab code is the core of this video analysis approach since it calculates the distance covered by the vehicles in metres, allowing to define the trajectories in the space(m)-time(s) diagram from which microscopic traffic data can be extracted thereafter. This code first calculates the cumulative distance covered by the vehicles (in pixels) from the corrected vehicle's trajectories. Subsequently, the code constructs the 'equivalence curve', which correlates the 'equivalence points' (y-axis) with the cumulative distance in pixels covered by the reference vehicle along the stretch (x-axis). An example of this table for the road stretch 1-R is depicted in Figure 4.7. The reader may realize the area underneath the curve is equal the distance covered by the reference vehicle in metres. Assuming that every vehicle follows the exact same path through the lane as the reference vehicle, this curve can also be used to obtain the distance in metres covered by the rest of the vehicles in that lane.

The 'equivalence curve' essentially is a fitted curve to the 'equivalence points' obtained from the second code. In order to find the type of curve that best fits the data points, a goodness-of-fit assessment of different models was conducted and it is explained in the following section. Both a graphical and empirical assessment showed that the exponential 2 model was found to be the best fitting curve to the data points. Figure 4.7 depicts the fitted curve of stretch 1-R to the equivalence points depicted in Table 4.2. The fitted curve is extended until it crosses the

y-axis at a value of 0.25 m/px, which corresponds to the last point on the road captured by the camera. In order to better understand the meaning of this curve, one could consider a vehicle crossing the flooded stretch at constant speed, in other words covering the same distance per time unit. Indeed, when the vehicle is far away from the camera, it covers shorter distance in pixels yet the area underneath the curve (i.e. distance covered by the vehicle in meters) is larger. This will return the same distance as when the vehicle is close to the camera, where it covers larger distance in pixels yet the area under the curve is smaller.

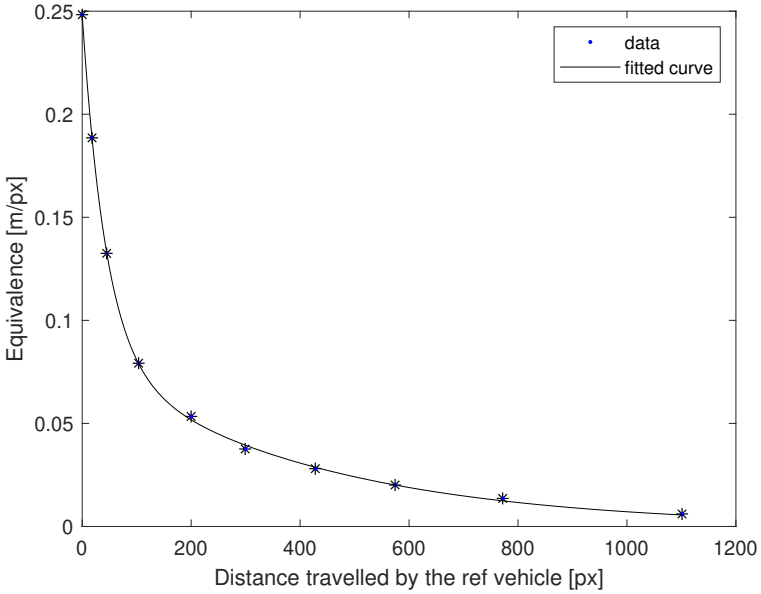

Figure 4.7: Equivalence curve of video 1-R.

The third Matlab code introduces the cumulative distance (in pixel) covered by each vehicle on the x-axis of the equivalence curve and re-locates it a distance equal to Δtot_i, so that it compensates for the rotation movements of the camera. Finally, by integrating the curve, the distances covered by each vehicle in meters and in time intervals of 1 second are obtained. This allows to plot the vehicles trajectories in the space(m)-time(s) diagram. It is worth noting that when the rotation angle of the camera is larger, a new section of the road stretch becomes visible in the image. To solve this issue, the equivalence curve is extended at both ends deriving the corresponding 'equivalence points' needed for computing the integral. The distance covered by a vehicle in meters is calculated as follows:

$$\int_{p1}^{p2} f(x)dx = \int_{p1}^{p2} (ae^{bx} + ce^{dx})dx = \frac{a}{b}[e^{bp2} - e^{bp1}] + \frac{c}{d}[e^{dp2} - e^{dp1}] \tag{4.1}$$

Where $f(x)$ is the exponential 2 function, and $p1$ and $p2$ are the limits of the integral which correspond to the start and end point of the cumulative distance covered by each vehicle along the flooded stretch.

Evaluating Goodness-of-Fit

The 'cftool' of Matlab was used to conduct a graphical and empirical assessment of different models in order to find the best fit to the data points. From the full range of models, the exponential 2 and Gaussian 2 were selected. Subsequently, goodness-of-fit statistics were computed in order to empirically assess both models. In Table 4.4 the value of the statistics calculated

for both models for stretch 1-R are shown. Since there is practically no difference, the simplest model or the one with lowest number of coefficients was finally selected, and that is the exponential 2. The same applies for the rest of the videos and directions, so that three equivalence curves with different parameters a, b, c and d were estimated in total.

Stretch 1-R			
Model	Expression	Good-of-fit statistics	
Exponential 2	$f(x) = a \cdot e^{bx} + c \cdot e^{dx}$	SSE	8,4767e-06
		R-square	0,9997
		dfe	5
		Adj. R-square	0,9996
		RMSE	0,0013
Gaussian 2	$f(x) = a_1 \cdot e^{-\left(\frac{x-b1}{c1}\right)^2} + a_2 \cdot e^{-\left(\frac{x-b2}{c2}\right)^2}$	SSE	2,7691e-04
		R-square	0,9909
		dfe	3
		Adj. R-square	0,9757
		RMSE	0,0096

Table 4.4: Goodness-of-fit statistics of the selected models.

4.2.6 Outputs

The third Matlab code plots the trajectories of vehicles in the space(m)-time(s) diagram. As an example, the trajectory of the reference vehicle of stretch 1-R is depicted in Figure 4.8, which corresponds to the Mercedes Benz displayed on Figure 4.6.

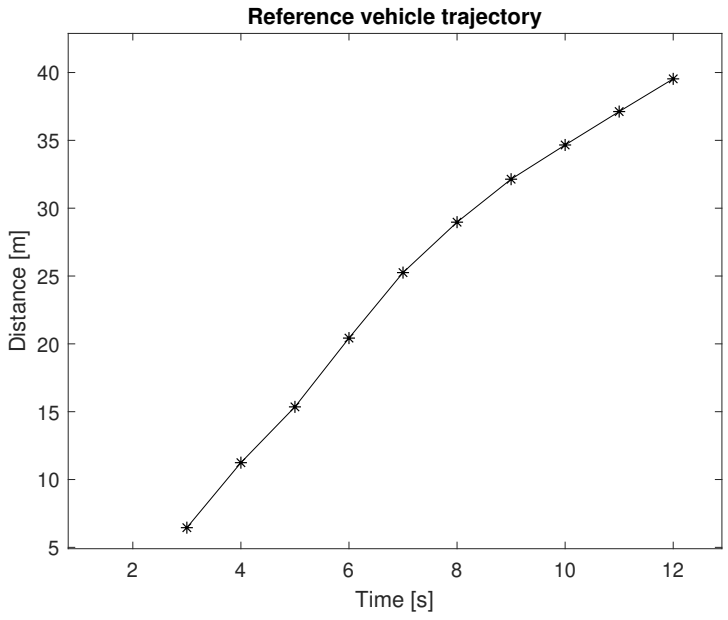

Figure 4.8: Reference vehicle trajectory stretch 1-R.

The y-axis contains the cumulative distance covered by the vehicle in metres, whereas the x-axis shows the video seconds. From the trajectory one may realize the length of the flooded stretch is about 40 metres. The reference vehicle takes around 8 seconds to traverse the flooding and it slowing down as it moves along the stretch. This can be seen from the slope of each of the segments, that is the velocity of the vehicle. It enters the flooded stretch at a speed of 17 km/h and leaves it at speed of 9 km/h approximately.

In addition, the third code also returns a Matlab structure array that contains the corresponding microscopic traffic variables, i.e. speeds, time headways and spacing for each of the vehicle tracked along the stretch. These microscopic variables are calculated as the horizontal and vertical distances between consecutive trajectories. The spacing is derived for those video seconds in which at least, two vehicles are crossing the stretch, and it is equal to the difference between the cumulative distances covered by the leader and the follower. In other words, the spacing corresponds to the vertical distance between vehicle's trajectories for a certain time. Time headways are however obtained at predefined cross-sections along the stretch, which need to be specified in the inputs of the third code. Unlike spacing, time headways are derived as the horizontal distance between the vehicle's trajectories at a specific location on the road stretch. Figure 4.9 depicts the trajectories of vehicles 3 and 4 of stretch 1-L. Figure 4.10 contains a screenshot of the Matlab structure array corresponding to stretch 1-L where the previous vehicles are highlighted.

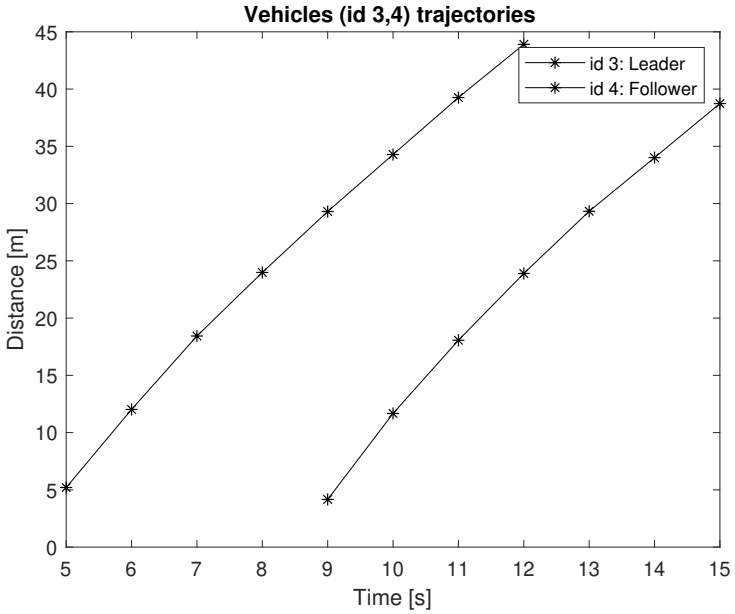

Figure 4.9: Vehicles (id 3 and 4) trajectories. Stretch 1-L.

From the vehicle structure array, one can see that both vehicles traverse the flooding at an average speed of 20 km/h approximately. Moreover, vehicle id 4 keeps an average spacing of 22 metres with its leader. Finally, the time headways are calculated at different locations along the stretch (i.e. at a cumulative distance of 10, 15, 20, 25, 30 and 35 meters), obtaining practically the same value of 4 seconds.

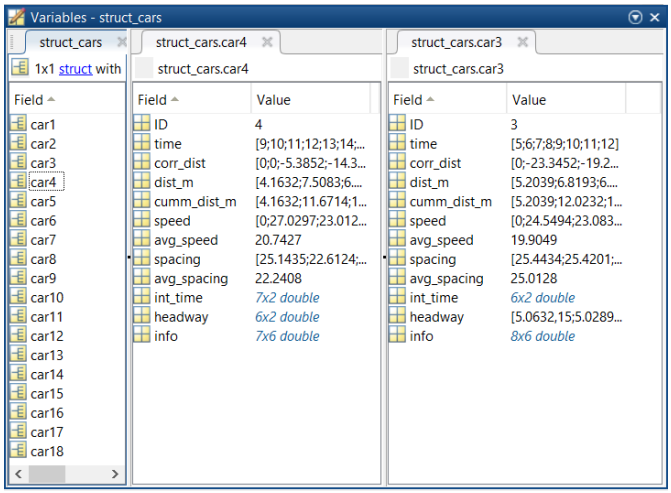

Figure 4.10: Vehicle structure array Matlab. Stretch 1-L.

A total of 51 vehicles trajectories are extracted by applying the 3SVAA to the videos of Perth. From the first one, practically the same number of vehicles are analysed in both directions, that is 18 vehicles on stretch 1-L and 21 vehicles on stretch 1-R. The lowest amount of data is obtained from the second video, stretch 2-L with a total of 12 vehicles trajectories. Nevertheless, microscopic traffic data (i.e. vehicle speed, time headways and spacing) are extracted at multiple points along the stretches, resulting in a larger data set.

4.3 Uncertainty or Error Analysis

In Section 3.2 of the previous chapter, the concepts of accuracy and precision of a measuring system were introduced and related to random and systematic measurement errors. Random errors were defined as statistical fluctuation (in either direction) in the measured data due to the precision limitations of the measurement instrument. This type of errors can be evaluated through statistical analysis and can be reduced by averaging over a large number of observations.

A data collection plan was designed with the aim of estimating the uncertainty associated to the 3SVAA when it comes to measure vehicle speed from video recordings. A list of potential systematic errors were considered for the design of the data collection plan. First, car's speedometers do not show the real speed at which vehicles are travelling, and that is why a GPS speedometer was used instead. As it is explained in Section 3.2, this thesis assumes that GPS speedometers provide an accurate value of vehicle speed, since under normal conditions they compute errors down to about 0.1 and 0.2 m/s. Furthermore, the author found in the province of Granada (Spain) two road stretches very similar in road layout to the ones in Perth. Besides, some references were taken from the videos in order to position the camera in a similar location during the data collection activities. Besides, the experimental driver was asked to drive on the opposite side of the road in order to recreate the driving in the UK. The results of the data collection are depicted in Tables 4.5, 4.6 and 4.7, from which the errors can be defined as the differences between the considered 'true speed' or GPS speed and the speed provided by the 3SVAA. One can clearly see that the speed differences, δx_i, fluctuate in either direction for the measured data, which brings the author to assume that only random errors exist. These errors can therefore be evaluated through statistical analysis, and that is why the uncertainty associated to the 3SVAA when measuring vehicle speed from video recording is calculated as the standard deviation of the speed differences.

$$s = \sqrt{\frac{\delta x_1^2 + \delta x_2^2 + ... + \delta x_N^2}{N-1}} = \sqrt{\frac{\sum(\delta x_i^2)}{N-1}} \tag{4.2}$$

Where δx_i^2 is equal to the squared difference between GPS speed and the speed obtained by applying the 3SVAA, while N is equal to the number of speed measurements. In this case, a standard deviation of $s = 1.46$ is obtained, which is the maximum error committed by the 3SVAA when it comes to measure vehicle speed at a confidence level of 68%. In order to obtain the maximum error committed at a confidence level of 95% the standard deviation is 1.96 times s and equal to $\pm$ **2.86** km/h.

Possible random error sources are, for instance the error committed when tracking the vehicles manually in the first Matlab code. Likewise, there is an error when tracking the reference point along the video that is used to compensate for the rotation movements of the camera. Other possible error sources could be the way the equivalence curve is constructed; first, the reference vehicle length is also tracked by manually clicking on the terminal points of the reference vehicle. Second, the equivalence curve is a fitted function to the equivalence points, and therefore it has an error associated to the fit. The reader may remember the calculation of the distances covered by the vehicles (in metres) are obtained by using the equivalence curve. These are all examples of possible random error sources, yet there could be others the author of this thesis is not aware of.

As it is also explained in the previous chapter, this thesis also provides the uncertainty associated to headway measurements. During the data collection activities was not possible to measure neither time headways nor spacing due to lack of equipment and devices, and hence a different technique is conducted to measure the error associated to the 3SVAA when it comes to measure time headways. A frame-by-frame analysis technique was conducted instead to measure, using a grid, the elapsed time between the front of the lead vehicle and the front of the following vehicle. The difference between these values, considered as 'true headway values', and those obtained through the 3SVAA are used to estimate the headway measurement error. These differences also show fluctuation in either direction, and hence they are considered random errors. Therefore, the uncertainty is again reported using the standard deviation, obtaining a value of $s = 0.38$ seconds. The maximum error committed by the 3SVAA when it comes to measure time headways with a confidence level of 95% is equal to $s = \pm$ **0.74 seconds**.

Stretch	Car Speedometer	GPS Speedometer	3SVAA (Matlab)	Speed diff. (δxi)	Speed diff. Squared (δxi^2)
1-L	15 km/h	12 km/h	13.37 km/h	-1.37	1.8769
	20 km/h	17 km/h	18.57 km/h	-1.57	2.4649
	25 km/h	22 km/h	20.01 km/h	1.99	3.9601
	30 km/h	27 km/h	29.34 km/h	-2.34	5.4756
	35 km/h	32 km/h	31.12 km/h	0.88	0.7744
	40 km/h	37 km/h	35.60 km/h	1.40	1.9600
	45 km/h	42 km/h	40.56 km/h	1.44	2.0736

Table 4.5: Speed differences stretch 1-L.

Stretch	Car Speedometer	GPS Speedometer	3SVAA (Matlab)	Speed diff. (δxi)	Speed diff. Squared (δxi^2)
1-R	16 km/h	13 km/h	12.12 km/h	0.88	0.7744
	19 km/h	16 km/h	14.94 km/h	1.06	1.1236
	24 km/h	21 km/h	21.93 km/h	-0.93	0.8649
	30 km/h	27 km/h	27.43 km/h	-0.43	0.1849
	35 km/h	32 km/h	30.71 km/h	1.29	1.6641
	39 km/h	36 km/h	34.01 km/h	1.99	3.9601
	44 km/h	41 km/h	42.36 km/h	-1.36	1.8496

Table 4.6: Speed differences stretch 1-R.

Stretch	Car Speedometer	GPS Speedometer	3SVAA (Matlab)	Speed diff. (δxi)	Speed diff. Squared (δxi^2)
2-L	11 km/h	8 km/h	9.54 km/h	-1.54	2.3716
	17 km/h	14 km/h	14.62 km/h	-0.62	0.3844
	19 km/h	16 km/h	17.31 km/h	-1.31	1.7161
	25 km/h	22 km/h	21.18 km/h	0.82	0.6724
	29 km/h	26 km/h	26.95 km/h	-0.95	0.9025
	35 km/h	32 km/h	32.64 km/h	-0.64	0.4096
	40 km/h	37 km/h	39.67 km/h	-2.67	7.1289

Table 4.7: Speed differences stretch 2-L.

4.4 Validation

The reader may realize the three microscopic variables, namely vehicle speed, time headways and spacing are related to each other through the fundamental relationship of traffic, so that a theoretical validation can be conducted to validate the 3SVAA. To do so, a Pearson correlation coefficient is calculated from the spacing values obtained through the 3SVAA and those derived by applying the fundamental relationship (equation 3.1). A Pearson correlation coefficient between two metric variables is calculated by:

$$r_{XY} = \frac{\sum_{i=1}^{n}(X_i - \overline{X})(Y_i - \overline{Y})}{\sqrt{\sum_{i=1}^{n}(X_i - \overline{X})^2}\sqrt{\sum_{i=1}^{n}(Y_i - \overline{Y})^2}} \tag{4.3}$$

Where X_i and Y_i correspond to the spacing values obtained through the 3SVAA and the fundamental relationship of traffic, n is the sample size which in this case is equal to 14. Albeit the sample size is quite short, this correlation provides the reader with an idea of the validity of the 3SVAA. The Pearson correlation coefficient varies from -1 to 1. A value equals to 1 means that the two variables are perfectly positively linearly. In this case, a value equals to 0.96 was obtained.

4.5 Flooding Depth Measurements

The flooding depth is inferred from the proportion of the tyre's height (i.e. distance between the base of the tread to the rim) that is submerged for those specific vehicles whose brand and model can be identified by observing the videos. However, the reader may realize the uncertainties associated when deriving the flood depth using the tyre's height as a reference; first, there are irregularities on the road surface that leads to wrong estimations at certain locations. Second, the splash back of the vehicles when moving through the flooding makes it difficult to define the exact proportion of the tyre height that is submerged. Additionally, it is not possible to see the tyre model for the selected vehicles. Finally, the flattening of the tyre under the weight of the car or due to lack of pressure leads to inaccurate estimates. That is why the author provides a flood depth error bound for each road stretch, which is defined based on the different tyre sizes available in the market for the selected vehicles [3][4][5].

Three vehicles for which the brand and model can be observed in the videos are first selected. The flood depth is inferred from the proportion of the tyre's height submerged, which in case of stretch 2-L is the entire height, whilst in stretches 1-L and 1-R the proportion is estimated in 1/3 and 2/3 respectively. However, for any vehicle brand and model, different tyre sizes are available in the market so that the flood depth is estimated as the average value of all possible tyre sizes available for the selected vehicles. Therefore, the flood depth measurement error on each stretch is calculated as the standard deviation of the tyre sizes available for the chosen cars. The average is calculated to unify the errors obtained on each stretch.

[3] https://www.wheel-size.com/size/volkswagen/transporter/2010/
[4] https://www.wheel-size.com/size/mercedes/e-class/2008/
[5] https://www.wheel-size.com/size/bmw/1-series/2007/

Stretch	A94 Perth Road (video 1)		A93 Isla Road (video 2)
Direction	L	R	L
Flooding depth	45 ± 15 mm	65 ± 15 mm	125 ± 15 mm

Table 4.8: Estimation of the flooding depth and its measurement error.

Finally, the length of the flooding on each stretch can be estimated from the vehicle's trajectories obtained through the 3SVAA, more specifically from the cumulative distances covered by the vehicles. The length of the waterlogging is approximately 40 and 30 meters in Perth Road and Isla Road stretch respectively.

4.6 Conclusions

In this chapter, the 3SVAA developed by the author of this thesis is presented and has been applied to videos that show vehicles driving through two waterlogged stretches part of the A94 and A93 Major Roads in Scotland (UK). This chapter, together with Appendix 6, in which the Matlab codes are included can be used as a guide of how to implement the 3SVAA to extract microscopic traffic variables from video recording. The proposed video analysis approach is a manual process that requires the analyst to track individually every vehicle displayed on the videos to derive its trajectory. This could turn into a tedious process if one disposes of videos of longer duration. Nevertheless, with the advent of real time object detection algorithms the vehicle tracking process could be automatized, so that the video analysis is simplified allowing the analyst to obtain in an effortless way a higher number of trajectories in less time. Additionally, the human error committed when tracking the vehicles manually along the road stretch will be removed. However, these algorithms are implemented in more advanced programming languages that require the analyst to have some previous experience before its use.

Since the author lacks of information regarding the camera used to record the videos in Perth and Isla Road stretches, the traditional camera calibration procedure could not be performed. Instead, an alternative distortion correction was implemented in the 3SVAA through the so-called 'equivalence curves'. As it is explained in the error analysis of this chapter, there is uncertainty associated to the construction of these curves as they are fitted curves to the 'equivalence points'. Therefore, it is important the video analyst can work with the camera that is utilized to record the videos, so that the traditional camera calibration procedure can be conducted. This would allow to measure the size of any object in the video in world units, and hence to accomplish a more accurate video analysis.

Finally, this chapter also conducts an error analysis to derive the uncertainty associated to the 3SVAA when it comes to measure vehicle's speed and time headways. A data collection plan was carried out in the home town of the author of this thesis in order to define the speed measurement error as the standard deviation of the considered 'true' speed (i.e. GPS speed) and the velocity obtained through the 3SVAA. Unfortunately, due to lack of equipment, it was not possible to measure neither time headways nor the spacing during the data collection activities, and therefore the headway error was calculated through a frame-by-frame analysis technique. However, nowadays more vehicles are equipped with sensors and/or cameras that measure the distance with the vehicle in front, which would allow to collect time headways and

spacing data on the field. In doing so, the three microscopic variables could be validated and their corresponding measurement errors would be defined more precisely.

Nonetheless, a more accurate validation of the 3SVAA could be conducted by installing radars or loop detectors at the same location of the camera, allowing to collect speed, headway and spacing data while recording the videos. This will enable to compare the values obtained through the 3SVAA with data gathered by these digital devices with measurement errors practically negligible. However, this equipment is expensive and difficult to acquire and would also need the permission of the government to be installed on public roads.

Chapter 5

Analysis & Final Results

In this chapter, the multilevel analysis approach proposed by the author of this thesis to study driving adaptation effects at two complementary levels (i.e. microscopic and macroscopic) is implemented using microscopic data obtained from the previous chapter. First, a microscopic analysis is accomplished in Section 5.1, where changes in microscopic variables of vehicles travelling through the A94 and A93 road stretches are analysed at three different flood depths. By doing so, the second research question can be answered:

What changes in microscopic variables (i.e. vehicle speed and time headways) occur when vehicles travel under different flood depths?

Furthermore, two functions are estimated in Section 5.2 that correlate average vehicle speed and average headway with flood depth, allowing to assess driving adaptation effects over a continuous flood depth interval. Then, the multilevel analysis approach explained in Section 3.3 is applied to extend the study to the macroscopic level. In Section 5.3, macroscopic traffic parameters are derived from their microscopic counterparts, which enables to study the impact of flood depth on free-flow speed and capacity variables. For the first time, part of the fundamental diagrams of vehicles travelling under different flood depths are estimated, which leads to the answer of the fourth and last research question:

What changes in macroscopic traffic parameters (i.e. free-flow speed and capacity) occur when vehicles travel under different flood depths?

Finally, the results are compared to those found in previous research under other adverse weather conditions, which contributes to extending the comparison of weather-related impacts on traffic flow operations.

5.1 Microscopic Analysis

In this section, changes in microscopic traffic parameters under different flood depths are studied from the data obtained by means of the video analysis conducted in the previous chapter. As it is illustrated in Figure 3.1, the development/adaptation of microscopic traffic models in adverse conditions requires the analysis of microscopic traffic variables (i.e. vehicle speed and headway) in such conditions. Therefore, this section studies how these traffic parameters change when flooding conditions become more severe, that is when flood depth increases.

First, a criteria is set up to distinguish between vehicles driving in car-following and free-driving mode, which will help to differentiate between traffic states (congestion or free-flow state). Therefore, vehicles are grouped in two categories: those driving in free-driving mode and those driving in and car-following mode according to the criteria defined in [66]. Subsequently, this is verified by observing the videos to make sure that, indeed the classification responds to the behavioural actions displayed on the videos. The free-driving mode considered in this thesis is defined as the one maintained by a driver that is not influenced by other road users. According to the latter author, a short headway does not always imply car-following, since for instance a large speed difference between the leaders and the followers may imply the vehicles are not in car-following mode. That is the reason why the classification between free and following drivers will be based on both time headway and relative speed criterion. Therefore, a driver i is considered to be in car-following mode if:

$$h_i < h^* \tag{5.1}$$

and

$$|v_{i-1} - v_i| < \Delta v^* \tag{5.2}$$

Where v_{i-1} is the speed of the follower and v_i the speed of the leader. The boundary values h^* and Δv^* are equal to 7 seconds and 2.5 m/s respectively.

As it is explained in the literature review of this thesis, it is recognized that drivers tend to reduce their speed or/and increase time headway under adverse weather conditions. Figure 5.1 depicts the time headway frequency obtained on each flooded stretch analysed in the previous chapter under flooding depths of 45, 65 and 125 $\pm$ 15 mm, which have been renamed as flood depth 1, 2 and 3 respectively. Although this figure contains the headway values of vehicles driving in both car-following and free mode according to the previous criteria, very large time headways were excluded.

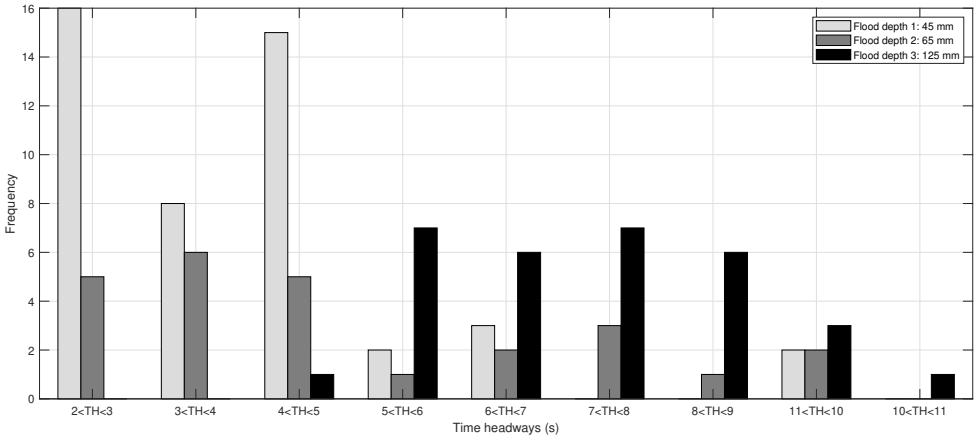

Figure 5.1: Time headways under different flooding depths.

According to the figure, the majority of headway values found in the less flooded stretch (i.e. 45 mm) lies between 2 and 5 seconds, having the largest headway frequency between 2 and 3 seconds. This seems logical since the flooding conditions are less severe, and hence drivers maintain shorter headways with their leaders. Although the majority of the headway values in the second stretch (i.e. 65 mm) also lies between 2 and 5 seconds, the frequencies are practically half of those found in the less flooded stretch. Besides, headway values found in the second

most flooded stretch spread over larger headway intervals compared to those found in the less flooded one. Finally, only values higher than 5 seconds were found in the most flooded stretch (i.e. 125 mm), lying the majority between 5 and 9 seconds. The frequencies found in this interval in the flooded stretch are more than double the ones found in the previous stretch. This suggests that drivers tend to keep larger distances with their leaders when the flooding conditions become more severe. Indeed, by observing the videos one realizes that those vehicles driving in car-following mode leave some space to their leaders before entering the flooding. This could be explained by the fact that drivers seem to wait right upstream the flooding area to make sure the vehicle in front crosses the stretch safely, and then followers usually copy their leader's trajectories along the flooded stretch.

Figure 5.2 depicts the frequency of speeds found at the different flooded stretches. The speed values displayed in the figure are the average speeds maintained by each vehicle when crossing the waterlogged stretch. This figure includes average speed values of vehicles travelling in both car-following and free mode. As it was expected, the lowest speeds correspond to those vehicles travelling through the most flooded stretch, with values between 5 to 20 km/h, with a maximum average speed of 19.6 km/h. The largest speed frequency is found within the interval from 10 to 15 km/h. The values corresponding to the second most flooded stretch seem to be normally distributed around an average value of 25 km/h, while those found in the less flooded stretch follow a similar distribution, yet translated to the right and having an average of 29 km/h approximately. There is some vehicles crossing the less flooded stretch at speeds of around 42 km/h, which are the largest values found across the three road stretches, yet still below the speed limit of 30 mph ($\approx 50km/h$), and which correspond to vehicles driving in free mode.

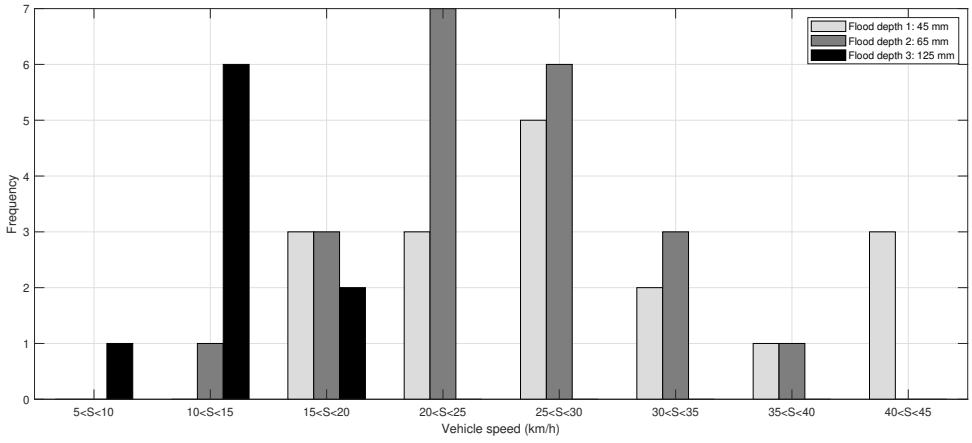

Figure 5.2: Vehicle speeds under different flooding depths.

In the second video (i.e. stretch 2-L), the camera captures the road section right upstream the waterlogging, which allows to observe driver's behaviour when they enter the flooding. By observing the video, one will essentially recognize three driving behaviours; the first one occurs when a queue of vehicles builds upstream the flooding area, which usually happens when the leading vehicle stops before the waterlogging. This situation followed by an increase in traffic demand leads to congestion upstream the flooding, and therefore vehicles to traverse the stretch in car-following mode. This has been referred to as *'Scenario 1'* in Figure 5.3. Other drivers however, are able to freely cross the stretch as they do not encounter any other vehicle on the same lane, yet they are constrained by a vehicle coming from the opposite direction (R) which normally travel through the middle part of the road. This has been referred to as *'Scenario 2'*.

This makes the vehicle slow down before getting in the flooding and also forces it to strictly cross the stretch through its lane (L) where flood depth is slightly higher due to the road gradient. This has been represented with the light grey arrow in the figure. Finally, there are couple of vehicles that are able to freely traverse the stretch without being constrained by any vehicle on the road stretch, which have been included within *'Scenario 2'*, and their trajectories have been represented in the sketch with a light blue arrow. As these vehicles do not encounter any other car passing by, they cross the stretch through the middle part at higher speeds.

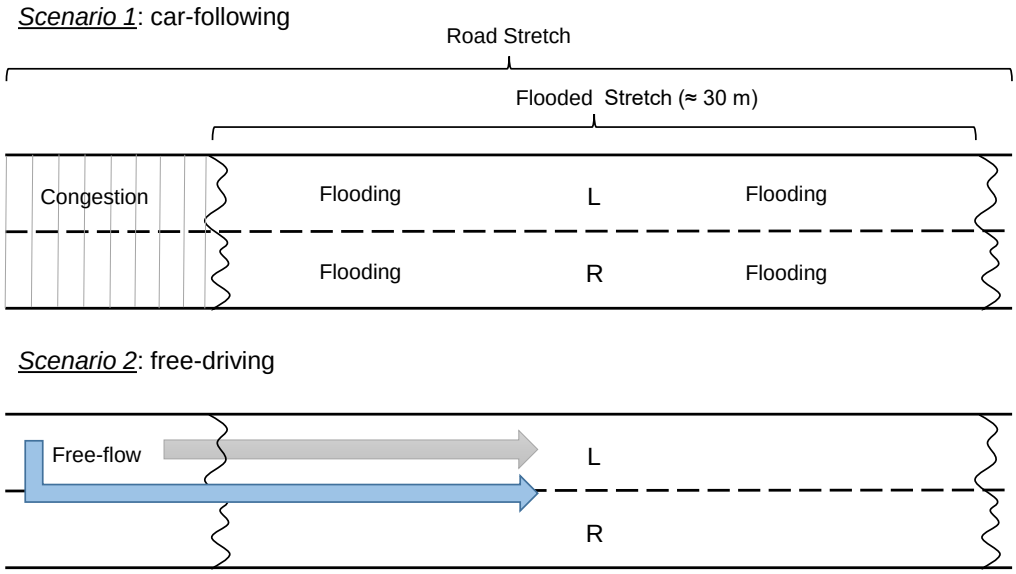

Figure 5.3: Sketch of the two traffic scenarios in stretch 2-L.

In order to analyse drivers speed variation (i.e. acceleration and deceleration) along the flooded stretch 2-L, some examples of vehicle's speed over time have been plotted and depicted in Figure 5.8 corresponding to *'Scenario 1'*, that is vehicles travelling in car-following mode. Additionally, two examples of vehicles driving in free-mode are included in Figure 5.11. The lowest speed values highlighted in blue, correspond to the instant of time at which vehicles enter the flooding area, that is when the two front wheels get in contact with the waterlogging. The first point on each plot represents the second before vehicles enter the flooding.

From Figure 5.8, one can see that the speed variation along the stretch of those vehicles travelling in car-following mode follows practically the same pattern. Cars slow down as they get closer to the waterlogging reaching the lowest speed values, between 1.2 to 3.2 m/s (blue points), the moment which the two front wheels get in contact with water. As it is explained in Figure 5.3 (*'Scenario 2'*) the stop of some leading vehicles before the flooding causes the followers to slow down practically to a standstill. In contrast, the highest speeds, between 3.8 and 5.8 m/s are reached when vehicles are leaving the flooding area. The average deceleration rate found when vehicles are approaching to the flooding is equal to 0.54 m/s^2, while the average acceleration rate right after reaching the lowest speed is equal to 0.48 m/s^2.

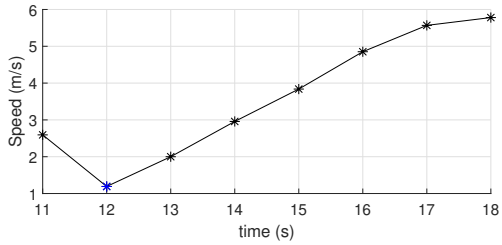

Figure 5.4: Vehicle id 2

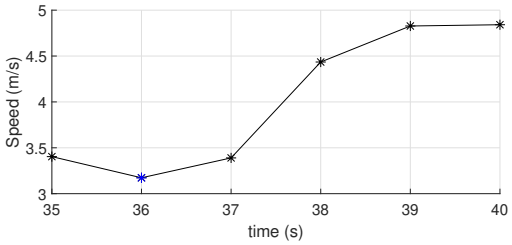

Figure 5.6: Vehicle id 5

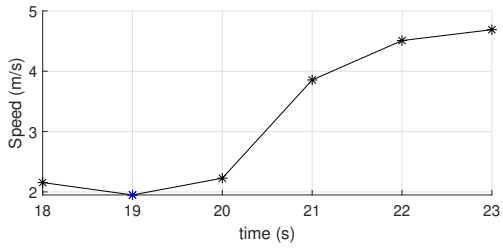

Figure 5.5: Vehicle id 3

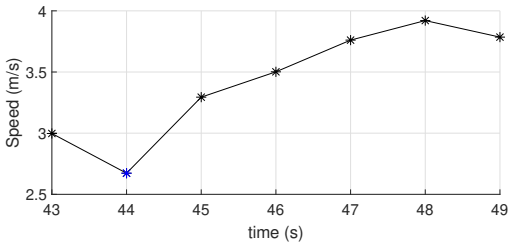

Figure 5.7: Vehicle id 6

Figure 5.8: Speed over time of vehicles driving in car-following mode on stretch 2-L.

From Figure 5.11 one can see that speed variation over time of those vehicle driving in free-mode follows practically the same pattern as the previous ones. Vehicles represented by the light grey arrow in Figure 5.3 also slow down almost to standstill before entering the flooding, since they are constrained by a vehicle coming from the opposite direction who is traversing the stretch through the middle part of the road. However, the average deceleration rate is slightly lower than in the previous case and equal to 0.42 m/s^2, whereas the acceleration rate is significantly higher and equal to 1.12 m/s^2.

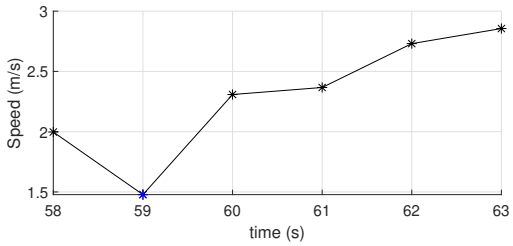

Figure 5.9: Vehicle id 7

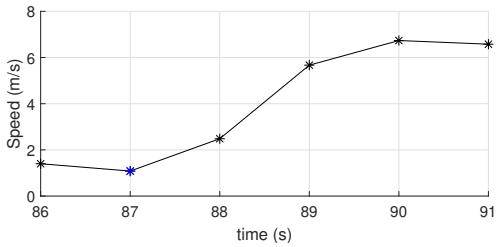

Figure 5.10: Vehicle id 9

Figure 5.11: Speed over time of vehicles driving in free-driving mode on stretch 2-L.

5.2 Flood depth Impact Assessment

The aim of this section is to provide with two functions that relate average vehicle's speed and average time headway with flooding depth by fitting two models to the data obtained in the previous chapter by means of the 3SVAA, and data from previous literature. In the speed case, two fitting curves are plotted; one corresponding to those vehicles driving in car-following mode and the other one to those that are in free-driving mode. In the time headway case however, the function is estimated using time headways of those vehicles driving in car-following mode. The car-following criteria introduced in Section 5.1 is applied to categorize vehicles according to their driving mode. The significance of these curves is that they provide traffic practitioners with the possibility of including driving adaptation effects under flooding conditions within microscopic traffic simulation models.

5.2.1 Speed-Flood depth Function

As it is explained in Section 2.5 of the literature review, some authors attempted to study diver's speed adaptation under flooding conditions in the past. In particular, [2] proposed a depth-disruption function for correlating vehicle's speed with flood depth, which was constructed combining data from previous experimental studies, safety literature, expert's opinion and data collected by observing videos that show vehicles driving through flooded stretches in Perth and Bromsgrove (UK). However, the authors derive an average vehicle speed at two different flood depths by considering just one vehicle in each video. They calculate the speed dividing distance covered by the vehicle over a fixed time period using road markings as reference points. The reader may realize the uncertainty involved in this estimation; first, the road markings in the video of Perth, which is the same one analysed in this thesis are barely visible due to waterlogging. Besides, the vehicle selected in that video is constrained by its leader since it is driving in car-following mode. Therefore, in order to estimate a more reliable average speed, vehicles driving in both car-following and free mode need to be considered separately in the analysis. Finally, the function proposed by the authors includes data points collected in different types of roads (e.g. motorways, major roads...), leading to a biased function as vehicle speed differ significantly according to the type of road in which it is measured.

Table 5.1 displays the data used to estimate both speed curves of vehicles driving in car-following and free mode. Points 1, 2 and 3 correspond to the average speed calculated from the microscopic data extracted through 3SVAA when it was applied to the videos of Perth. The speed measurement error with a confidence level of 95% is equal to $\pm$ 2.86 km/h, which is represented in the plot by vertical error bars. The flooding depth estimation and the measurement error are explained in Section 4.5. Finally, point 4 corresponds to the speed limit of the A94 and A93 road stretches in which the videos were recorded, while point 5 is taken from previous literature.

Both the A94 and A93 road stretches have a speed limit of 30 mph ($\approx$ 50 km/h), which has been set as the vehicle speed in dry conditions, that is at 0 mm of water depth. Nevertheless, different authors have found that drivers tend to reduce their speed under light rain, that is when road pavement becomes wet, yet the flood depth is still considered 0 mm. The questionnaire of [16] shows there is a speed decrease of 15.7% under light rain, which has been represented by point 4 (i.e. flood depth equals to 0 mm). Finally, the right end of the curve, point 5, corresponds to a flood depth of 300 mm. Different experimental and theoretical studies on car stability in floodwaters [26,45,46] have defined a certain threshold value of flooding depth at which vehicles start floating. This also connects with the guide of road design from [47] that provides a road closure indicator based on a combination of depth and velocity of flow over the road and is defined when the total head (depth and velocity of flow) at any point across the carriageway is equal to 0.3 m.

			Car-following	Free-driving
Point no.	Reference	Flood depth (mm)	Avg. Speed (km/h)	Avg. Speed (km/h)
1	Video 1_L	45 ± 15	27.3 ± 2.86	31.6 ± 2.86
2	Video 1_R	65 ± 15	24.4 ± 2.86	26.4 ± 2.86
3	Video 2_L	125 ± 15	14.1 ± 2.86	16.9 ± 2.86
4	Speed limit + Previous literature	0 (dry conditions) 0 (wet pavement)	50 – 7.90	50 – 7.90
5	Previous literature	300	0	0

Table 5.1: Average vehicle speed under different flood depths.

Furthermore, the guideline of [35] developed a draft interim criteria for stationary vehicles stability considering three classes, namely small passenger cars, large passenger cars and 4WD vehicles. For small passenger cars the flood depth for which stationary vehicles lose stability is also set at 0.3 m. Therefore, this thesis considers the most restrictive one, that is for small passenger cars to set the vehicle speed at 300 mm equal to 0 km/h of water depth.

The type of speed function was found by conducting a goodness-of-fit assessment of potential curves that meet the following selection criteria:

1. Constraint: vehicle speed equals to 0 km/h at a flood depth of 300 mm.
2. Constraint: vehicle speed equals to 50 km/h at a flood depth of 0 mm.
3. Strictly decreasing along the flood depth interval from 0 mm to 300 mm. In the microscopic analysis was found that average vehicle speed decreases as water depth increases.
4. No inflection points along the flood depth interval from 0 mm to 300 mm.
5. A model is considered to have a good fit if the adjusted R-square is close to 1 and it has a low RMSE.
6. If two models have similar goodness-of-fit, the one that passes through the horizontal and vertical error bars estimated will be selected.
7. If two models have similar goodness-of-fit and both functions pass through the horizontal and vertical error bars, then the one with the lowest amount of coefficients, that is the less complexed model will be selected.

A total of four functions were selected for further analysis: lineal, polynomial, exponential and reverse polynomial model. According to the selection criteria, the polynomial function was discarded since it does not strictly decrease along the flood depth interval from 0 mm to 300 mm; it reaches a minimum value around 250 mm. The lineal model was also discarded since when the function is raised to meet the first criteria, it leads to a poor fit of the data points. Nonetheless, all these functions were plotted and displayed in Figure 5.12, which allows to graphically assess the goodness-of-fit.

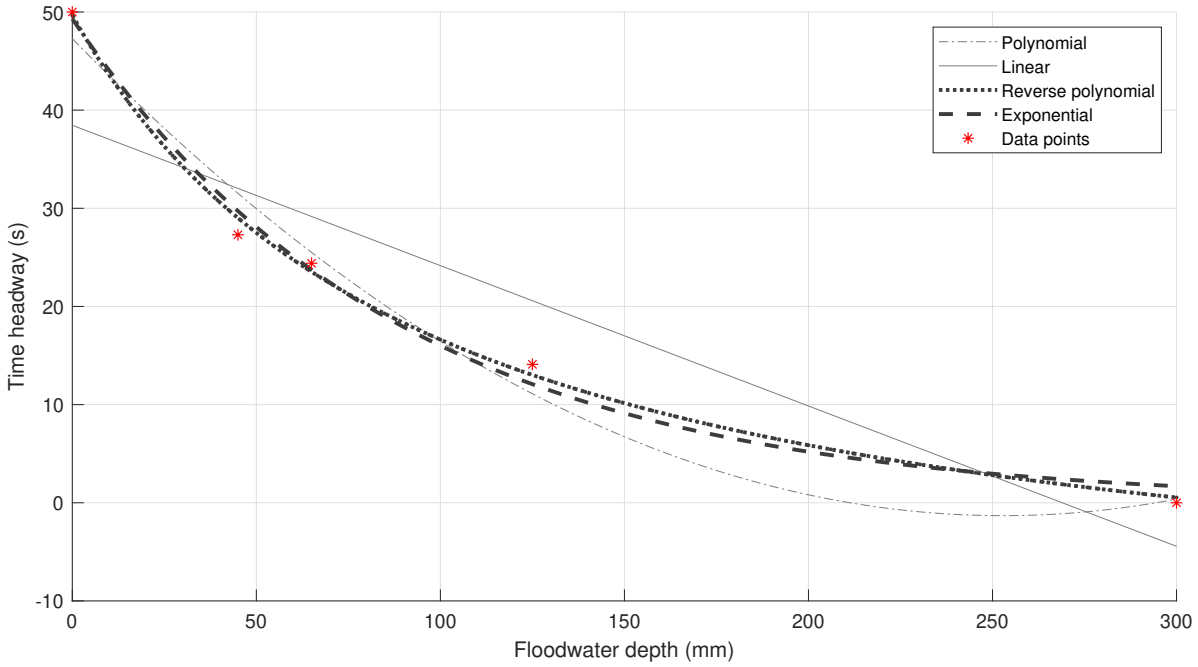

Figure 5.12: Graphical evaluation of the goodness-of-fit.

According to the above figure, the exponential and the reverse polynomial show a better fit to the data points, and hence were selected as potential functions for further evaluation. Table 5.2 shows the RMSE and adjusted R-square statistics for each model. Although both functions show practically the same values in both statistics, the reverse polynomial has lower RMSE than the exponential model. However, both functions were plotted in Matlab to see whether they pass through the horizontal and vertical error bounds. Only the reverse polynomial does it, and therefore it is selected as the best fitting model.

Model	Expression	Good-of-fit statistics	
Exponential	$f(x) = a \cdot e^{bx}$	Adj. R-square	0.987
		RMSE	2.137
Reverse polynomial	$f(x) = \frac{1}{(ax+b)} + c$	Adj. R-square	0.992
		RMSE	1.622

Table 5.2: Goodness-of-fit statistics of the selected models.

It is found that the average speed of vehicles driving in car following and free mode decreases with an increase of water depth in urban road stretches with speed limit around ($\approx 50 km/h$). More specifically, the average speed of vehicles driving in car-following and free mode follows the reverse polynomial function displayed in Equation 5.3 and 5.4 respectively. Both curves were plotted in Matlab and displayed in Figure 5.13.

$$Car following : v(d) = \frac{1}{(1.67 \cdot 10^{-4} \cdot d + 0.02)} - 15.29 \tag{5.3}$$

$$Free - driving : v(d) = \frac{1}{(1.02 \cdot 10^{-4} \cdot d + 0.01)} - 22.46 \tag{5.4}$$

Where $v(d)$ is vehicle speed as a function of water depth d.

5.2.2 Headway-Flood depth Function

To the best knowledge of the author of this thesis, this is the first time that a relationship between depth of standing water and time headways is developed and represented in a function. As it is explained in the literature review, different authors have studied in the past the impact of adverse weather conditions on time headways (e.g. rain, fog...), yet there is no research available on the impacts of flood depth on time headways. In this section, the average gross time headway (i.e. the distance in time between the rear bumper of the leading vehicle and the rear bumper of the following vehicle) of those vehicles driving in car-following mode is calculated under the estimated flood depths. A function is fitted to these data points and data obtained from previous literature to relate average time headway with flood depth.

Data from previous literature are used to define time headways in dry conditions on urban roads with similar speed limits to the A94 and A93 road stretches in Perth. The authors of [67] collected time headways in dry conditions on a two carriageway urban arterial in Southampton (UK) by using a probe vehicle. The aim of the study was to examine whether the headway chosen by a driver is influenced by a range of situational variables (i.e. type of vehicle being followed, changes in traffic flow, road type and day to day variation in driver's behaviour). The time headway found vary between 1.06 and 2.54 seconds.

The authors of [68] collected time headways in dry conditions also in urban roads. The aim of the research was to report on the effectiveness of two hand-held roadside signs admonishing drivers not to tailgate (i.e. to follow the leader with a headway of considerably less than 2 seconds). The authors excluded from the data collected those vehicles that were driving more than 4 seconds behind the vehicle ahead, since they were considered not to be driving in car-following mode. The authors found that drivers followed with an average headway of 2.11 seconds when the sign was absent.

Therefore, based on the previous studies this thesis uses the time headway interval found in [67] to define the left end of the headway curve in dry conditions. An assumption is made to define the right end of the curve, that is when the water depth is equal to 300 mm. This assumption needs to be in line with past experimental and theoretical studies on car stability in floodwaters that are explained in the previous sub-section. The flood depth threshold value of 300 mm proposed by some authors suggests that, if time headways increase with flood depth, the headway value when vehicles lose their stability, and hence start floating, could be assumed to be infinite. This will thus make the function to have an asymptote at point x=300. It makes sense if one imagines that at the threshold value, vehicle lose the contact with ground, and therefore they are washed away by floodwaters, so that the concept of headway would not apply any more. Nonetheless, it is quite unclear how would headway values distribute over the flood depth range from 125 to 300 mm since there is not any intermediate data point available in that range. Therefore, in order to provide with a more reliable model, the author of this thesis decided to estimate a curve that extends from 0 to 125 mm of floodwater depth. Table 5.3 shows the data points through which the headway curve was fitted.

			Car-following
Point no.	Reference	Flood depth (mm)	Avg. Headway (s)
1	Video 1_L	45 ± 15	3.20 ± 0.74
2	Video 1_R	65 ± 15	3.40 ± 0.74
3	Video 2_L	125 ± 15	6.53 ± 0.74
4	Previous literature	0 (dry conditions)	1.80 ± 0.74

Table 5.3: Average vehicle headway under different flood depths.

The first three points are calculated by averaging time headways of those vehicle that cross the flooded stretches in car-following mode. The measurement error associated to time headway values with a confidence level of 95% is equal to ± 0.74 seconds. The reader may realize there is practically no difference between time headways in video 1-L and 1-R, being the average value at 45 mm slightly lower. Nonetheless, from the table one can clearly see that average time headway increases with flooding depth having the maximum value (6.53 seconds) at 125 mm. It is worth noting point 4 corresponds to the mean of the time headway interval found by [67] in dry conditions, which is equal to 1.80 seconds. It worth noting the distance from the mean to both ends of the interval (0.74 seconds) is coincidentally equal to the headway error measurement found at a level of confidence of 95%.

The same procedure carried out for the speed case is followed again to find the best fitting model to the data points displayed in Table 5.3. The model selection criteria for the headway case slightly varies from the speed case:

1. Constraint: the headway at 0 mm of flood depth must lie within the headway range 1.80 $\pm 0.74s$.
2. Strictly increasing along the flood depth interval from 0 mm to 125 mm. In the microscopic analysis was found that average time headway increases with water depth.
3. No inflection points along the flood depth interval from 0 mm to 125 mm.
4. A model is considered to have a good fit if the adjusted R-square is close to 1 and it has a low RMSE.
5. If two models have similar goodness-of-fit, the one that passes through the horizontal and vertical error bars estimated in each data point will be selected.
6. If two models have similar goodness-of-fit and both functions pass through the horizontal and vertical error bars, then the one with the lowest amount of coefficients, that is the less complexed model will be selected.

Two potential functions met the selection criteria, namely the polynomial of second degree and the exponential model. However, the exponential function shows slightly better goodness-of-fit statistics (i.e. adjusted R-square closer to 1 and a lower RMSE), and therefore it was finally selected as the best fitting model. The mathematical expression of the model is defined in Equation 5.5. The estimated curve was plotted in Matlab and displayed in Figure 5.14.

Model	Expression	Good-of-fit statistics	
Polynomial (degree 2)	$f(x) = ax^2 + bx + c$	Adj. R-square	0.968
		RMSE	0.356
Exponential	$f(x) = a \cdot e^{bx}$	Adj. R-square	0.986
		RMSE	0.234

Table 5.4: Goodness-of-fit statistics.

$$Carfollowing : h(d) = 1.88 \cdot e^{0.01 \cdot d} \tag{5.5}$$

Where $h(d)$ is time headway as a function of water depth d.

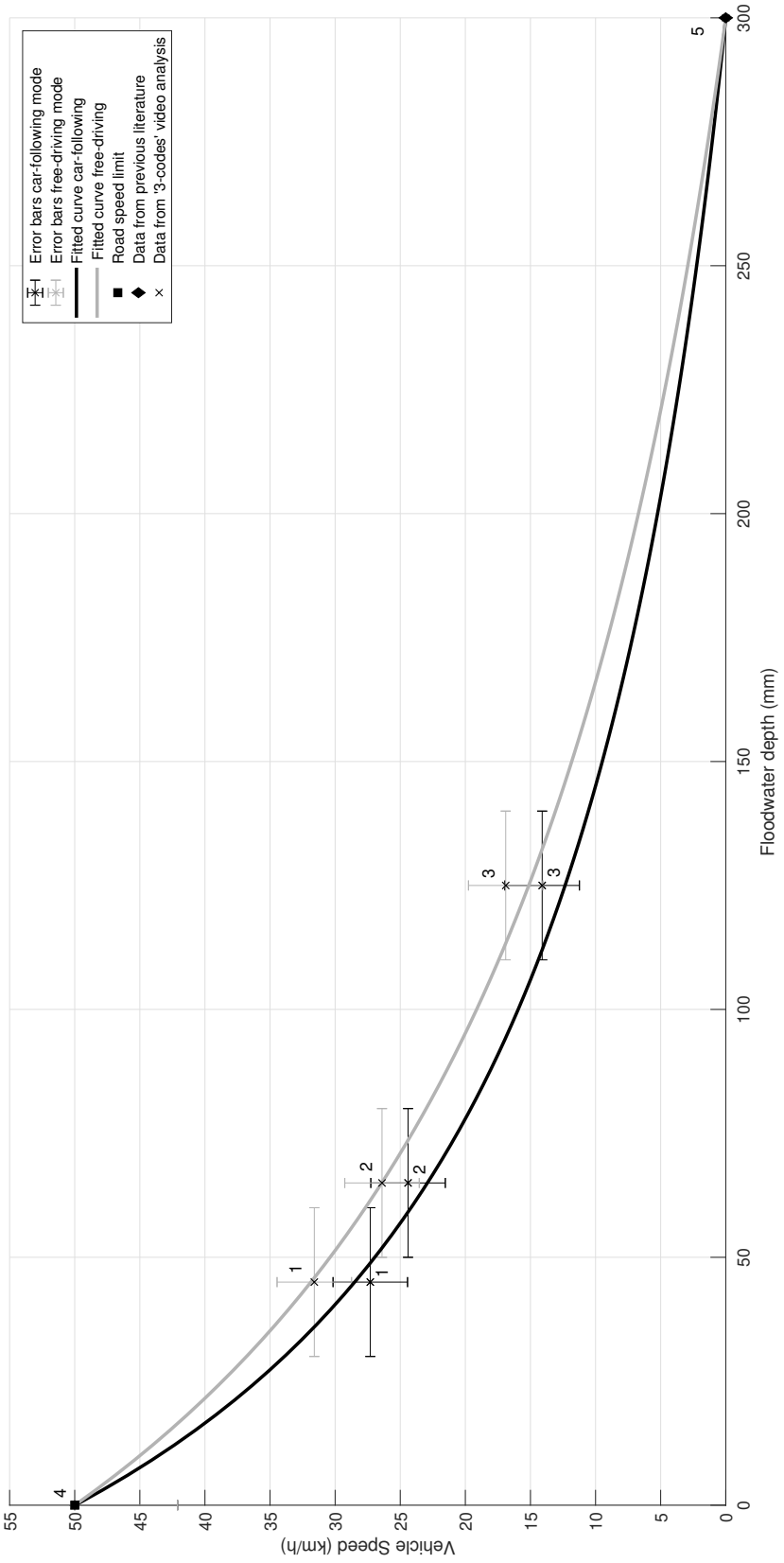

Figure 5.13: Speed-flood depth function for vehicles in car-following and free-driving modes.

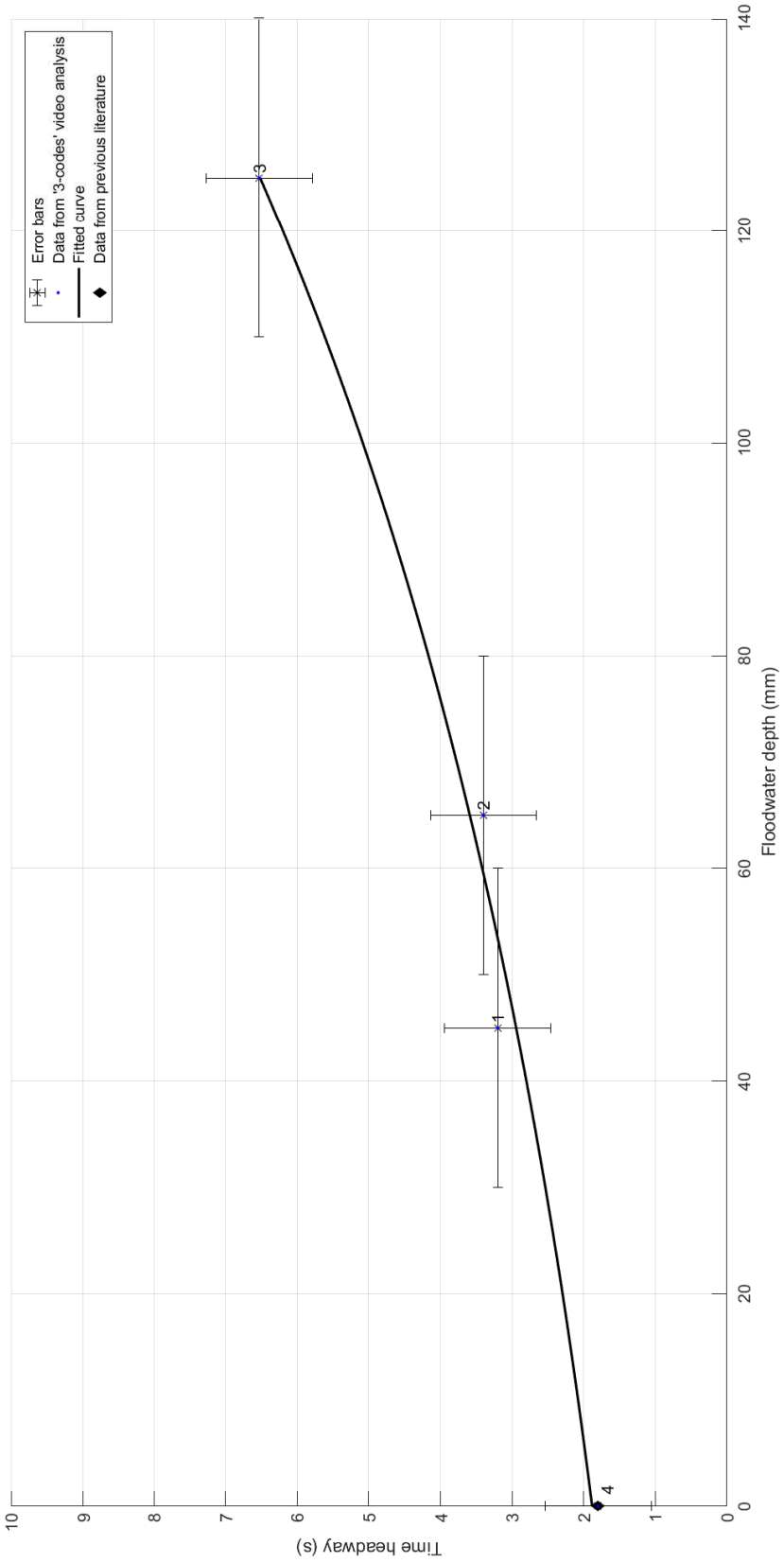

Figure 5.14: Headway-flood depth function for vehicles in car-following mode.

5.3 Macroscopic Analysis

As it is mentioned in Section 2.5 of the literature review, a large number of weather-related effects have been proved to influence driving behaviour, and hence traffic flow operations. In the past, many authors have done research on the impacts of weather conditions (e.g. rain, snow, fog, cold and high temperatures) on traffic flow parameters, specially on free-flow speed and capacity reduction due to heavy/light rain and snow. Some of these authors also estimated the fundamental diagrams of vehicles travelling under such conditions, by studying the changes in macroscopic traffic variables, namely average speed (u_i), flow (q_i) and density (k_i). According to [18], the fundamental diagram is the basis of macroscopic traffic simulation and a valuable tool for traffic management. However, to the best knowledge of the author of this thesis, there is no research available on the impacts of flooding conditions on traffic flow operations, and therefore the fundamental diagrams of vehicles driving through different flooding conditions have not been estimated yet. For the first time, this thesis applies a multilevel driving behaviour analysis to the data obtained through the 3SVAA to assess flooding impacts on macroscopic traffic parameters from the their microscopic counterparts studied in Section 5.1.

The outcome of this analysis is the estimation of the fundamental diagram's free-flow branches of vehicles travelling under different flooding depths. In doing so, the impacts of flooding conditions on free-flow speed and capacity can be estimated on road stretches with speed limit of 30 mph ($\approx 50km/h$). Nevertheless, due to the short data set obtained from the video analysis, the estimated macroscopic parameters should be considered as rough estimations and therefore should not be generalized in no case. That is also why a triangular fundamental diagram was adopted for the analysis since its approximation requires lower amount of data compared to other models.

First, it is explained how free-flow speed and capacity can be estimated based on the data set obtained from the video analysis. Secondly, it also explains how the triangular fundamental diagrams of vehicles travelling under different flooding depths are estimated based on macroscopic parameter values. The reader may see this section has been divided into two sub-sections corresponding to each of the videos analysed in the previous chapter, namely the A94 Perth Road and the A93 Isla Road stretch. Finally, the results obtained in this section are also compared to those found in previous studies on the impacts of adverse weather conditions on traffic flow operations.

5.3.1 Macroscopic Traffic Parameters

In order to define the uncongested branch of a triangular fundamental diagram, only two parameters need to be estimated, and those are the free-flow speed and the free-flow capacity, see Figure 3.5. Free speed or desired speed can be defined as the speed driven when the driver is not influenced by any other road user [54]. The free speed is influenced by characteristics of the vehicle, the driver, the road, road conditions such as weather and traffic rules, etc. The reader may see free speed depends on many factors that make the true value be unknown, and that is why estimation techniques are usually conducted to derive its value for a certain road and under pre-defined conditions. This is known as right censored data, since data points considered will always be below a certain value. A number of different approaches are available for estimating the free speed of a road under pre-defined conditions. However, all these methods require a larger data set than the one obtained for this multilevel analysis, so that an alternative estimation will be therefore conducted.

In this case, the free-flow speed has been estimated by averaging the speed of those vehicles that are in free-driving mode according to the car-following criteria introduced in Section 5.1. It is assumed that drivers who are not influenced by other road users are able to choose their

own speed for crossing the flooded stretches. Therefore, it is important to bear in mind that the free-flow speed is highly dependent on the situation captured on the videos, which is influenced by several aspects such as time period, road conditions, type of vehicles captured, etc. This means that it is important to be careful when it comes to the generalization of the macroscopic parameter values since the assumptions made can lead to biased estimations of free-speed on the road stretches subject of study.

The same applies to the estimation of the road stretch capacity. In general, the capacity of a traffic facility can be defined as the maximum hourly rate at which vehicles can be reasonably expected to traverse a cross-section of a roadway during a given time period under prevailing roadway, traffic and control conditions [54]. According to the *American Highway Capacity Manual* [69] any change in the prevailing conditions will result in a change in the capacity of the facility for a specific time period. Moreover, capacity is assumed to be of a stochastic nature due to the differences in individual driving behaviour and changing road, traffic and weather conditions. In order to estimate the capacity of a road stretch under prevailing conditions, data need to be collected at different road cross-sections, that is far and right upstream/downstream the location.

The reader may realize then that with the short data set obtained from the video analysis together with the impossibility of analysing traffic states at different cross-sections upstream and downstream the stretch, practically no solid conclusions can be drawn from the free-flow capacity estimations. Therefore once again, every estimated value should be taken only as a guide value.

5.3.2 Video 1: A94 Perth Road Stretch

Unfortunately in video 1, the camera's field of vision only captures the flooded stretch. This means that neither the road section upstream nor the one downstream the flooding are visible in the recording. As it is explained in the previous section, to estimate the free-flow capacity of a road stretch, information about the traffic estates upstream and downstream the location are required. As this information is not available, assumptions about traffic states will be made according to what is observed from the videos.

It is worth remembering that if a triangular shape of the fundamental diagram is assumed, the slope of the free-flow branch can be estimated either by using the free-flow speed or by defining the free-flow capacity point. For those vehicles driving on stretch 1-L (45 mm), only the free-flow speed can be estimated since there is not any evidence that shows the free-flow capacity is reached at any time along the video. Therefore, it is calculated by averaging the speed of those vehicles driving in free-mode, which is equal to $u_{1L} = 31.6\ km/h$ (see Table 5.1). Having this value, the slope of the uncongested branch of the triangular fundamental diagram can be drawn, yet with the information available the free-flow capacity point cannot be defined.

Notwithstanding, a fleet of 10 vehicles crosses the flooded stretch on the right lane at high speeds while keeping very short time headways. Indeed, these vehicles were travelling at an average speed of 27.71 km/h which is slightly higher than the average free-flow speed found in this lane, while keeping the shortest headways with their leaders according to the headway distribution shown in the microscopic analysis, that is an average value of 2.79 s. The street view option of *Google Maps* was used to find potential traffic elements (e.g. traffic lights, signs, pedestrian crossings...) that could cause a queue of vehicles upstream or downstream the location, yet none were found. Therefore, this group of 10 vehicles will be used to give a rough estimation of the free-flow capacity value of stretch 1-R under a flood depth of 65 mm.

Table 5.5 depicts the estimated values of macroscopic parameters at free-flow capacity that are used to approximate the free-flow branch of the triangular fundamental diagram of vehicles travelling through stretch 1-R under water depth of 65 mm. The fundamental relationships displayed in Table 3.2 are used to derive macroscopic variables from their microscopic counterparts.

Video	Flood depth	Traffic state	Avg. Speed (u)	Avg. Headway (h)	Flow (q)	Density (k)
1-R	65 ± 15 mm	Free-flow capacity	u_{1R}= 27.7 km/h	h_{c1}= 2.79 s	q_{c1}= 1292 veh/h	k_{c1}= 47 veh/km

Table 5.5: Macroscopic variables stretch 1-R.

The above table suggests two possible values of free-flow speed for those vehicles driving on stretch 2-L. The first one $u_{1R} = 26.4\ km/h$, obtained by averaging the speed of those vehicles driving in free-mode, while the second one $u_{1R} = 27.7\ km/h$ is obtained by deriving the mean speed of the fleet of vehicles crossing the stretch at capacity. Yet, the reader may see that the average speed value is practically the same. Therefore, the free-flow branch can be drawn having the average speed and headway of those vehicles crossing the stretch at free-flow capacity. Using the fundamental relationship, the flow at capacity (q_{c1}) and the critical density (k_{c1}) values can be obtained. Figure 5.15 depicts the estimation of the free-flow branches corresponding to stretch 1-L and 1-R. The first one is represented by a dashed arrow since it was not possible to define the free-flow capacity point, while the second one is depicted by a solid black line.

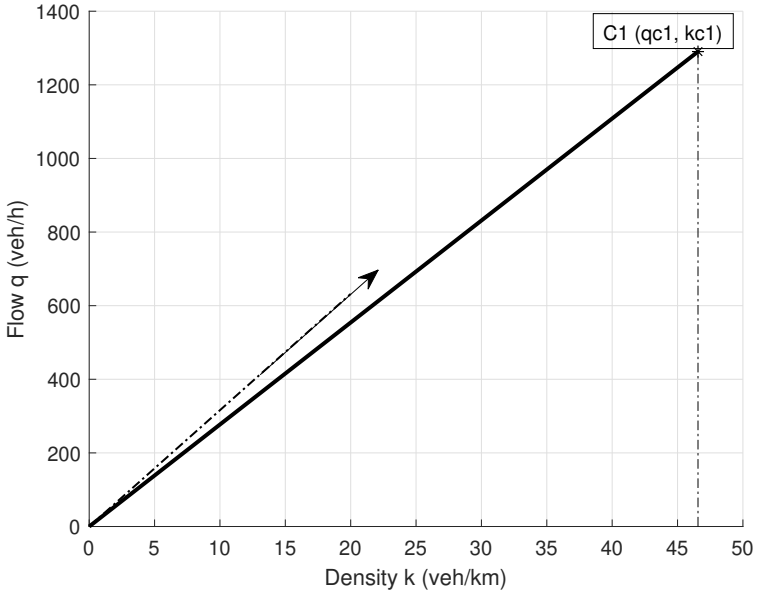

Figure 5.15: Free-flow branches of vehicles driving under 45 and 65 mm of flood depth.

5.3.3 Video 2: A93 Isla Road Stretch

Unlike video 1, in video 2 the camera's field of vision captures the cross-section right upstream the flooded stretch, and hence it enables the analyst to distinguish between different traffic scenarios that were already introduced in Section 5.1 and represented in Figure 5.3. When the

traffic demand on the road is lower than the capacity of the flooded stretch, vehicles are able to cross it in free-driving mode. The free-flow speed was estimated in the previous section and it is equal to $u_{2L} = 16.9\ km/h$. However, there is a certain instant in which a vehicle is blocking the passage as it seems to be waiting to the car coming on the opposite direction to leave the stretch free. This situation followed by an increase of traffic demand on the road leads to a queue of vehicles building upstream the flooded area, and hence vehicles traversing the stretch in car-following mode when the congestion releases. The average speed of vehicles crossing the stretch in car-following mode was calculated in the previous section and it is equal to 14.1 km/h. The reader may see this speed is lower than the free-speed (u_{2L}), which suggests that a capacity drops may exist when vehicles enter the flooding area. Therefore, using the time headways of those vehicles that are queueing upstream the location, the queue discharge rate (q_{d2}) and the critical density (k_{c2}) can be estimate using the fundamental relationship. Since it is assumed there is a critical density (k_{c2}) value for both the queue discharge rate and free-flow capacity, the capacity point (q_{c2}) can be found in the fundamental diagram at the intersection between the free-flow branch and a vertical line from the critical density value.

Video	Flood depth	Traffic state	Avg. Speed (u)	Avg. Headway (h)	Flow (q)	Density (k)
2-L	125 ± 15 mm	Q. discharge rate	u_{d2}= 14.1 km/h	h_{d2}= 6.53 s	q_{d2}= 552 veh/h	k_{c2}= 39 veh/km

Table 5.6: Macroscopic variables stretch 2-L.

Figure 5.16 depicts the free-flow branch of the triangular fundamental diagram of vehicles travelling under a flood depth of 125 mm on stretch 2-L, which has been estimated from the queue discharge rate value and the free-flow speed (i.e. slope of the uncongested branch). The free-flow capacity point is also highlighted in the figure and has a value of 661 veh/h approximately, practically half of the capacity found in stretch 1-R. The capacity drop estimated is equal to 16.5% in the most flooded stretch (i.e. 125 mm), while the free-flow capacity reduction compared to the second most flooded stretch (i.e. 65 mm) is equal to 49%.

5.3.4 Comparison with other studies

As it is explained in Section 2.5 of the literature review, several researchers have measured the extent to which traffic flow and capacity are affected by adverse weather conditions. Specially, studies have focused on investigating highway capacity and free-flow speed reduction due to heavy/light rain and snow compared to dry conditions. Less research can be found on the impacts of adverse weather conditions on urban roads. In [41], the authors give an estimation of road capacity and free flow speed in urban roads (with speed limit of 50 km/h) under different adverse weather conditions. This latter study together with the ones that analyse highway/freeway capacity and free-flow speed under adverse weather conditions, are used in this section for comparing the results obtained in the previous section.

Free-flow Speed comparison

The authors of [70] examined data collected at a four-lane section interstate freeway in Idaho (US) by using automatic traffic counters during both good and bad weather conditions. The authors provide an estimate of free-flow speed for a range of weather conditions (e.g. rain, snow, low visibility and wind) and compare it with the results obtained by other researchers. The authors derived a multiple regression free-flow speed model that indicate the individual effects of the weather variables on passenger-car speed. Pavement conditions were represented

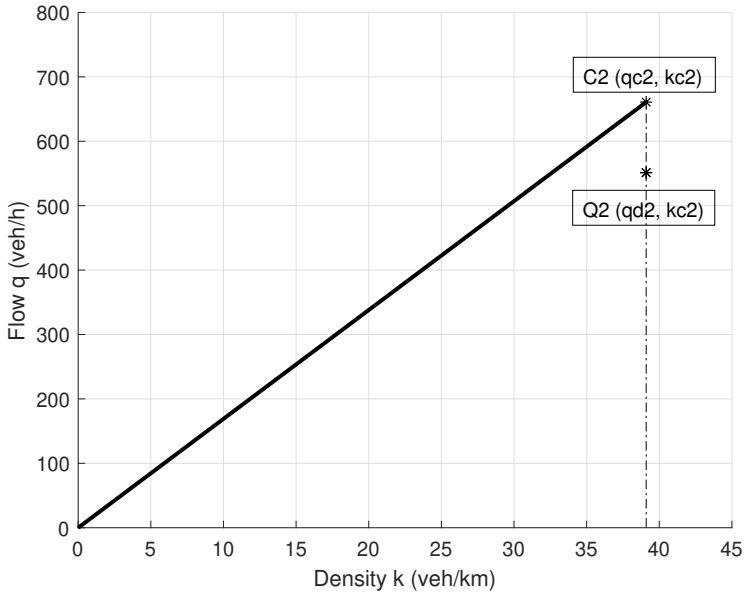

Figure 5.16: Free-flow branch of vehicles driving under 125 mm of flood depth.

by two indicator variables for wet or snow-covered pavement. Wind speed was represented as an indicator variable with 24 km/h as the critical wind speed, and finally visibility represented as a two-part function with a critical visibility of 0.28 km. From the model parameters one can see the effects of the various weather factors on passenger-car speed.

$$Speed = 100.2 - 16.4snow - 9.5wet + 77.3vis - 11.7win \tag{5.6}$$

A wet surface reduces the free-flow speed by 9.5 km/h, whereas a snow-covered surface reduces the speeds by 16.4 km/h. The reader may see that the authors do not further explain what do they considered as a 'wet' or 'snow-covered' surface. The model parameters also show that when the wind speed exceeds 24 km/h, the free-flow speed drops by an average of 11.7 km/h, and when visibility is lower than 0.28 km passenger-car speeds decline by 0.77 km/h for every 0.01 km below the critical visibility. Additionally, the authors provide a bar chart in which they compare their results with previous studies on the impacts of adverse weather conditions on free-flow speed.

Figure 5.17 depicts the free-flow speed reduction found in other studies together with the results obtained by [70]. In [71], the author studied the effects of rain and snow on speed-flow-occupancy relationship in a freeway in Canada using loops detectors, and they conclude that:

- Light rain caused a drop of 2 km/h.
- Light snow caused a drop of 3 km/h.
- Heavy rain caused a drop of 5 to 10 km/h.
- Heavy snow caused a drop of 38 to 50 km/h.

The authors of [39] argues that although the work of the latter authors are insightful, they used an extremely small data set, only 6 clear days, 2 rainy days and 2 snowy days. Therefore the first authors estimated the relationship between highway capacity and traffic speed on congested freeway in the Minneapolis - St. Paul (the Twin Cities) metropolitan area from a data set collected during a period of 4 years. From their results one can conclude that:

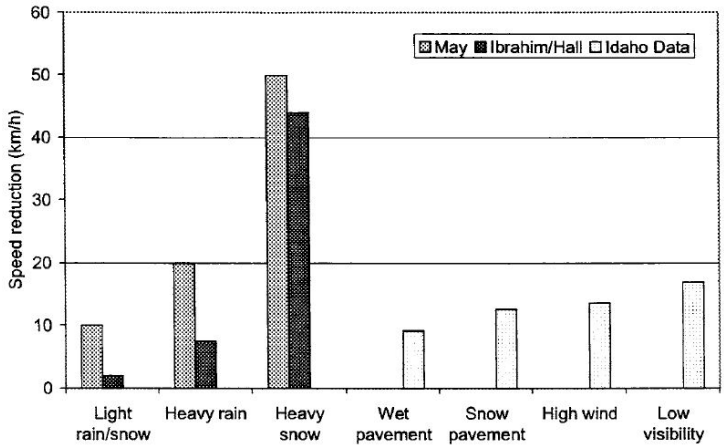

Figure 5.17: Speed reduction found by the authors under different weather conditions. [70].

- Light rain causes a drop of around 2 km/h approximately.
- Heavy rain causes a drop from 4.2 to 6.4 km/h approximately.
- Light snow causes a drop from 4.5 to 9 km/h approximately.
- Heavy snow causes a drop from 10 to 14.5 km/h approximately.

The reader may see both authors found similar speed reduction for light/heavy rain and light snow, yet there is a huge difference in the value found under heavy snow. The results found by [39] are more reliable since their data set is far larger than the one collected by [71]. Additionally, the above results come from data collected on highways or freeways with speed limits above 100 km/h. This thesis have analysed major road stretches in Perth, Scotland (UK) with speed limits of 30 mph (i.e. around 50 km/h). As it has been previously mentioned, the variation of free-flow speed and capacity depends on many other factors besides inclement weather conditions, and those are among others the distance selected by individual drivers which in turn depends on the type of vehicle and road. That is why the research of [41] is also included within this comparison as it studies free-flow speed and capacity variability on urban roads under rain and snow conditions. Data were collected using loop sensors on major roads with speed limit of 50 km/h in the approach of a signalized intersection in the urban area of Vienna (Austria). Two methods for estimating the capacity and free-flow were used by the authors, those are the product limit method for estimating the distribution of capacity, whilst a weighted harmonic mean (WHM) was utilized for estimating the free-flow speed.

The authors used two different methods for estimating the free-flow speed that provide similar results. First method uses single vehicle measurements and the time gap between consecutive vehicles, while the second one uses aggregated data. However, according to the authors, if the data is aggregated it is not possible to calculate time gaps, and therefore free-flow traffic situations are estimated by considering traffic flow observations. By doing so, only the mean speed of all the vehicles and the aggregated number of vehicles is known which does not allow to clearly determined the free-flow situations. Figure 5.18 displays the free-flow speed reduction based on the two different methods described above referred by the authors as 'gap' and 'flow'. Both methods show a reduction of free-flow speed under different conditions of rain and snow that are classified within the following categories:

– Category 1: no rain or snow.

– Category 2: rain intensity lower than 0.25 mm/h.

– Category 3: rain intensity higher than 0.25 mm/h and lower than 1 mm/h.

– Category 4: rain intensity higher than 1 mm/h and lower than infinite.

– Category 5: snow intensity higher than 0.2 $mm/2h$ and lower than 0.8 $mm/2h$.

– Category 6: snow intensity higher than 0.8 $mm/2h$ and lower than infinite.

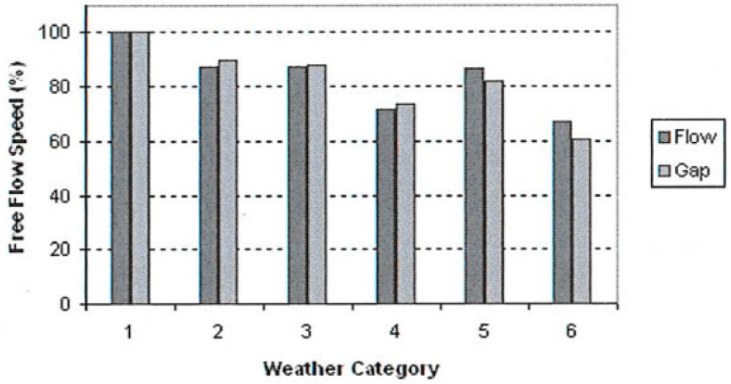

Figure 5.18: Reduction of free-flow speed based on 'Gap' and 'Flow' under different weather categories. Values are related to a free-flow speed of 42 km/h (100%). [41].

Categories 2 and 3 can be classified within light rain. However, the reader may see that the authors define one category in which the rain/snow intensity interval has an infinite end point. No need to say that the impact on rain conditions on free-flow speed will significantly change for high intensities. Therefore, it is not accurate to define a category that covers an infinite range of rainfall intensities.

According to the figure, there is a free-flow speed of 42 km/h in dry conditions, i.e. category 1. Speed drops practically the same, around the 10% of the speed in dry conditions for rainfall intensities of categories 2 and 3, which can be considered as light rain. For intensities above 1 mm/h and up to infinite the speed reduction with respect to dry conditions is around 30% of the speed in dry conditions. The highest drop corresponds to snow intensities above 0.8 $mm/2h$ up to infinite, around 60% of the speed in dry conditions (i.e. a drop of 16.8 km/h). Therefore, the free-flow speed reduction under different conditions of rain and snow can be presented as follows:

– No rain or snow: free-flow speed of 42 km/h.

– Light rain: free-flow speed drops around 4.2 km/h.

– Medium and heavy rain: free-flow speed drops around 12.6 km/h.

– Light snow: free-flow speed drops around 8.4 km/h.

– Medium and heavy snow: free-flow speed drops 16.8 km/h.

Figure 5.19 gathers the results of the above studies and includes the ones found in the macroscopic analysis conducted in this thesis. For those authors who provides a speed decrease interval, the average value is the one depicted in the figure. The flood depth categories 1, 2 and 3 correspond to a floodwater depth of 45, 65 and 125 $\pm$ 15 mm respectively. It is important to bear in mind that the free-flow speed reduction values under flood depth 1, 2 and 3 are calculated assuming the speed limit on Perth and Isla road stretches as the free-flow speed in dry conditions.

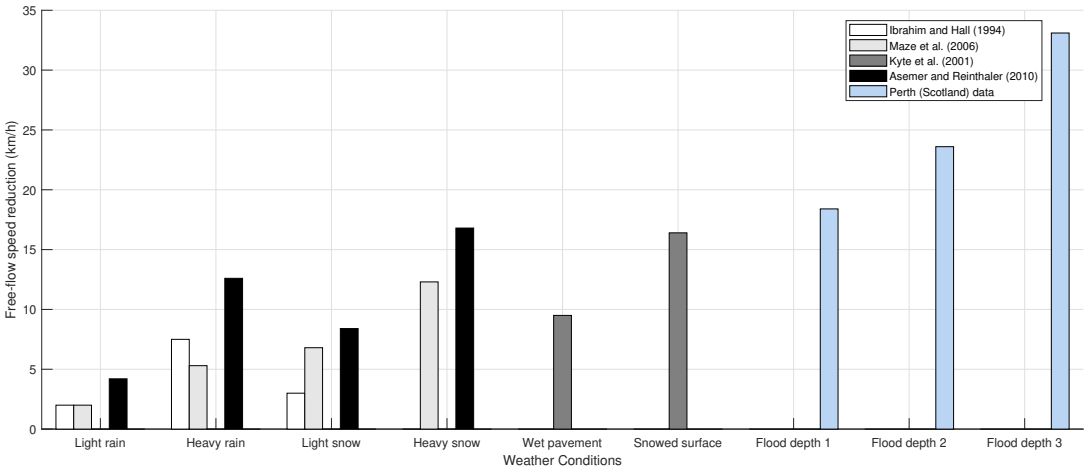

Figure 5.19: Free-flow speed reduction under different weather conditions.

It is important to be careful when comparing the results of the previous studies, since first they come from data collected across different types of roads (i.e. freeways, urban roads), having therefore different speed limits and road layout. Additionally, these studies were conducted in different countries so that regional differences may exist, and thus could have an influence on the free-flow speed variation. From the figure one may first realize that the speed reductions found by [41] under light/heavy rain and snow in an Austrian urban road are higher than those found by [39] in a US freeway under the same conditions. The reasons behind these results are unclear, yet regional differences, the type of road or the location where the data were collected could be potential factors affecting the speed reduction. The rainfall intensities measured in both studies were similar, and the data collection technique conducted to measure speed was the same (loops detectors).

According to the figure, the impact of heavy snow on passenger-car speed found by [41] is practically the same as the one found in this thesis under a flood depth of 45 $\pm$ 15 mm, lying between 15 and 20 km/h. These results are also similar to the speed decrease found by [70] due to snowed-covered surface. However, the latter authors do not provide any measurement of the height of snow under that category, which makes the estimation to be quite uncertain. The same occurs to the speed reduction caused by wet pavement, in which the authors do not provide with any indication of water depth. If these authors refer to 'wet pavement' as the state of the asphalt right after precipitation takes place, then the speed reduction seem to be in line with the results found in this thesis; average vehicle's speed decreases when flooding conditions become more severe.

From the figure one can clearly see that the highest impact on free-flow speed was found by [71] and it occurs under heavy snow resulting in a speed decrease from 38 to 50 km/h in a Canadian freeway. Yet, [39] conclude in their study that the latter authors used an extremely small set of data, which could have made the results being biased. The speed reduction found by the

latter authors under heavy snow in a US freeway is less than half of the speed drop found by the first ones and it lies between 10 and 14.5 km/h, which is considered as a more reasonable value. Therefore, removing the speed decrease value estimated by [71] under heavy snow from the comparison, one can see that flooding causes the highest impacts on vehicle's speed among the different weather conditions, with the highest speed drop of 33.1 km/h at 125 mm of water depth.

Free-flow Capacity comparison

The authors of [39] provides an estimation of the highway capacity reduction due to different adverse weather conditions. From the observations, the authors illustrate (not taken from actual data) the pattern that could be expected when the leading edge of the uncongested portion of occupancy and flow data plots are taken during clear weather, and then data taken during increasingly more severe weather (e.g. rain and snow).

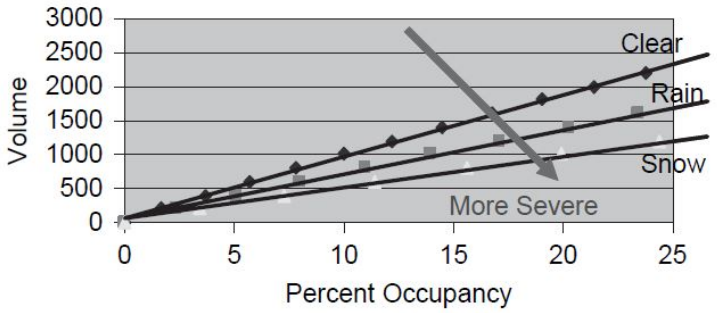

Figure 5.20: Occupancy and flow relationship as weather becomes more severe. [39]

From the above figure, one can clearly see how the slope of the uncongested branch (i.e. free-flow speed) decreases as the weather becomes more sever. Those are drivers reducing their speed and increasing the time headway, leading to a flow reduction and thus a reduced highway capacity. This is also in line with the results found in the macroscopic analysis, which are depicted in Figure 5.21. It can be seen the uncongested branch of the triangular fundamental diagram becomes less steep with an increase of flood depth. There is a clear increase of vehicles headway (or density reduction) as the road becomes more flooded, which yields to a decrease of the free flow capacity value. According to the figure, the free-flow capacity drops around 48% when flooding depth increases from 65 mm to 125 mm, which is equals to a reduction of around 631 veh/h.

Figure 5.22 was included in the study of [39], where one can see the results of capacity and speed reduction during rain and snow of increasing intensity. According to the authors, these results are in line with those reported in the *Highway Capacity Manual* [69]. They found that heavy rains (more than 6.35 mm/h) reduce freeway capacity by an average of 14%, whilst heavy snows (more than 12.7 mm/h) cause the highest impact lowering the capacity by an average of 22% compared to clear conditions. That is approximately a drop of 326 veh/h during heavy rain and a decrease of 517 veh/h under heavy snow. One can see that the capacity drop found in this thesis when flooding depth increases from 65 mm to 125 mm is more than double the one found by [39] in US freeways under heavy snow.

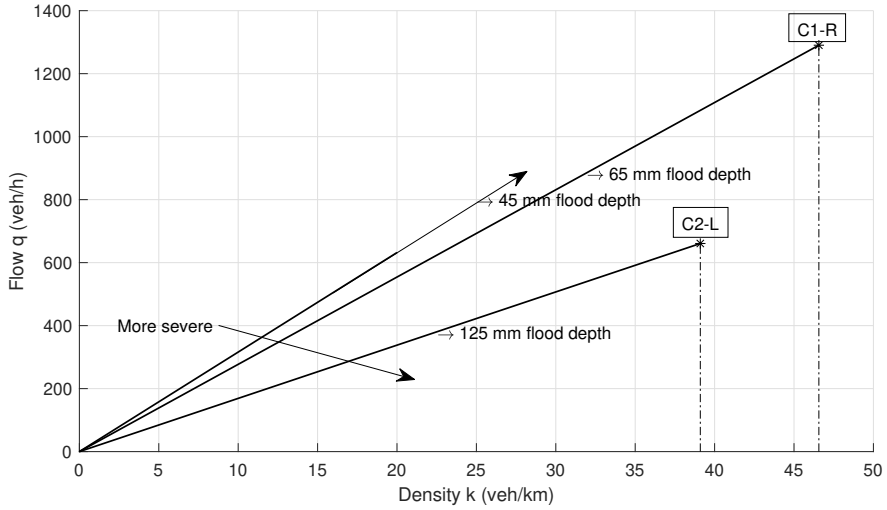

Figure 5.21: Free-flow branches of vehicles driving under different flooding depths.

Weather Variable	Intensity	Capacity (vph)	Percent Reduction Compared to Clear	Speed (mph)	Percent Reduction Compared with Clear
Rain	0	2318		66.2	
	0–0.01 in./h	2272	2	64.9	2
	0.01–0.25 in./h	2152	7	63.6	4
	>0.25 in./h	1992	14	62.2	6
Snow	0	2318		66.2	
	≤0.05 in./h	2220	4	63.4	4
	0.06–0.1 in./h	2117	9	60.7	8
	0.11–0.5 in./h	2064	11	59.9	9
	>0.5 in./h	1801	22	57.2	13

Figure 5.22: Average impact of weather on freeway capacity and speed. [39]

5.4 Main Findings & Discussion

In this chapter and for the first time, a multilevel analysis approach has been conducted to study driving adaptation effects under flooding conditions at two complementary levels, namely microscopic and macroscopic level. First, a microscopic analysis was accomplished using disaggregate traffic data obtained from the video analysis conducted in the previous chapter, and subsequently the study was extended to a macroscopic level. This allowed to analyse the impacts of flood depth on free-flow speed and capacity, and therefore to estimate part of the fundamental diagrams of vehicles travelling under 45, 65 and 125 mm $\pm 15mm$ water depth. Furthermore, two separate functions that relate average vehicle's speed and average headway with water depth were estimated providing traffic practitioners with the possibility of including driving adaptation effects under flooding conditions within microscopic traffic simulation models.

However, it is important to note the short data set used in this multilevel analysis, which is the results of having analysed videos of short duration (from 2 to 5 minutes video). Therefore, the reader must be sceptical with the results derived from the analysis since, among other reasons they could not be proved to be statistically significant. With a much larger data set, the empirical distributions of speed and time headways under the three flood depths can be determined, so that they can be modelled on the basis of an analytical model in order draw more reliable conclusions from the comparison between different flooding conditions. This type of study can be found in [18] in which a statistical analysis of the time headway distribution

under dry and rainy conditions is conducted. In that study, the authors collected individual data from a total of 66,271 vehicles in dry conditions, 52,870 vehicles in light rain and 22,642 vehicles in medium rain using double loop sensors.

Therefore, it is important to be very careful when it comes to the generalization of the conclusions drawn from this analysis. Notwithstanding, this is the first time a multilevel driving behaviour analysis under flooding conditions is accomplished, and therefore should be seen as a methodological guide for carrying out future research on micro and macroscopic driving behaviour under flooding conditions.

Although changes in microscopic parameters could not be proved to be statistically significant, the speed and headway frequency distributions clearly show that flood depth influences microscopic parameters; drivers tend to reduce their speed and increase time headways with respect to their leaders as the flooding conditions become more severe. In the less flooded stretch (45 mm), an average headway value of 3.20 s is found, whereas a value of 3.40 s is obtained in the second stretch (65 mm). Finally, an average headway value of 6.53 s is found in the third and most flooded stretch (125 mm). The short difference between stretch 1 and 2 of only 20 mm in flood depth might explain the small discrepancy between the average headway values. In stretch 3 however, the flood depth is almost double than in the second with an increase of the average headway of 3.13 s.

In the speed analysis, the lowest speed values correspond to those vehicles travelling through the most flooded stretch, ranging from 5 to 19.6 km/h. The average speed values of vehicles travelling in car-following and free mode on the most flooded stretch are equal to 14.1 and 16.9 km/h respectively. An increase of approximately 10 km/h is found when the flood depth reduces to 65 mm for vehicles travelling in both driving modes. A small speed increase is though observed when the flood depth reduces to 45 mm, being the average speed equals to 27.3 km/h for those vehicles in car-following mode and 31.6 km/h for those in free-driving mode. In other words, there is a free-flow speed drop of 16.5% when flood depth goes from 45 to 65 mm, whereas a drop of 36.0% exists when flood depth goes from 65 to 125 mm.

The average speed and headway values found under the three flood depths, together with data from literature were used to estimate two functions that correlate average vehicle speed and headway with water depth. In the speed case, two curves corresponding to vehicles driving in car-following and free-mode were estimated over a flood depth interval ranging from 0 mm (dry conditions) to 300 mm (threshold value at which vehicles start floating). After an graphical and empirical goodness-of-fit assessment, the reverse polynomial model turned to be the best fit (see equations 5.3 and 5.4). In the headway case however, only one curve was estimated corresponding to those vehicles driving in car-following mode over a flood depth that ranges from 0 mm (dry conditions) to 125 mm. Unlike vehicle speed, time headway increases exponentially when flooding conditions become more severe (see equation 5.5). The significance of these curves is that they can be used to develop/adapt microscopic models needed for simulating the impacts of flooding on road traffic. As it is explained in the introductory chapter of this thesis, several authors have attempted to introduce driving adaptation effects under flooding conditions within microscopic models in order to simulate road traffic under such conditions.

With this purpose in mind, [2] already estimated a depth-disruption function that relates flood depth to traffic speed (see Figure 2.6) by fitting a second degree polynomial function to data from previous experimental studies, safety literature, expert's opinion and data collected by observing videos. Besides, the authors use data that were collected in different types of roads (e.g. motorways, major roads) and across different countries. The reader may realize that average vehicle speed varies considerably depending on the type of road and country in which it is measured. Moreover, the polynomial function was discarded from the analysis as it does not meet the criteria established by the author of this thesis; the function does not strictly decrease

along the flood depth interval from 0 to 300 mm. Instead, it reaches the minimum speed value around 250 mm, while according to the criteria the average speed must be equal to 0 km/h at the threshold value of 300 mm (see Figure 5.12).

Subsequently, the study was extended to the macroscopic level by using the fundamental relationship that correlates macroscopic variables with their microscopic counterparts. This allowed to assess the impacts of flood depth on macroscopic traffic parameters, namely free-flow speed and capacity, and therefore to estimate the free-flow branches of the triangular fundamental diagrams. Due to the scarce data obtained from the video analysis combined with the short camera's field of view, the author could not analyse traffic states at different cross-sections upstream and downstream the flooding. This is necessary in order to give a reliable estimate of the free-flow capacity and speed of a road stretch. Therefore, the reader should be careful when it comes to the generalization of the outcomes.

The estimated free-flow branches of the triangular fundamental diagrams of vehicles travelling under three different flood depths are included in Figures 5.15 and 5.16. In Perth Road stretch, the camera only captured the waterlogging, and hence it was not possible to estimate the capacity point in stretch 1-L. However, in stretch 1-R the free-flow capacity could be estimated from a fleet of 10 vehicles that crosses the stretch at the highest speed while keeping the shortest headways according to the frequency distributions. The free-flow capacity estimated in a major road stretch of approximately 50 km/h under a flood depth of 65 mm is equal to 1,292 veh/h. In the second video however, the camera captures the road section right upstream the flooding which allowed to derived the queue discharge rate when vehicles enter the flooding. A value of 552 veh/h is obtained, which in turns enabled to define the capacity point of stretch 2-L at 661 veh/h. This yields to a capacity drop of 16.5% when flood depth increases from 65 to 125 mm. Additionally, a free-flow capacity reduction of almost the 50% is obtained with this increase of flood depth.

The majority of research carried out on the impacts of adverse weather phenomena on traffic flow operations provide the free-flow speed and capacity drop under predefined weather conditions compared to dry conditions. In order to compared the results obtained in this thesis with previous studies, the author has derived the free-flow speed drop taking place under the three flood depths compared to dry conditions, assuming that the average speed at 0 mm of water depth is equal to the speed limit of the road stretch ($\approx 50km/h$). Unfortunately, the author did not dispose of any video of vehicles travelling under dry conditions on those, so that the average free-flow speed in such conditions could not be proved to be 50 km/h. The results however, seem to be in line with those found in previous studies under different weather conditions, although the majority collected data on motorways/freeways and not on urban roads. Only one research was found that studies the impacts of rain and snow on an urban road with speed limit of $50km/h$. Therefore, one should be careful when comparing these results since neither regional differences nor the road layout effects are included in the analysis.

The free-flow speed drop of 18.4 km/h found under a flood depth of 45 mm is higher than the one found by [70] under 'wet pavement' (9.5 km/h) in a US freeway, and very similar to the speed drop under 'snowed-covered surface' found by the same authors (16.4 km/h). This latter value is practically the same as the one found by [41] in an Austrian urban road under heavy snow (16.8 km/h). This suggests that snowy conditions could have similar effects on free-flow speed than flooding conditions with water depth of 45 mm. Furthermore, a speed drop of 23.6 km/h and 33.1 mm are found under floodwater depths of 65 and 125 mm respectively, being the latter one the weather condition that causes the highest impact on free-flow speed among those studied in the past.

Finally, the free-flow capacity reduction found in previous studies under heavy rain and snow varies between 15% and 30% in motorways/freeways, which is much lower than the 49% found in this thesis when flood depth increases from 65 to 125 mm. Nonetheless, it was shown that vehicles almost go to standstill and crossing the most flooded stretch at a very low speed while keeping large headways. This yields to a steeper decline of density and flow compared to the one that could be observed in a motorway under rain or snow conditions, where vehicles are travelling at higher speeds while keeping shorter headways.

Chapter 6

Conclusions & Suggestions for Future Research

Flooding events as a result of intense precipitation, is one of the predominant causes of weather-related disruption to the transport sector in urban cities. According to several climate scenarios, heavy rainfall events will become more frequent and intense in the future leading to more severe flooding across urban cities. Transportation systems are the backbone of modern societies, and therefore ensuring their resilience against adverse weather conditions has become an essential aspect of governing and managing sustainable cities. Therefore, transportation networks need to be designed and managed in such a way that operate during and after adverse weather conditions occur. That is why flood risk professional and urban planners need firstly to understand the impacts of flooding, and secondly predict those impacts in order to build flood resilient cities.

With the advent of transport simulation models, experts are able to predict the geographic location, severity and impacts of flooding events on the road network. This allows to test resilience measures and traffic strategies to efficiently cope with the impact of flooding events, and hence returning the road network performance to nearly initial levels. These model techniques essentially combine a flood simulation model and a microscopic traffic simulation for modelling the impacts of flooding on the road network. However, this microscopic models require the study of driving adaptation effects under flooding conditions, which in turns required to collect microscopic traffic data in such conditions. Just a few authors have attempted to study microscopic driving behaviour under flooding conditions, yet according to the author of this thesis they have used data collection techniques that are highly questionable in terms of suitability for the type of data to be acquired. Therefore, this thesis provides with a new methodology that combines an alternative data collection technique together with a multilevel approach analysis to study driving adaptation effects under flooding conditions at two complementary levels, namely microscopic and macroscopic level.

To do so, first a video analysis procedure called the *'3-Step Video Analysis Approach'* (3SVAA) implemented in Matlab was developed by the author to extract microscopic traffic data from video recording that show vehicles driving under different flooding conditions (i.e. flood depths). This brings to the answer of the first research question proposed in this study:

How can microscopic traffic data (i.e. vehicle speed, time headways and spacing) of individual vehicles travelling through flooding be obtained?

Besides, a data collection plan was conducted in the home town of the author of this thesis (Granada, Spain) in order to define the speed error committed by the 3SVAA when it comes to measure vehicle's speed. A speed measurement error equal to $\pm 2.86 km/h$ was estimated at a confidence level of 95%. Unfortunately, due to lack of equipment and necessary devices, it was not possible to measure neither time headways nor spacing during the data collection activities. However, a manual frame-by-frame analysis technique was carried out to estimate the time headway measurement error. It is found that the maximum time headway error committed by the 3SVAA is equal to $\pm 0.74 s$ at a confidence level of 95%. The latter technique is not precise when it comes to measure vehicle spacing, since the authors did not dispose of the real size of objects displayed on the videos in order to build an scaled grid. Therefore, the spacing measurement error could not be defined, and that is the reason why this variable was not used in the microscopic and macroscopic analysis. Nonetheless, nowadays more vehicles are equipped with sensors and/or cameras that measure the distance with the vehicle in front, which would allow to easily collect spacing data in the field. In doing so, the spacing measurement error could be defined the same way the speed measurement was estimated. This will be accomplished in future studies.

From the microscopic traffic data (i.e. vehicle speed, time headways and spacing) obtained by means of the 3SVAA, changes in those parameters can be analysed at different flood depths, and then the study can be extended to the macroscopic level through a multilevel analysis approach by correlating macroscopic variables with their microscopic counterparts. This enables to analyse the impacts of flooding conditions on macroscopic variables, namely the free-flow speed and capacity, which in turns allows to estimate part of the fundamental diagrams of vehicles driving through flooding. In the past, several authors have studied the impacts of adverse weather conditions on traffic flow operations by analysing changes in the relationships between macroscopic variables through the use of the classical fundamental diagram. However, the majority of these studies focuses on the impacts of day-to-day weather conditions such as light/heavy rain or snow. The author of this thesis therefore realized that there is no research available on the impacts of floodwaters on macroscopic variables, and therefore no one has provided with an estimate of the fundamental diagram of vehicles driving through predefined flooding conditions.

The proposed methodology was implemented through an empirical study that consisted on analysing by means of the 3SVAA two videos of vehicles crossing three waterlogged stretches part of the A94 and A93 major roads in Perth, Scotland (UK). In doing so, individual traffic data were extracted at three different flood depths (45, 65 and 125 mm), so that changes in microscopic variables (i.e. vehicle speed and headways) were analysed at the three water depths. This brings to the answer of the second research question:

What changes in microscopic variables (i.e. vehicle speed and time headways) occur when vehicles travel under different flood depths?

From the microscopic data extracted, the speed and time headway frequency distributions were plotted, reflecting an increase of headways and a decrease of speed when flooding conditions become more severe, that is with an increase of flood depth. The lowest speed values correspond to those vehicles driving through the most flooded road stretch (125 mm), whereas the largest speeds correspond to those driving through the less flooded stretch (45 mm). A limitation of this analysis is the small data set extracted from the videos of Perth, which is the result of their short duration. Therefore, the reader must be sceptical with the results derived from the analysis since, among other reasons they could not be proved to be statistically significant. With a larger data set, the empirical distributions of speed and time headways under the three

flood depths can be determined, so that they can be modelled on the basis of an analytical model in order draw more reliable conclusions from the comparison between different flooding conditions.

By using the average speed and time headway values found at different flood depths combined with more data from literature, two functions were estimated that correlate average vehicle speed and headway with floodwater depth. Those essentially are fitted curves to the data points, which in the speed case two curves are plotted corresponding to vehicles driving in car-following and free-mode. To the best knowledge of the author of this thesis, this is the first time that a relationship between depth of standing water and time headways is developed and represented in a function. Both a graphical and empirical goodness-of-fit assessment were conducted and it is found that vehicle's speed decreases in the flood depth interval [0-300 mm] following a reverse polynomial function. In contrast, it is found that time headway increases exponentially in the flood depth interval [0-125 mm]. The significance of these curves is that they can be used to develop/adapt microscopic models needed for simulating the impacts of flooding on road traffic. As it is explained in the introductory chapter of this thesis, several authors have attempted to introduce driving adaptation effects under flooding conditions within microscopic models in order to simulate road traffic under such conditions.

Subsequently, the study was extended to the macroscopic level through the multilevel analysis approach that correlates macroscopic variables with their microscopic counterparts. This led to the answer of the third research question:

How can macroscopic traffic variables (i.e. average speed, flow and density) of vehicles travelling through flooding be obtained from their microscopic counterparts?

This enabled to assess the impacts of flood depth on macroscopic traffic parameters, namely free-flow speed and capacity, and therefore to estimate the free-flow branches of the triangular fundamental diagrams of vehicles travelling under three flood depths (i.e. 45, 65 and 125 mm). It is found that the uncongested branches become less step with an increase of flood depth. The free-flow speed drops by 16.5% when flood depth increases from 45 to 65 mm, and by 36.0% when flood depth goes from 65 to 125 mm. Besides, a free-flow capacity reduction of the 49% is found when flood depth increases from 65 to 125 mm due to a substantial decrease of vehicle's speed and an increase of headways when flooding conditions are more severe. Finally, it was only possible in the most flooded stretch to estimate the discontinuity in the fundamental diagram or capacity drop equals to 16.5% between the free-flow capacity and the queue discharge rate. This brings to the answer of the fourth and last research question proposed in this thesis:

What changes in macroscopic traffic parameters (i.e. free-flow speed and capacity) occur when vehicles travel under different flood depths?

As it has been mentioned along the thesis, a major limitation of this research is the short data set obtained from the video analysis. A total of 51 vehicles trajectories are extracted by applying the 3SVAA to the videos of Perth. This is the result of having analysed short videos (i.e. between 2 and 5 minute videos). From the vehicle's trajectories, microscopic traffic data (i.e. vehicle speed, time headways and spacing) were extracted at different locations along the stretch. However, this was not enough to conduct a statistical analysis of the results, which would have led to more reliable conclusions when comparing changes in microscopic parameters under different flood depths. Therefore, the results obtained from the empirical study should be taken as a guide values. Notwithstanding, the aim of this research is to provide with a systematic methodology to study driving adaptation effects under flooding conditions at both microscopic and macroscopic levels, and hence this study should be taken as a methodological guide to conduct future research on the topic.

The aim of future research on this topic should focus on the collection of a larger data set in order to statistically prove changes in micro and macroscopic parameters under different flood depths. A data set of around hundred vehicles per road stretch should be enough to conduct a statistical analysis of the results, which would allow to draw more solid conclusions. With the advent of machine learning, real time object detection algorithms could be used to automatically track vehicles, simplifying the video analysis process enormously. This would allow the analyst to obtain in an effortless way a higher number of vehicle's trajectories in less time. Additionally, the human error committed when tracking the vehicles manually along the road stretch will be removed. However, these algorithms are implemented in more advanced programming languages that require the analyst to have some previous experience before its use. If this is the case, the objective would be then to record videos of larger duration using cameras with wider field of view strategically placed at the site in order to capture the road sections upstream and downstream the flooding.

In doing so, more accurate values of free-flow speed, capacity and queue discharge rate will be estimated, allowing to complete the entire fundamental diagram of vehicles travelling through predefined flooding conditions. Therefore, if a single camera does not provide with the whole picture, multiple recorders should be installed. It is essential to capture different traffic states (i.e. free-flow conditions and congestion) in order to obtain enough data that allow to estimate the complete fundamental diagrams. Furthermore, video cameras should be placed on different types of roads (e.g. motorways, urban roads, local roads...) and across different countries. This will allow to include regional differences within the analysis. Besides, it is important to distinguish between peak hours and non-peak hours as well as classify vehicles according to their sizes. The cameras could be mounted in side firing poles or overhead together with radars that measure vehicle speed and headways in order to conduct a more accurate validation of the measurements. As it is explained in the methodology of this thesis, the advantage of video analysis is that it enables to visualize unexpected actions that drivers can undertake when adverse conditions become more severe, providing insightful information to study driver's behaviour under such conditions. It is worth noting the camera should be placed within a protective case to prevent damage from extreme weather and to avoid vandalism and theft. Besides, through the use of hydrologic simulation models, hot spots can be easily identified across the road network before the flooding takes place. Finally, depth gauges should be placed at the site in order to provide with more accurate measurements of flood depth along the road stretch.

Finally, if more studies are conducted in the future, the average speed and headway functions estimated in this thesis can be validated. If new average values of speed and headway are derived at different flood depths, they can be plotted on these functions to verify whether the reverse polynomial and exponential models are indeed the best fit to the data points. A graphical and empirical assessment should be again conducted, and in case new data suggest a change of the type of curve, then new models need to be proposed. More data will also allow to define the shape of the headway function within the interval [125-300 mm] which could not be defined in this research due to lack of data. It is important to verify if time headways continue increasing after a flood depth of 125 mm with the aim of finding the maximum value of this function. Validating the models proposed in this thesis is essential in order to provide traffic practitioners with more accurate curves to be introduced within microscopic models for simulating road traffic under flooding conditions. This will enable experts to evaluate complex traffic situations, so that new traffic strategies can be designed to counter the impacts of adverse weather events, and therefore building more resilient transport systems.

"Muchas son las criaturas del mundo que ven, menos las que miran, pocas las que observan y señaladas las que experimentan"

Jorge Wagensberg

Bibliography

[1] J. Clark and G. Daigle, "The importance of simulation techniques in its research and analysis," in *Winter Simulation Conference: Proceedings of the 29 th conference on Winter simulation*, vol. 7, pp. 1236–1243, Citeseer, 1997.

[2] M. Pregnolato, A. Ford, S. M. Wilkinson, and R. J. Dawson, "The impact of flooding on road transport: A depth-disruption function," *Transportation research part D: transport and environment*, vol. 55, pp. 67–81, 2017.

[3] E. Hooper, L. Chapman, and A. Quinn, "The impact of precipitation on speed–flow relationships along a uk motorway corridor," *Theoretical and applied climatology*, vol. 117, no. 1-2, pp. 303–316, 2014.

[4] T. Cresswell, *On the move: Mobility in the modern western world*. Taylor & Francis, 2006.

[5] R. Faturechi and E. Miller-Hooks, "Measuring the performance of transportation infrastructure systems in disasters: A comprehensive review," *Journal of infrastructure systems*, vol. 21, no. 1, p. 04014025, 2014.

[6] B. Arkell and G. Darch, "Impacts of climate change on london's transport systems," in *Proceedings of The Institution of Civil Engineers-Municipal Engineer*, vol. 159, pp. 231–237, 2006.

[7] M. J. Hammond, A. S. Chen, S. Djordjević, D. Butler, and O. Mark, "Urban flood impact assessment: A state-of-the-art review," *Urban Water Journal*, vol. 12, no. 1, pp. 14–29, 2015.

[8] M. Snelder and S. Calvert, "Quantifying the impact of adverse weather conditions on road network performance," *European Journal of Transport and Infrastructure Research*, vol. 16, no. 1, 2016.

[9] J. Yin, D. Yu, Z. Yin, M. Liu, and Q. He, "Evaluating the impact and risk of pluvial flash flood on intra-urban road network: A case study in the city center of shanghai, china," *Journal of hydrology*, vol. 537, pp. 138–145, 2016.

[10] S. N. Jonkman and I. Kelman, "An analysis of the causes and circumstances of flood disaster deaths," *Disasters*, vol. 29, no. 1, pp. 75–97, 2005.

[11] G. FitzGerald, W. Du, A. Jamal, M. Clark, and X.-Y. Hou, "Flood fatalities in contemporary australia (1997–2008)," *Emergency Medicine Australasia*, vol. 22, no. 2, pp. 180–186, 2010.

[12] Z. Zheng, J. B. Lee, M. Saifuzzaman, and J. Sun, "Exploring association between perceived importance of travel/traffic information and travel behaviour in natural disasters: A case study of the 2011 brisbane floods," *Transportation Research Part C: Emerging Technologies*, vol. 51, pp. 243–259, 2015.

[13] D. for Transport, *Transport Resilience Review:A review of the resilience of the transport network to extreme weather events*. Department for Transport, Great Minster House 33 Horseferry Road, London SW1P 4DR, United Kingdom., 2014.

[14] P. M. Murray-Tuite, "A comparison of transportation network resilience under simulated system optimum and user equilibrium conditions," in *Proceedings of the 2006 Winter Simulation Conference*, pp. 1398–1405, IEEE, 2006.

[15] K. Pyatkova, A. S. Chen, S. Djordjević, D. Butler, Z. Vojinović, Y. A. Abebe, and M. Hammond, "Flood impacts on road transportation using microscopic traffic modelling techniques," in *Simulating Urban Traffic Scenarios*, pp. 115–126, Springer, 2019.

[16] B. Su, H. Huang, and Y. Li, "Integrated simulation method for waterlogging and traffic congestion under urban rainstorms," *Natural Hazards*, vol. 81, no. 1, pp. 23–40, 2016.

[17] J. Zhu, Q. Dai, Y. Deng, A. Zhang, Y. Zhang, and S. Zhang, "Indirect damage of urban flooding: Investigation of flood-induced traffic congestion using dynamic modeling," *Water*, vol. 10, no. 5, p. 622, 2018.

[18] R. Billot, N.-E. El Faouzi, and F. De Vuyst, "Multilevel assessment of the impact of rain on drivers' behavior: standardized methodology and empirical analysis," *Transportation research record*, vol. 2107, no. 1, pp. 134–142, 2009.

[19] S. N. Jonkman, "Global perspectives on loss of human life caused by floods," *Natural hazards*, vol. 34, no. 2, pp. 151–175, 2005.

[20] M. Gad-el Hak, *Large-scale disasters: prediction, control, and mitigation*. Cambridge University Press, 2008.

[21] R. G. Hoogendoorn, B. van Arem, and K. A. Brookhuis, "Longitudinal driving behavior in case of emergency situations: an empirically underpinned theoretical framework," *Procedia-Social and Behavioral Sciences*, vol. 80, pp. 341–369, 2013.

[22] M. Snelder, H. Van Zuylen, and L. Immers, "A framework for robustness analysis of road networks for short term variations in supply," *Transportation Research Part A: Policy and Practice*, vol. 46, no. 5, pp. 828–842, 2012.

[23] E. M. Victoria, *Emergency Management Manual Victoria*. Victoria State Government, Emergency Management Victoria, GPO Box 4356, Melbourne, Vic 3001., 2018.

[24] B. of Meteorology, *National Arrangements for Flood Forecasting and Warning*. Commonwealth of Australia, National Climate Centre, Bureau of Meteorology, GPO Box 1289K, Melbourne VIC, 3001., 2018.

[25] E. M. Victoria, *Flood Sub-Plan*. Victoria State Government, 121 Exhibition Street, Melbourne VIC 3000., 2016.

[26] E. Martínez-Gomariz, M. Gómez, B. Russo, and S. Djordjević, "Stability criteria for flooded vehicles: A state-of-the-art review," *Journal of Flood Risk Management*, vol. 11, pp. S817–S826, 2018.

[27] S. N. Jonkman, M. Bo**c**karjova, M. Kok, and P. Bernardini, "Integrated hydrodynamic and economic modelling of flood damage in the netherlands," *Ecological economics*, vol. 66, no. 1, pp. 77–90, 2008.

[28] S. C. Calvert and M. Snelder, "A methodology for road traffic resilience analysis and review of related concepts," *Transportmetrica A: transport science*, vol. 14, no. 1-2, pp. 130–154, 2018.

[29] B. Immers, A. Bleukx, J. Stada, C. Tampere, and I. Yperman, "Robustness and resilience of road network structures," in *NECTAR Cluster Meeting on Reliability of Networks*, 2004.

[30] L. Chen and E. Miller-Hooks, "Resilience: an indicator of recovery capability in intermodal freight transport," *Transportation Science*, vol. 46, no. 1, pp. 109–123, 2012.

[31] A. Kaviani, R. G. Thompson, A. Rajabifard, G. Griffin, and Y. Chen, "A decision support system for improving the management of traffic networks during disasters," in *37th Australasian Transport Research Forum (ATRF), Sydney, New South Wales, Australia*, 2015.

[32] H. S. Mahmassani, *Incorporating weather impacts in traffic estimation and prediction systems*. U.S. Department of Transportation, Research and Innovative Technology Administration, 2009.

[33] R. Hranac, E. Sterzin, D. Krechmer, H. A. Rakha, M. Farzaneh, M. Arafeh, *et al.*, "Empirical studies on traffic flow in inclement weather," 2006.

[34] J. Kim, H. S. Mahmassani, R. Alfelor, Y. Chen, T. Hou, L. Jiang, M. Saberi, Ö. Verbas, and A. Zockaie, "Implementation and evaluation of weather-responsive traffic management strategies: insight from different networks," *Transportation Research Record*, vol. 2396, no. 1, pp. 93–106, 2013.

[35] W. research laboratory, *Australian Rainfall and Runoff: Appropriate safety criteria for people*. The University of New South Wales, 110 King Street Manly Vale, NSW 2093, 2011.

[36] R. G. Hoogendoorn, G. Tamminga, S. P. Hoogendoorn, and W. Daamen, "Longitudinal driving behavior under adverse weather conditions: Adaptation effects, model performance and freeway capacity in case of fog," in *13th International IEEE Conference on Intelligent Transportation Systems*, pp. 450–455, IEEE, 2010.

[37] S. C. Calvert and M. Snelder, *Influence of weather on traffic flow: An extensive stochastic multi-effect capacity and demand analysis*. Institute for Transport Studies in the European Economic Integration, 2016.

[38] B. L. Smith, K. G. Byrne, R. B. Copperman, S. M. Hennessy, and N. J. Goodall, "An investigation into the impact of rainfall on freeway traffic flow," in *83rd annual meeting of the Transportation Research Board, Washington DC*, Citeseer, 2004.

[39] T. H. Maze, M. Agarwal, and G. Burchett, "Whether weather matters to traffic demand, traffic safety, and traffic operations and flow," *Transportation research record*, vol. 1948, no. 1, pp. 170–176, 2006.

[40] W. J. van Stralen, S. C. Calvert, and E. J. Molin, "The influence of adverse weather conditions on probability of congestion on dutch motorways," *European Journal of Transport and Infrastructure Research*, vol. 15, no. 4, 2015.

[41] J. Asamer and M. Reinthaler, "Estimation of road capacity and free flow speed for urban roads under adverse weather conditions," in *13th International IEEE Conference on Intelligent Transportation Systems*, pp. 812–818, IEEE, 2010.

[42] J. Hogema, "Effects of rain on daily traffic volume and on driving behaviour," tech. rep., 1996.

[43] K. L. Broughton, F. Switzer, and D. Scott, "Car following decisions under three visibility conditions and two speeds tested with a driving simulator," *Accident Analysis & Prevention*, vol. 39, no. 1, pp. 106–116, 2007.

[44] S. Caro, V. Cavallo, C. Marendaz, E. R. Boer, and F. Vienne, "Can headway reduction in fog be explained by impaired perception of relative motion?," *Human factors*, vol. 51, no. 3, pp. 378–392, 2009.

[45] J. Xia, R. A. Falconer, X. Xiao, and Y. Wang, "Criterion of vehicle stability in floodwaters based on theoretical and experimental studies," *Natural hazards*, vol. 70, no. 2, pp. 1619–1630, 2014.

[46] M. Kramer, K. Terheiden, and S. Wieprecht, "Safety criteria for the trafficability of inundated roads in urban floodings," *International journal of disaster risk reduction*, vol. 17, pp. 77–84, 2016.

[47] Austroads, *Guide to Road Design Part 5: Drainage-General and Hydrology Considerations*. Level 9, 287 Elizabeth Street Sydney NSW 2000 Australia, 2018.

[48] M. Brackstone and M. McDonald, "Car-following: a historical review," *Transportation Research Part F: Traffic Psychology and Behaviour*, vol. 2, no. 4, pp. 181–196, 1999.

[49] R. Hoogendoorn, "State-of-the-art driving theory and modeling in case of adverse conditions," *Delft University of Technology, Delft*, 2010.

[50] S. Krauß, P. Wagner, and C. Gawron, "Metastable states in a microscopic model of traffic flow," *Physical Review E*, vol. 55, no. 5, p. 5597, 1997.

[51] S. Krauß, *Microscopic modeling of traffic flow: Investigation of collision free vehicle dynamics*. PhD thesis, Dt. Zentrum für Luft-und Raumfahrt eV, Abt. Unternehmensorganisation, 1998.

[52] K. Pyatkova, A. S. Chen, D. Butler, and S. Djordjević, "Modelling road transport congestion due to flooding," in *International Conference on Urban Drainage Modelling*, pp. 517–521, Springer, 2018.

[53] S. Robinson, *Simulation: the practice of model development and use*. Macmillan, 2003.

[54] W. Daamen, C. Buisson, and S. P. Hoogendoorn, *Traffic simulation and data: validation methods and applications*. CRC Press, 2014.

[55] W. Daamen, Y. Yuan, D. Duives, and S. Hoogendoorn, "Comparing three types of real-time data collection techniques: counting cameras, wi-fi sensors and gps trackers," *Proceedings of the Pedestrian and Evacuation Dynamics*, 2016.

[56] J. Taylor, *Introduction to error analysis, the study of uncertainties in physical measurements*. 1997.

[57] C. L. Kimberlin and A. G. Winterstein, "Validity and reliability of measurement instruments used in research," *American journal of health-system pharmacy*, vol. 65, no. 23, pp. 2276–2284, 2008.

[58] N. Golafshani, "Understanding reliability and validity in qualitative research," *The qualitative report*, vol. 8, no. 4, pp. 597–606, 2003.

[59] *Uncertainty of measurement - part 3: Guide to the expression of uncertainty in measurement (GUM:1995) = incertitude de mesure: partie 3: guide pour lexpression de lincertitude de mesure*. ISO, 2008.

[60] P. R. Bevington and D. K. Robinson, *Data reduction and error analysis for the physical sciences*. McGraw-Hill, 3rd ed., 2010.

[61] T. Witte and A. Wilson, "Accuracy of non-differential gps for the determination of speed over ground," *Journal of biomechanics*, vol. 37, no. 12, pp. 1891–1898, 2004.

[62] V. Knoop, *Introduction to Traffic Flow Theory*. Delft University of Technology, 2018.

[63] W. Daamen, "Lecture notes in empirical analysis for transport and planning, chapter 10: Traffic estimation," November 2018.

[64] B. Persaud and V. Hurdle, "Freeway capacity: definition and measurement issues," in *International Symposium on Highway Capacity*, 1991.

[65] D. Westland, "Potential methods to forecast the actual highway capacity. highway capacity and the level of service. proceedings of the international symposium on highway capacity, karlsruhe, germany," 1991.

[66] M. M. Minderhoud, H. Botma, and P. H. Bovy, "Assessment of roadway capacity estimation methods," *Transportation Research Record*, vol. 1572, no. 1, pp. 59–67, 1997.

[67] M. Brackstone, B. Waterson, and M. McDonald, "Determinants of following headway in congested traffic," *Transportation Research Part F: Traffic Psychology and Behaviour*, vol. 12, no. 2, pp. 131–142, 2009.

[68] P. G. Michael, F. C. Leeming, and W. O. Dwyer, "Headway on urban streets: observational data and an intervention to decrease tailgating," *Transportation research part F: traffic psychology and behaviour*, vol. 3, no. 2, pp. 55–64, 2000.

[69] T. R. Board, *Highway Capacity Manual*. 2101, Constitution Avenue, NW, Washington, DC 20418, 2000.

[70] M. Kyte, Z. Khatib, P. Shannon, and F. Kitchener, "Effect of weather on free-flow speed," *Transportation Research Record*, vol. 1776, no. 1, pp. 60–68, 2001.

[71] A. T. Ibrahim and F. L. Hall, *Effect of adverse weather conditions on speed-flow-occupancy relationships*. No. 1457, 1994.

[72] S. M. Turner, W. L. Eisele, R. J. Benz, and D. J. Holdener, "Travel time data collection handbook," tech. rep., United States. Federal Highway Administration, 1998.

Appendix A

Data Collection Plan

The present data collection plan is developed with the aim of defining the uncertainty associated to the 3SVAA when it comes to measure vehicle's speed from video recording. As a measurement system, it is subjected to errors or uncertainties that need to be evaluated in order to estimate the level of confidence associated to the measures. This data collection is designed to validate solely the speed measurements provided by the proposed video analysis approach.

The data collection activities are planned to be conducted the 23rd of June (2019) in a small village located in the province of Granada (Spain), which is the home town of the author of this thesis. Figure A. 1 depicts on the left the location of the city of Granada in Andalucía (Spain), and on the right the site where the activities will take place in a small village called Escúzar in the province of Granada.

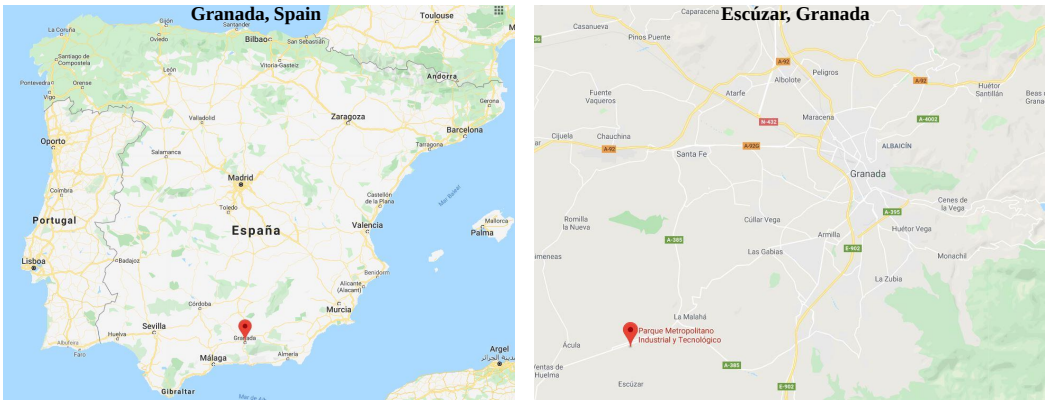

Figure A. 1: Location of Escúzar in the province of Granada (Spain). Google maps.

Two road stretches very similar to the ones displayed on the videos of Perth were chosen for conducting the data collection. Those are located in an industrial and technological park in Escúzar (Granada), which still has some areas under construction making the site a suitable place with low traffic to efficiently perform the data collection activities.

Research purpose and objectives

As it is already mentioned in the introduction, the objective of this data collection plan is to define the speed measurement error committed by the 3SVAA when analysing vehicle's speed from video recording. To do so, an experimental vehicle will be recorded crossing two road stretches in dry conditions at known speeds. Subsequently, the 3SVAA will be used to obtained

from the videos, the speed at which the experimental vehicle was supposed to be travelling at. The speed measurements obtained will then be compared to the real speed at which the vehicle actually crossed the road stretches. However, the true value of a measure may never be known, yet the author of this thesis assumes that a GPS speedometer provides an accurate value of speed. Therefore, the difference between the considered true speed value or GPS speed and the speed computed when applying the 3SVAA enables to define the speed measurement error committed. Considering all this, the main research question is formulated as follows:

What is the speed measurement error committed by the 3SVAA when it measures vehicle speed from video recordings?

The main research question yields to the following sub-question:

What is the difference between the speed measurements reported by the 3SVAA and the 'true speed' or GPS speed at which the vehicle is actually travelling at?

The answer of the research questions will guide to successfully complete the data collection plan. This plan is based on the data collection process explained in [72]. First section defines the research questions and objectives. The information and data needs for answering the research questions are presented in first section. Section 2 contains the research scope and assumptions, followed by the data collection technique used in this plan in section 3 and data collection scheduling in section 4. Finally, the setup of a pilot study to improve the effectiveness of the data collection performance is included in section 6. Section 7 defines unusual or adverse weather conditions that will lead to the cancellation of the data collection activities. At the end of the document, the speed tables to be completed during the activities are included in Tables A. 3, A. 4 and A. 5.

Research scope and assumptions

The accuracy of a measure is defined by [59,60] as 'the closeness agreement between the measured value and a true or accepted value', or in other words it refers to the deviation of a measurement from its true or accepted value. Such deviations can have two components, namely systematic and random errors. According to [60], systematic errors are reproducible inaccuracies that are consistently in the same direction and are difficult to detect. In contrast, random errors are however statistical fluctuations (in either direction) in the measured data due to the precision limitations of the measurement system. Therefore, the data collection plan is designed so that as many potential systematic errors as possible are removed

First, a search was made by the author to find two road stretches very similar in layout to those analysed in Perth and Isla road. An industrial and technological park located in a small village in the province of Granada called Escúzar provides with suitable road stretches with practically no traffic during the day to conduct the activities. Having low amount of traffic is key to successfully complete this data collection since it allows both the driver and the camera operator to freely perform their activities without having any conflict with other road users. Figure A. 2 shows a screenshot of the road stretches selected for the data collection.

Furthermore, some references were taken in the videos of Perth in order to place the camera in a similar position regarding height and distance from the road. Besides, the driver will be asked to drive on the opposite side of the road in order to recreate the driving in the UK. In addition, it is important to know that car's speedometers do not show the real speed of a vehicle, and that is why a GPS speedometer is used instead to correct for the speed difference. The driver

Figure A. 2: Screenshot of the two road stretches during a visit to the site. Escúzar, Granada (Spain).

will be recorded driving at different speeds ranging from 10 to 45 km/h too be sure the increase of speed does not influence the quality of the measure provided by the 3SVAA. Therefore, the experimental vehicle will be recorded crossing the stretches at different constant speeds ranging from 10 to 45 km/h in speed intervals of 5 km/h. Keeping constant speed along the stretch makes much easier to control the speed at every point. Finally, it is worth noting that is not necessary to have flooding conditions since after all, the objective is to find the measurement error associated to the 3SVAA when it measures vehicle speed from video recording.

The data collection activities will take place on Sunday, the 23rd of June (2019), which is probably the day of the week with the lowest traffic load. It is important to choose a time period of the day that enables the person responsible for recording the videos to carry out the tasks in pleasant weather conditions. Due to the high temperatures in this location during the summer, the time period selected to conduct the activities is between 9.00 to 13:30.

Information and data needs

The research objectives and research questions presented in the first section of this data collection plan defines the information needs. This information is subsequently translated into data needs, which are the starting points for the reminder of the data collection plan.

The measurement perspective of the data needed is microscopic as the speed of an individual vehicle is recorded. Moreover, the measurement objective of the data is local since the experimental vehicle will be recorded travelling at certain speed through two specific road stretches. In order to define the difference between the GPS speed value and the speed obtained through 3SVAA, the following data are needed:

- Video recording of an experimental vehicle crossing two specific road stretches at a constant speed ranging from 10 to 45 km/h in speed intervals of 5 km/h.
- Speed displayed on the experimental vehicle speedometer when crossing the road stretches.
- GPS speed of the experimental vehicle when crossing the road stretches.
- Speed of the experimental vehicle obtained when the videos are analysed through the 3SVAA afterwards.

Data collection techniques

For microscopic and local data, two data collection techniques are available, namely video cameras and probe vehicles. The second techniques was discarded since it requires the use of a vehicle equipped with devices that store position, speed and travel time, which the author does not dispose of. Besides, this technique requires the presence of an expert who is familiar with all the devices the vehicle is instrumented with. Nevertheless, it is important to know that a probe vehicle would have allowed to measure time headways and spacing, so that their validation could have also been conducted. For the speed validation, videotaping is an easier, faster an less expensive data collection technique, and it was therefore chosen as the preferred technique for the purpose at a hand. In addition, a simple experiment will be conducted to find the difference between GPS speed and the velocity displayed on the car's speedometer.

Video taping and analysis

A total of 14 videos (7 videos per direction) will be taped in the first road stretch, which is the one similar to the A94 Perth Road stretch. Only 7 videos will be taped in the second stretch, this is the one similar to the A93 Isla road stretch. This is because in the video only display vehicles coming from one direction, while in the first video vehicles are captured crossing the road in both directions. The reference speed to be maintained by the driver when crossing the road section ranges from 15 to 45 km/h in the first stretch and from 10 to 40 km/h for the second stretch, both in speed intervals of 5 km/h. Two people are needed to carry out the activities; an experimental driver and a person in charge of recording the videos (i.e. camera operator). Both will be in contact at every moment through a phone call conversation. The driver will use the hands-free kit of the car, while the camera operator will use headphones for operating convenience.

The driver will probably find some difficulties to reach the exact reference speeds when crossing the stretches, yet this will not be an issue as long as the driver writes down the actual speed at which he/she is travelling at. To make sure the driver maintains a constant speed, the cruise control of the car will be activated. Nevertheless, this device is not available when driving at low speeds, so that the driver will have to manually maintain a constant speed when driving at low speed ranges (<30 km/h). However, the experimental car disposes of a digital speedometer that enables the driver to clearly visualized the speed. To make sure the driver always completes a run (i.e. cross the stretch at a certain constant speed), the road stretch captured by the camera will be signalized with two cones marking. Therefore, the driver will drive on the left lane (L), turn around in the so-called 'manoeuvring area' and drive back on the other lane (R) until he/she completes all the runs. The manoeuvring areas will also be signalized and will be placed approximately 100 metres away from the last cone that indicates the end of the road stretch captured by the camera. In doing so, the driver will have enough space to fix the speed before crossing the stretch. In case the driver is not able to reach the desired speed, he/she will called it a 'failed attempt', so that the person responsible for the video taping will not start recording the video. Then, the driver will turn around and go back to the manoeuvring area to start again the run. Tables A. 3 and A. 4 are the ones that need to be filled in during the activities, and a two copies will be handed in to the driver who has to fill in the second column called 'Car Speedometer'. First columns contains the reference speeds at which the driver should be crossing the stretch, whilst the second column contains the actual speed at which the vehicle is crossing the stretch. The ideal scenario would be that both columns are equal, yet due to external factors the speed could slightly vary.

The camera operator will first attached the camera to a tripod that will allow to record the videos from a higher position as it is done in the A94 Perth Road stretch. The operator will

stand on the side walk and will place the camera in a way that it captures practically the same perspective as in the videos of Perth. To do so, the operator will be given some references that are taken from the videos of Perth in order to help him/her correctly placed the camera. Then, the operator will just have to press play every time the vehicle is approaching the road stretch, i.e. around 10 metres before the first cone, and press stop once the vehicle passes the second cone. It is essential the operator says in loud voice the corresponding reference speed at which the vehicle is supposed to be crossing the stretch. This will make much easier the identification of the videos afterwards.

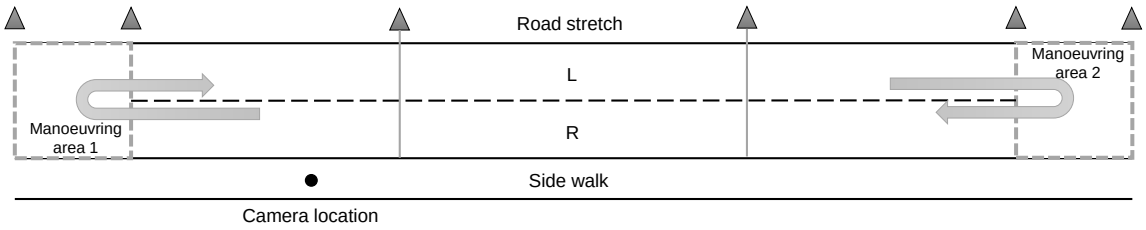

Figure A. 3: Sketch of the road stretch and the manoeuvring areas.

All the videos recorded during the data collection will be analysed by means of the 3SVAA, which will return the speed measurements that need to be compared thereafter with the GPS speed. The following section explains the experiment that will be conducted to obtain the considered 'true speed' value or GPS speed.

Speed experiment

A simple speed experiment aiming at defining the difference between the speed displayed on the car's speedometer and the GPS speed will be conducted during the pilot study, which will take place one week before the actual data collection plan. Being the camera operator in this experiment the passenger of the experimental vehicle, he/she will note down both the speed displayed on the car's speedometer and the GPS speed while the driver maintains different constant speeds ranging from 5 km/h to 50 km/h in speed intervals of 5 km/h. Table A. 5 shows the table that needs to be filled in by the passenger during the experiment. More details about this speed experiment are introduced within the 'Pilot study' section of this plan.

Schedule and equipment

In order to performed well-organized data collection activities, a complete schedule need to be developed in order to properly inform the data collection personnel of their specific responsibilities.

Date	Time period	Data collection personnel	Arrival time	Road stretch	Starting point	Activity duration
Sunday, 23rd June	AM	Driver	8:30	1	Manoeuvring area 1	9:00 – 11:00
Sunday, 23rd June	AM	Camera operator	8:30	1	Camera location	9:00 – 11:00
Sunday, 23rd June	PM	Driver	12:00	2	Manoeuvring area 1	12:30 – 13:30
Sunday, 23rd June	PM	Camera operator	12:00	2	Camera location	12:30 – 13:30

Table A. 1: Data collection schedule.

Both the driver and the camera operator will arrive to the site about half an our before starting the data collection activities. First, the operator needs time to place the camera at the right position on the side walk. Subsequently, the driver will call the operator using the hands-free kit of the car. If the communication is good enough, the driver will start crossing the first stretch on the left lane and they will dispose of two hours to complete the activities in the first road stretch. Subsequently, a 45 minutes break is planned before starting the activities at the second stretch, which can be spent on resting and moving the equipment to the second stretch. It is important both the driver and the camera operator spend around 15 minutes after the activities to double check the data gathered.

With the regard to the equipment needed to successfully complete all the data collection activities, the following list has been developed:

- Normal passenger car with its technical specifications
- Any type of camera/phone that records videos at a frame rate of 25 fps or higher
- Two mobile phones
- Camera tripod
- Reference sheet to help place the camera on the right location in stretch 1: 1 unit
- Reference sheet to help place the camera on the right location in stretch 2: 1 unit
- One reflective vest
- Six cones marking
- Writing material: 2 clipboards, 2 pencils and 2 rubbers
- Speed table stretch 1: four units
- Speed table stretch 2: four units
- Speed table form for pilot study: one unit

Pilot study

The pilot study together with the speed experiment will be conducted one week before the data collection plan. That is on Sunday, the 16th of June (2019) from 9:00 to 11:30. The main objective of the pilot study is to become familiar with the data collection equipment and process and to identify unexpected issues that may jeopardise the performance of the data collection activities.

The pilot study activities will mainly consist on recording 9 videos of the experimental vehicle crossing both stretches at different constant speeds. The driver will cross the first road stretch in both directions at speed of 15-30-45 km/h, and the second stretch only in one direction at speeds of 10-20-40 km/h. This will be enough to become familiar with the process and to identify possible issues that may arise not just during the activities, but when analysing the videos in the studio afterwards. Before carrying out the pilot study, a simple experiment to define the difference between the GPS speed and the speed displayed on the car's speedometer will be conducted. The schedule of the activities to be developed during the pilot study are depicted in Table A. 2.

The speed experiment will take place at the first road stretch and will last for half an hour. As a passenger of the experimental vehicle, the camera operator will fill in the speed table depicted

Date	Time period	Activities	Personnel	Arrival time	Road stretch	Starting point	Activity duration
Sunday, 16th June	AM	Speed experiment	Driver + camera operator	8:30	1	Manoeuvring area 1	9:00 – 9:30
Sunday, 16th June	AM	Data collection	Driver	9:30	1	Manoeuvring area 1	9:30 – 10:30
Sunday, 16th June	AM	Data collection	Camera operator	9:30	1	Camera location	9:30 – 10:30
Sunday, 16th June	AM	Data collection	Driver	9:30	2	Manoeuvring area 1	10:30 – 11:30
Sunday, 16th June	AM	Data collection	Camera operator	9:30	2	Camera location	10:30 – 11:30

Table A. 2: Pilot study schedule.

in Table A. 5 by using a GPS speedometer. The task of the driver is to maintain the speeds shown in the first column of the table while the operator notes down the speed at which the vehicle is actually travelling at, which corresponds to the one displayed on the GPS device. For the data collection, one hour will be enough time to record 9 videos, 6 at the first road stretch and 3 at the second road stretch.

The recorded videos will be analysed on the days following the pilot study by through the 3SVAA. This is essentially a quality control of the data to identify equipment problems or data discrepancies that may arise during the performance of the data collection activities or afterwards during the video analysis process. This will allow to make changes in the plan, the organisation or the equipment to ensure correct performance of the final data collection activities.

Extreme or unusual conditions

Extreme weather or unusual conditions may threaten the data collection, leading to the cancellation of the activities. Heavy rain or strong winds can make difficult to maintain constant speed or can reduce the visibility of the driver compromising his/her safety. Furthermore, it can lead the camera tripod to fall or reduce the quality of the video recordings if the camera lens is covered by raindrops. Nevertheless, the southern Spain climate is a hot-summer Mediterranean climate characterised by dry and warm summers with high sunshine levels. Therefore, the probability of cancelling the activities due to extreme weather conditions will be very low. In any case, it is important to check the weather forecast couple days before both the pilot study and the actual data collection to make sure the weather will allow the correct performance of the activities.

Moreover, it is also important to check that the devices (e.g. GPS speedometer, camera, tripod...) are working properly before moving to the site, since an equipment malfunctioning can also cause the cancellation of the activities. It is also essential to make sure there is no traffic on the road stretches when recording the videos. The presence of other vehicles when the experimental car is crossing the stretch may lead to errors in the video analysis. Therefore, it is important to make sure the experimental car is visible at every moment along the stretch. In principle, this should not be an issue since the traffic load at the park is extremely low. Nonetheless, it is recommended to ask the security guard for permission to close the road stretches to traffic during the activities to make sure there will not be any other vehicle present when the video taping is being conducted. The security guard can be found at the main entry of the park at the security post.

Stretch	Reference speed	Car Speedometer	GPS Speedometer	3SVAA (Matlab)	Speed diff. (δxi)	Speed diff. Squared (δxi^2)
1-L	15 km/h					
1-R	15 km/h					
1-L	20 km/h					
1-R	20 km/h					
1-L	25 km/h					
1-R	25 km/h					
1-L	30 km/h					
1-R	30 km/h					
1-L	35 km/h					
1-R	35 km/h					
1-L	40 km/h					
1-R	40 km/h					
1-L	45 km/h					
1-R	45 km/h					

Table A. 3: Speed table road stretches 1-R and 1-L.

Stretch	Reference speed	Car Speedometer	GPS Speedometer	'3-codes' Method (Matlab)	Speed diff. (δxi)	Speed diff. Squared (δxi^2)
2-L	10 km/h					
2-L	15 km/h					
2-L	20 km/h					
2-L	25 km/h					
2-L	30 km/h					
2-L	35 km/h					
2-L	40 km/h					

Table A. 4: Speed table road stretch 2-L.

Car Speedometer (km/h)	GPS Speedometer (km/h)	Speed difference (km/h)
5		
10		
15		
20		
25		
30		
35		
40		
45		
50		

Table A. 5: Speed table to be filled in during the pilot study.

Appendix B

The 3SVAA Matlab Codes

Matlab Code 1

```
trajectory = struct();
% Introduce video format .mp4, .MOV, .avi...
files = dir("*.mp4");
% Introduce the position of the video file within the folder
i = 1;
vid = VideoReader(files(i).name);
numFrames = vid.NumberOfFrames;
frameRate = round(vid.FrameRate);
k=1;
sec = 1;
% Select the lane on which vehicles are driving
direction = "L";
trajectory(1).vehicleID = 1;
for j = 1:frameRate:numFrames
frame = read(vid,j);
% imtool(frame) for manual
imshow(frame);
[x,y] = getpts;
for m = 1:length(x)
trajectory(k).direction = direction;
trajectory(k).frameNumber = j;
trajectory(k).seconds = sec;
trajectory(k).vehicleNumber = m;
trajectory(k).x = x(m);
trajectory(k).y = y(m);
k = k+1;
end
% If frameRate = round(vid.FrameRate):
sec = sec + 1;
close all;
end
% Save a table file in Matlab
save("trajectory-L-1.mat","trajectory");
```

Matlab Code 2

```
% Introduce video format .mp4, .MOV, .avi...
files = dir("*.mp4");
% Introduce the position of the video file within the folder
i = 1;
vid = VideoReader(files(i).name);
frameRate = round(vid.FrameRate);
equivTable = [];
k = 1;
for j = 1:frameRate:numFrames
frame = read(vid,j);
% imtool(frame) for manual
imshow(frame);
[x,y] = getpts;
equivTable(k).frameNumber = j;
equivTable(k).x4 = x(1);
equivTable(k).y4 = y(1);
equivTable(k).x5 = x(2);
equivTable(k).y5 = y(2);
equivTable(k).widthInX = x(2) - x(1);
equivTable(k).widthInY = y(2) - y(1);
k = k + 1;
close all;
end
% Save a table file in Matlab
save("equivalenceTable-R-1.mat","equivTable")
```

Matlab Code 3

```
% 1. Inputs
% Equivalence points & Corrected trajectory table
filename_distcorr = 'EquivPoints_1_R';
d = readtable(filename_distcorr + ".xlsx");

filename_car = 'Trajectories_1_R_corrected';
car_data = readtable(filename_car + ".xlsx");

% Decide to show plots (1: show plot, 0: don't show plot)
make_plot = 1;

% Calculate headways at the following cumulative distances
lst_space = [22,24,26,28,30,32,34,36,38];


% 2. Read data and associate to variables
% Introduce frame length and width according to video properties
lenFrame = 720;
widFrame = 1280;

% Associate to (x,y) and (x1,y1) the terminal points of the length of the car at every frame in
which 'reference vehicle' is passing through
if filename_distcorr == "EquivPoints_1_L"
x = d.x4;
x1 = d.x5;
y = lenFrame - d.y4;
y1 = lenFrame - d.y5;

% Subtract widFrame and lenFrame to invert the graph for vehicles coming on the right lane
in order to have the (0,0) in the upper-left corner. This is where the (0,0) in pixels coordinates
is located
elseif filename_distcorr == "EquivPoints_1_R"
x = widFrame - d.x4;
x1 = widFrame - d.x5;
y = lenFrame - d.y4;
y1 = lenFrame - d.y5;
else
disp("Check file name...")
end

% Equivalence points
equi_width = d.EquivalenceWidth_m_px_ ;

% In order to calculate the cumulative distance covered by the reference vehicle (in pixels),
we need first to draw a line through the middle points of the tracked lengths. Use first degree
polynomial
middle_points = [(x+x1)/2, (y+y1)/2 equi_width];
```

```
fitted_curve_middle_pt = fit(middle_points(:,1), middle_points(:,2),
'poly1');

% Make the line start at the y-axis (x=0)
interp_zero = [0, fitted_curve_middle_pt.p2, 10000];
middle_points = [interp_zero; middle_points];
middle_points = sortrows(middle_points,1);


% 3. Estimate 'equivalence curve'
% Calculate the cumulative distance (px) covered by the reference vehicle
middle_point_dist = [];
cumm_dist = 0;

for i = 1:length(middle_points)-1
x_i  = middle_points(i,1);
x_i1 = middle_points(i+1,1);
y_i =  middle_points(i,2);
y_i1 = middle_points(i+1,2);

dist = sqrt((x_i1-x_i)^2 + (y_i1-y_i)^2);
cumm_dist = cumm_dist + dist;
middle_point_dist = [middle_point_dist; cumm_dist];
end
middle_point_dist = [0; middle_point_dist];

% Estimate the 'equivalence curve' by fitting a second degree exponential through data points
('equivalence points' - cumulative distance covered by the reference vehicle)
[fitted_curve,stats] = fit(middle_point_dist(2:end),
middle_points(2:end,3),'exp2');
middle_points(1,3) = fitted_curve(0);
equi_width = middle_points(:,3);
interp_zero = interp_zero(1:2);

% Show goodness-of-fit statistics
parametres=4;
rse = sqrt(sum((middle_points(2:end,3)./
fitted_curve(middle_point_dist(2:end))
- 1).^2)./(length(middle_point_dist(2:end)) - parametres))*100
stats


% 4. Create vehicle structure array with microscopic data
% Fill in structure array
correction_dist = car_data.d_tot;

unique_ids = unique(car_data.id);
struct_cars = {};
```

```
for i = 1:length(unique_ids)
currentcar = "car" + string(i);
struct_cars.(currentcar).ID = i;
end

for k = 1:length(unique_ids)
currentcar = "car" + string(k);
[rows, ~] = find(car_data.id==k);

if filename_distcorr == "EquivPoints_1_L"
x_car1 = car_data.x(rows);
y_car1 = lenFrame - car_data.y(rows);

elseif filename_distcorr == "EquivPoints_1_R"
x_car1 = widFrame - car_data.x(rows);
y_car1 = lenFrame - car_data.y(rows);
else
disp("Check file name...")
end

car_position = [x_car1, y_car1];
car_position = [interp_zero; car_position];

car_info = [];
car_cumm_dist = 0;

% Cumulative distance in pixels
for i = 1:length(car_position)-1
xcar_i  = car_position(i,1);
xcar_i1 = car_position(i+1,1);
ycar_i =  car_position(i,2);
ycar_i1 = car_position(i+1,2);

dist = sqrt((xcar_i1-xcar_i)^2 + (ycar_i1-ycar_i)^2);
car_cumm_dist = car_cumm_dist + dist;

% Fit the car cumulative distance (px) in the 'equivalence curve'
equi_location_distance = fitted_curve(car_cumm_dist);

car_info = [car_info; dist, car_cumm_dist, equi_location_distance];
end

struct_cars.(currentcar).time = car_data.Sec(rows);
corr_dist = [0; correction_dist(rows)];
struct_cars.(currentcar).corr_dist = corr_dist;

car_info = [car_info, car_data.Sec(rows)];
car_info = [0, 0, fitted_curve(0), 0; car_info];

% Cumulative distance in meters
```

```
lst_dist_meters = [];
car_cumm_dist_meters = 0;

for j = 1:size(car_info,1)-1
if filename_distcorr == "EquivPoints_1_L"
d1 = car_info(j,2) + struct_cars.(currentcar).corr_dist(j);
d2 = car_info(j+1,2) + struct_cars.(currentcar).corr_dist(j+1);
else
d1 = car_info(j,2) - struct_cars.(currentcar).corr_dist(j);
d2 = car_info(j+1,2) - struct_cars.(currentcar).corr_dist(j+1);
end

dist_meters = integrate(fitted_curve, d2, d1);
car_cumm_dist_meters = car_cumm_dist_meters + dist_meters;
lst_dist_meters = [lst_dist_meters; dist_meters, car_cumm_dist_meters];

struct_cars.(currentcar).dist_m(j,1) = dist_meters;
struct_cars.(currentcar).cumm_dist_m(j,1) = car_cumm_dist_meters;
end

% car info: distance, cum dist, equivalence, sec, distance meters, cumm dist meters
car_info = car_info(2:end,:);
car_info = [car_info lst_dist_meters];

% Calculate microscopic variables
% SPEED and AVERAGE SPEED
for j = 2:size(car_info,1)
delta_t = struct_cars.(currentcar).time(j,1) -
struct_cars.(currentcar).time(j-1,1);
delta_m = struct_cars.(currentcar).cumm_dist_m(j,1) -
struct_cars.(currentcar).cumm_dist_m(j-1,1);
speed = delta_m/delta_t*3.6;

struct_cars.(currentcar).speed(j,1) = speed;
end
currentcar;
struct_cars.(currentcar).avg_speed =
mean(struct_cars.(currentcar).speed(2:end,1));

% SPACING
if k ~=1
previous_car = k-1;
[rows_prev_car, ~] = find(car_data.id== previous_car);
time_current_car = car_data.Sec(rows);
time_prev_car = car_data.Sec(rows_prev_car);

same_time = intersect(time_current_car,time_prev_car);

for kk = 1:length(same_time)
KK = same_time(kk);
```

```
time_index_cc = find(struct_cars.(currentcar).time == KK);
time_index_pc = find(struct_cars.("car" +
string(previous_car)).time == KK);

cumm_dist_cc = struct_cars.(currentcar).
cumm_dist_m(time_index_cc);
cumm_dist_pc = struct_cars.("car" +
string(previous_car)).cumm_dist_m(time_index_pc);

spacing = cumm_dist_pc - cumm_dist_cc;
struct_cars.(currentcar).spacing(time_index_cc) = spacing;
end
if isfield(struct_cars.(currentcar),"spacing") == 1
struct_cars.(currentcar).spacing =
transpose(struct_cars.(currentcar).spacing);
struct_cars.(currentcar).avg_spacing =
sum(struct_cars.(currentcar).spacing,1)./
sum(struct_cars.(currentcar).spacing
~=0,1);
end
end

% TIME HEADWAYS
lst_int_time = [];

for i5 = 1:length(lst_space)
space = lst_space(i5);

idx_closest_pt = find(min(abs(struct_cars.
(currentcar).cumm_dist_m-space)) ==
abs(struct_cars.(currentcar).cumm_dist_m-space));
closest_pt_1 = struct_cars.(currentcar).
cumm_dist_m(idx_closest_pt);
time_1 = struct_cars.(currentcar).time(idx_closest_pt);

if space > struct_cars.(currentcar).cumm_dist_m(end) || space <
struct_cars.(currentcar).cumm_dist_m(1)
continue
elseif closest_pt_1 < space
closest_pt_2 = struct_cars.(currentcar).
cumm_dist_m(idx_closest_pt+1);
time_2 = struct_cars.(currentcar).time(idx_closest_pt+1);
else
closest_pt_2 = struct_cars.(currentcar).
cumm_dist_m(idx_closest_pt -1);
time_2 = struct_cars.(currentcar).time(idx_closest_pt -1);
end

f=fit([time_1; time_2], [closest_pt_1; closest_pt_2],'poly1');
param_a = f.p1;
```

```
param_b = f.p2;

associated_time = (space - param_b)/param_a;
lst_int_time = [lst_int_time;associated_time space];
end

struct_cars.(currentcar).int_time = lst_int_time;

TF = isfield(struct_cars.(currentcar),'int_time');

previous_car = "car" + string(k-1);
if k ~=1 &&  isempty(struct_cars.(currentcar).int_time) == 0 &&
isempty(struct_cars.(previous_car).int_time) == 0

current_int_time = struct_cars.(currentcar).int_time;
prev_int_time = struct_cars.(previous_car).int_time;

[tf,idx] = ismember(prev_int_time(:,2),current_int_time(:,2));
idx_prev_int_time = find(idx);
idx_current_int_time = idx(idx_prev_int_time);

lst_headway = [];

for i6 = 1:length(idx_current_int_time)
idx_i6_current = idx_current_int_time(i6);
idx_i6_prev = idx_prev_int_time(i6);

headway = current_int_time(idx_i6_current,1) -
prev_int_time(idx_i6_prev,1);
lst_headway = [lst_headway;
headway current_int_time(idx_i6_current,2)];
end
struct_cars.(currentcar).headway = lst_headway;
end


struct_cars.(currentcar).info = car_info;
end


% 5. Plots
if make_plot == 1
if filename_distcorr == "EquivPoints_1_L"

% Location of reference vehicle length middle points
figure()
plot(middle_points(:,1), middle_points(:,2),'k*')
hold on
plot(fitted_curve_middle_pt,'k', middle_points(:,1),
middle_points(:,2))
```

```
title("Location of length middle points")
xlabel("[px]")
ylabel("[px]")

% Equivalence points - Cum distance covered by reference vehicle
figure()
plot(middle_point_dist, equi_width,'k*')
ylabel("Equivalences [m/px]")
xlabel("Distance travelled by the ref vehicle [px]")

% Equivalence curve
figure()
plot(middle_point_dist, equi_width,'k*')
hold on
plot(fitted_curve,'k', middle_point_dist, equi_width)
ylabel("Equivalences [m/px]")
xlabel("Distance travelled by the ref vehicle [px]")

% Vehicles trajectories in the Space (m)-Time (s) diagram
figure()
for p1 = 1:length(unique_ids)
time_graph = struct_cars.("car" + string(p1)).time;
cumm_dist_graph = struct_cars.("car" + string(p1)).cumm_dist_m;
plot(time_graph, cumm_dist_graph, 'k-*')
hold on
end
xlabel("Time [s]")
ylabel("Distance [m]")

else

figure()
plot(middle_points(:,1), middle_points(:,2),'*')
hold on
plot(fitted_curve_middle_pt, middle_points(:,1),
middle_points(:,2))
title("Location of length middle points")
xlabel("[px]")
ylabel("[px]")

figure()
plot(middle_point_dist, equi_width,'k*')
ylabel("Equivalences [m/px]")
xlabel("Distance travelled by the ref vehicle [px]")

figure()
plot(middle_point_dist, equi_width,'k*')
hold on
plot(fitted_curve,'k',middle_point_dist, equi_width)
ylabel("Equivalence [m/px]")
```

```
xlabel("Distance travelled by the ref vehicle [px]")

figure()
for p1 = 1:length(unique_ids)
time_graph = struct_cars.("car" + string(p1)).time;
cumm_dist_graph = struct_cars.("car" + string(p1)).cumm_dist_m;
plot(time_graph, cumm_dist_graph, 'k-*')
hold on
end
xlabel("Time [s]")
ylabel("Distance [m]")
end
end
```